Morphological comparison of the feeding apparatus in herbivorous, omnivorous and carnivorous mudskippers (Gobiidae: Oxudercinae)

July 2021

Graduate School of Fisheries and Environmental Sciences,

Nagasaki University

Tran Xuan Loi

CONTENTS

ABSTRACT

CHAPTER I GENERAL INTRODUCTION

One of the major biological evolution of vertebrates during land invasion was the transition of feeding mechanisms from suction in aquatic animals to prehension in terrestrial ones. Due to large differences in physicochemical characteristics of air and water, suction feeding is impractical on land, and thus terrestrial vertebrates usually employ teeth on jaws for obtaining food. How feeding mechanisms modified in the Devonian transitional vertebrates is little known. Recent investigations of fossils and extant amphibious fishes have partly revealed how early terrestrial vertebrates might have obtained food in terrestrial environment, and suggested all of them being carnivorous. However, understanding of the feeding transition is incomplete due to only based on hard structures (fossils) or macrophagous carnivorous fishes. There is a fraction number of amphibious fishes, i.e., oxudercine gobies, showing a full spectrum of habitat transition from water to land and varying feeding habits; and surprisingly, their transition of feeding habit may be from herbivory/omnivory to carnivory. Comparison of feeding apparatus among this group of fish could not only shed light on their feeding transition, but also gain our understanding of the feeding transition in early land vertebrates due to their feeding faced analogous constraints. In this study, oxudercine gobies were used as model species to elucidate i) how feeding system of aquatic fish has transitioned as they invaded land, and ii) is there any possibility of early emergence of oxudercine gobies being herbivorous or omnivorous?

CHAPTER II MORPHOLOGY OF THE FEEDING APPARATUS IN THE HERBIVOROUS MUDSKIPPER, *Boleophthalmus pectinitrostris* (Linnaeus, 1758)

Among the mudskippers, *Boleophthalmus pectinirostris* is herbivorous and grazes on diatoms on exposed mudflats. In this study, we investigated the morphology of the feeding apparatus of this species to understand how feeding apparatus is modified for grazing on land.

Dentition, and the skeletal and muscular systems of the branchial basket were examined through macroscopic and microscopic dissection, scanning electron microscopy, and micro-computed tomography scanning. The results show that the feeding apparatus of the fish has been modified presumably to transport diatom cells from the mudflats surface to the digestive tract with minimum admixture of mud particles. The modifications include horizontal orientation of the lower jaw teeth, horizontally aligned, high-density gill rakers on the third (only on the posterior row) and fourth (both rows) gill arches, large pharyngeal plates bearing numerous fine teeth, and the musculoskeletal system related to the fourth epibranchial.

CHAPTER III MORPHOLOGICAL COMPARISON OF THE FEEDING APPARATUS IN THE MUDSKIPPERS: *Boleophthalmus boddarti* (Pallas, 1770), *Oxuderces nexipinnis* (Cantor, 1849), *Scartelaos histophorus* (Valenciennes, 1837), *Periophthalmus chrysospilos* Bleeker, 1852, AND *Periophthalmodon schlosseri* (Pallas, 1770)

In this study, the anatomy of the feeding apparatus of five oxudercine gobies, *Boleophthalmus boddarti* (moderately terrestrial, herbivorous), *Oxuderces nexipinnis* (nearly aquatic, herbivorous), *Scartelaos histophorus* (moderately terrestrial, omnivorous), *Periophthalmus chrysospilos* (highly terrestrial, carnivorous), and *Periophthalmodon schlosseri* (highly terrestrial, carnivorous) collected from a mudflat in Vietnam, was compared. *B. boddarti* and *O. nexipinnis* are characterized by a horizontal disposition of the dentary teeth, more densely spaced gill rakers on the posterior row of the third arch and both rows of the fourth arch, and large, ventrally curved pharyngeal plates bearing numerous fine teeth. *Ps. chrysospilos* and *Pn. schlosseri* have oral jaw bones with jaw-levers producing a greater biting force, rudimentary gill rakers, and pharyngeal plates studded with robust canine teeth. On the underside of the ventral plates, prominent ridges occur, onto which strong muscles attach. The jaw adductors are larger in these carnivorous mudskippers. *S. histophorus* shows an anatomical architecture which may be considered intermediate between these herbivorous and carnivorous species. On the basis of currently accepted relationships of oxudercine genera, their feeding

habits, and the morphology of the feeding apparatus, we hypothesize that the oxudercine gobies had been adapted to feeding microalgae in shallow water before expanding their niche onto land, and subsequently diverged to more specialized herbivorous (*Boleophthalmus*) and carnivorous groups (*Periophthalmus* and *Periophthalmodon*) feeding in higher intertidal habitats.

CHAPTER IV MORPHOLOGY OF THE FEEDING APPARATUS IN TWO OXUDERCINE GOBIES, *Parapocryptes serperaster* (Richardson 1846) and *Pseudapocryptes elongatus* (Cuvier 1816)

Oxudercine gobies are exceptional among fish, comprising of fully aquatic to highly terrestrial species. The previous study hypothesized gradual transition from herbivory to carnivory during their niche expansion onto land. In this study, the anatomy of the feeding apparatus of two oxudercine gobies, *Parapocryptes serperaster* and *Pseudapocryptes elongatus*, was investigated, both of which show low degrees of terrestriality and are therefore important for understanding initial stages of the alteration of feeding apparatus in these fishes. The feeding system of the two species is similar in having heterogeneous development of gill rakers among gill arches; strongly curved, large pharyngeal plates studded with numerous papilliform teeth; and configuration of both musculature and skeleton of the branchial basket. On the other hand, the number of teeth in *Pa. serperaster* is more than double than in *Pd. elongatus* for both premaxilla and dentary, while the size of the teeth in *Pa. serperaster* is only half that of *Pd. elongatus* for both length and width. Pharyngeal plates and associated muscular and skeletal elements are more posteriorly located in *Pd. elongatus*. These similarities and differences may be explained by different feeding habits of the two species, and might represent transition from herbivory to omnivory during early stages of niche expansion onto land by oxudercine gobies.

CHAPTER V MORPHOLOGY OF THE FEEDING APPARATUS IN TWO OXUDERCINE GOBIES, *Periophthalmus modestus* Cantor, 1842 and *Periophthalmodon septemradiatus* (Hamilton, 1822)

In order to gain understanding of the terrestrial feeding in mudskippers, morphology of feeding apparatus in the two carnivorous mudskipper species, *Periophthalmus modestus* and *Periophthalmodon septemradiatus*, was examined and compared to these of *B. boddarti*, *B. pectinirostris*, *Ps. chrysospilos*, and *Pn. schlosseri* achieved in preceding studies. Feeding morphological features of *B. boddarti* and *B. pectinirostris* are similar but show some differences in dentition morphometrics and tooth density on the pharyngeal plates, which could be because they graze on different terrestrial zones. Among the four carnivorous mudskippers, feeding apparatus of *Ps. modestus* is different by having no frontal fang-like teeth, smaller values of replacement teeth, standardized tooth length, and standardized tooth width on the oral jaws; the pharyngeal plates being studded with higher density of teeth and overlapping of the third and fourth pharyngobranchials, which could facilitate feeding soft and non-invasive prey. In conclusion, modifications of the feeding apparatus could aid feeding different types of prey.

CHAPTER VI GENERAL DISCUSSION AND FUTURE DIRECTION

Evolution of feeding apparatus during land invasion of vertebrates: The suction-to-biting transition coincides with flexible-to-firm modifications of the cranial structure, which is thought to have happened around the time that vertebrates invaded land. The prominent changes include loss of the operculogular series, reduction and modification of the branchial system, and rigidity of the lower jaws and skull roof, which facilitate biting. These modifications presumably occurred when vertebrates were still in aquatic environment, and all of early vertebrates were carnivorous. Although the feeding system of mudskippers mainly shares the morphology of typical fish, they show some modifications, i.e., horizontal disposition of dentary teeth, posterior development of gill rakers, large and curved pharyngeal plates bearing with numerous fine teeth in the herbivorous and omnivorous species; the musculoskeletal

system of the oral jaw produce strong biting and of the pharyngeal plates being well developed in the carnivorous species, presumably facilitating feeding on land. The present study also proposed that early emerged oxudercine gobies could be herbivorous or omnivorous species.

Adaptions of terrestrial grazing in herbivorous and omnivorous mudskippers: The primary challenge of the herbivorous and omnivorous mudskippers is to obtain food particles with less admixture of mud particles. The modifications of feeding apparatus in the herbivorous and omnivorous mudskippers being distinct from typical filter-feeding fishes are presumably adaptations of effective exploitation of food resources on land, but conformation of filtering mechanics should be further investigated by employing electromyography or detail analysis of feeding behavior.

Adaptations of terrestrial feeding in carnivorous mudskippers: Capability of terrestrial capturing and swallowing prey without relying on water (using teeth on jaws and the tongue) is the key factor allowing early vertebrates to expand their life on land. Most of extant amphibious fishes are able to capture prey on land but they must return into water for swallowing, except *Ps. kalolo* feeding without using water (Sponder and Lauder 1981). Findings in the present study partly revealed how mudskippers could handle prey on land. In order to gain more understanding of terrestrial feeding in this group of fish, detail investigations of their feeding mechanics, especially in high terrestrial species (*Periophthalmus* or *Periophthalmodon*), using electromyography, cinematography, or feeding behavior analysis could be fruitful.

Chapter I

GENERAL INTRODUCTION

One of the major biological evolution of vertebrates during land invasion was the transition of feeding mode from foraging for food in aquatic environment to preying on terrestrial environment. Based on relative movement of prey and water to the mouth, feeding in aquatic environment can be classified into three modes, i.e., ram feeding, suction feeding, and biting (Ferry et al. 2015). Ram feeding mainly relies on forward swimming of aquatic animals with mouth opened in order to engulf prey (Fig. I-1a). In this mode of feeding, the relative closing movement of the prey and predator is mainly contributed by the movement of the predator, and massive volumes of water flows through the mouth. Feeding of herring, basking shark, or blue whales is typical examples of ram feeding (Sanderson and Wassersug 1990; Carey and Goldbogen 2017). Suction feeding, widely employed by aquatic animals (Wainwright et al. 2015), is dependent on rapid expansion of the oropharyngeal cavity generating negative pressure drawing water and prey into the mouth. In this type of feeding, the movement of prey mainly contributes to the relative closing movement of the prey and predator (Fig. I-1b). Biting refers to grip and tear prey with teeth on the oral jaws. In this type of feeding, the movement of predator mainly contributes to the relative closing movement of the prey and predator, but volume of water flowing through the mouth is much less than in the ram feeding (Fig. I-1c). Whichever feeding mode is used, water plays an essential role as a medium of prey ingestion and/or intraoral transport. Due to air is much less density and viscosity compared to water, feeding modes employed by aquatic animals are impractical on land (Liem 1990; Norton and Brainerd 1993). Instead, terrestrial vertebrates capture prey using teeth on the oral jaws and the tongue to transport it into the esophagus (Schwenk and Rubega 2005). During land invasion by vertebrates which is though had occurred in the late Devonian Period (approximately 390 to 360 million years ago) (Clack 2012), feeding mechanism had to be evolved from suction to

biting. The questions of what form of feeding mode early terrestrial vertebrates could be employed and how morphological feeding apparatus could be modified from typical fish are still mysterious.

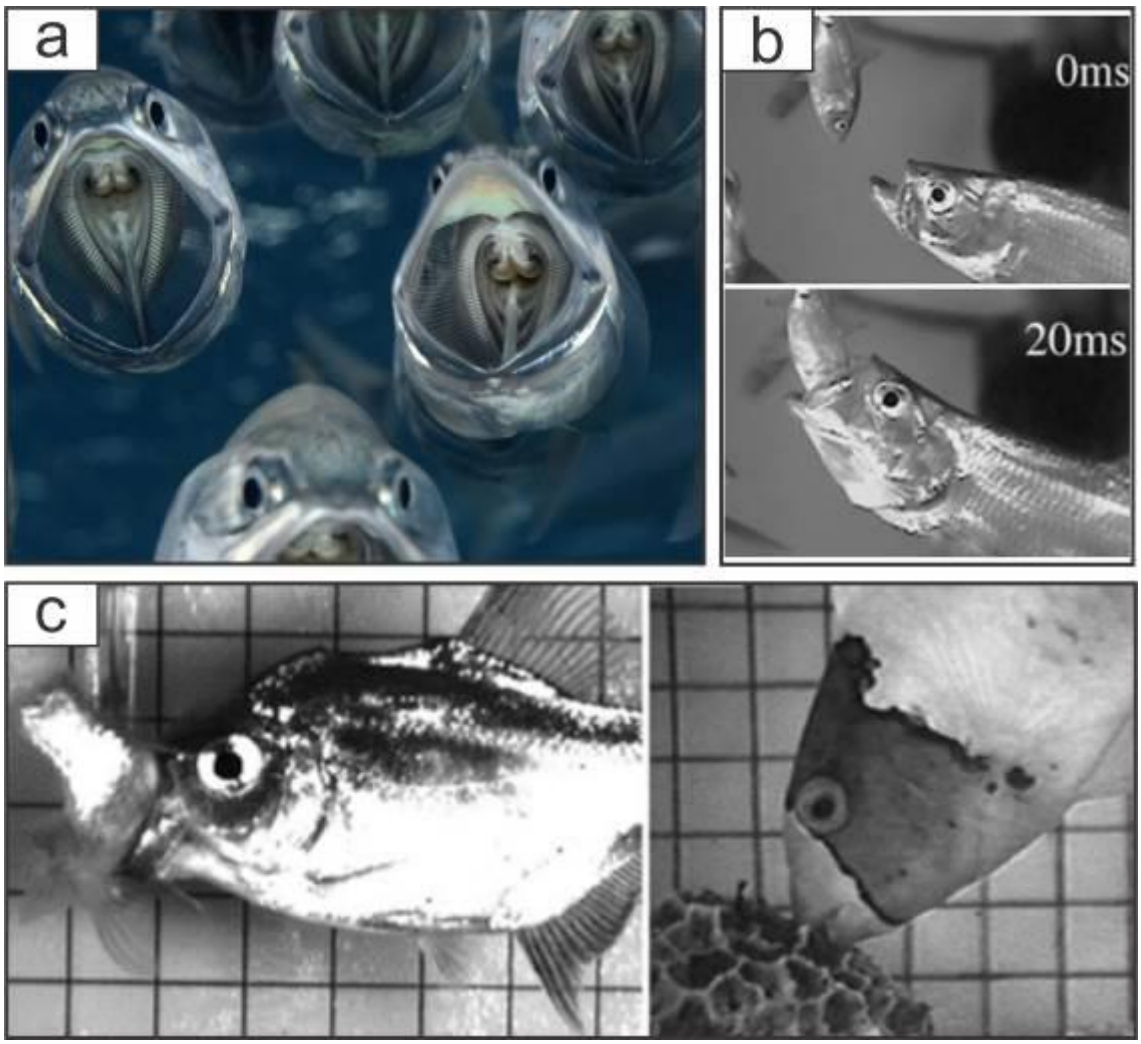

Fig. I- 1 Ram feeding in *Rastrelliger kanagurta* (**a**); suction feeding of *Megalops atlanticus* at 0ms (upper box) and 20 ms (lower box) (**b**); biting in *Catoprion mento* (left box) and *Cetoscarus bicolor* (right box) (**c**). Photos were modified from Tattersal (2018) for ram feeding and Westneat (2006) for suction feeding and biting.

Fossil evidences have being employed to infer an intermediate step in the evolution of terrestrial feeding (Markey and Marshall 2007; Ashley-Ross et al. 2013; Lemberg et al. 2021), which is only based on hard structures, but not soft structures or behavior. Examination of feeding mechanism of extant amphibious fish, i.e., facing analogous constraints as feeding in terrestrial environment, could also give more insight into the feeding transition, and recent findings showed how fish manage to capture prey in terrestrial environment. For example,

Channallabes apus (Günther, 1873) and *Erpetoichthys calabaricus* Smith, 1865 use their elongated body to lift and incline the anterior body in order to place the mouth on prey (Van Wassenbergh 2013; Van Wassenbergh et al. 2016). *Anableps anableps* (Linnaeus, 1758) and *Periophthalmus barbarus* (Linnaeus, 1766) possess capability of rotation the dentary at large angle and protrusion the premaxilla for orientating the gape toward the ground (Michel et al. 2014, 2015a, b). *Ps. barbarus* also uses their pectoral fins to lift the anterior body enabling the oral jaws to be placed on prey (Sponder and Lauder 1981; Michel et al. 2014). Whichever strategies are employed in terrestrial prey capture, the key factor of successful capture is the capability of placing the gape on prey (Heiss et al. 2018). Although giving how amphibious fish capture prey on land, these findings were based on macrophagous, carnivorous fishes feeding on immovable prey, which do not fully reflect feeding mechanism in their nature, and we have little knowledge about how the feeding system of aquatic fish has transitioned to those specialized terrestrial modes.

A small fraction number of amphibious fishes belonging to the subfamily Oxudercinae inhabits intertidal zones. They show a full range of transition from aquatic to terrestrial mode of life, and include herbivorous, omnivorous and carnivorous species feeding at the water's edge (Clayton 1993, 2017; Murdy and Jaafar 2017). Therefore, they are ideal models for studying the water-to-land transition of feeding mechanism. Natural distribution of oxudercine gobies is in mangroves or on mudflats, throughout the Indo-West Pacific and western coast of Africa. Their living habitats are tightly restricted to these ecosystems that makes them ideal bio-indicators for these habitats but also vulnerable to the habitat degradation and loss (Ansari et al. 2014; Parenti and Jaafar 2017).

The feeding cycle in vertebrates generally comprises five phases, capture, ingestion, intraoral transport, processing, and swallowing. Certain anatomical structures, i.e., the dentition, the gill rakers, the pharyngeal plates, and/or the skeletal and muscular systems of the branchial

baskets, are responsible for each feeding phase (Schwenk and Rubega 2005). In order to elucidate the aquatic-to-land transition of feeding apparatus, morphological comparison of the feeding organs among the mudskippers species were implemented. Ten mudskipper species, i.e., *Boleophthalmus boddarti* (Pallas, 1770), *Boleophthalmus pectinirostris* (Linnaeus, 1758) *Oxuderces nexipinnis* (Cantor, 1849), *Parapocryptes serperaster* (Richardson, 1846), *Pseudapocryptes elongatus* (Cuvier, 1816), *Scartelaos histophorus* (Valenciennes, 1837), *Periophthalmus chrysospilos* Bleeker, 1853, *Periophthalmus modestus* Cantor, 1842, *Periophthalmodon schlosseri* (Pallas, 1770), and *Periophthalmodon septemradiatus* (Hamilton, 1822), represented various life modes (from aquatic to terrestrial) in the intertidal zones and feeding habits were chosen. Among them, *B. boddarti*, *B. pectinirostris*, *O. nexipinnis* and *Pa. serperaster* are herbivorous; *P. elongatus* and *S. histophorus* are omnivorous; and *Ps. chrysospilos*, *Ps. modestus*, *Pn. schlosseri*, and *Pn. septemradiatus* are carnivorous. *Oxuderces nexipinnis*, *Pa*. *serperaster*, and *Pd*. *elongatus* spends most of their time in shallow tidal pools, *B. boddarti*, *B. pectinirostris*, and *S. histophorus* inhabits a moderately terrestrial environments, while *Ps. chrysospilos, Ps. modestus, Pn. schlosseri*, and *Pn. septemradiatus* are most terrestrial (Fig. I-2 and Table S1).

The thesis was organized into six chapters. In Chapter 1, general introduction of the water-to-land transition of feeding modes in vertebrates and the potential of using mudskippers as key models in bridging knowledge gap of this transition will be given. In Chapter 2, the morphology of feeding apparatus in *Boleophthalmus pectinirostris*, an herbivorous mudskipper distributed in the Ariake Sea, Japan, will be presented. In Chapter 3, the morphology of feeding apparatus among the five mudskipper species represented different feeding habits and water-to-land mode of life will be compared; and a hypothesis of the feeding habit transition will also be proposed. In order to consolidate the proposed hypothesis, the morphology of feeding apparatus in two herbivorous/omnivorous mudskippers showing low terrestriality (*Parapocryptes serperaster* and *Pseudapocryptes elongatus*, Chapter 4) and two carnivorous

species showing high terrestriality (*Periophthalmus modestus* and *Periophthalmodon septemradiatus*, Chapter 5) will be investigated. The last chapter provides general discussion of aquatic-to-terrestrial feeding transition in vertebrates and adaptations of terrestrial feeding in mudskippers.

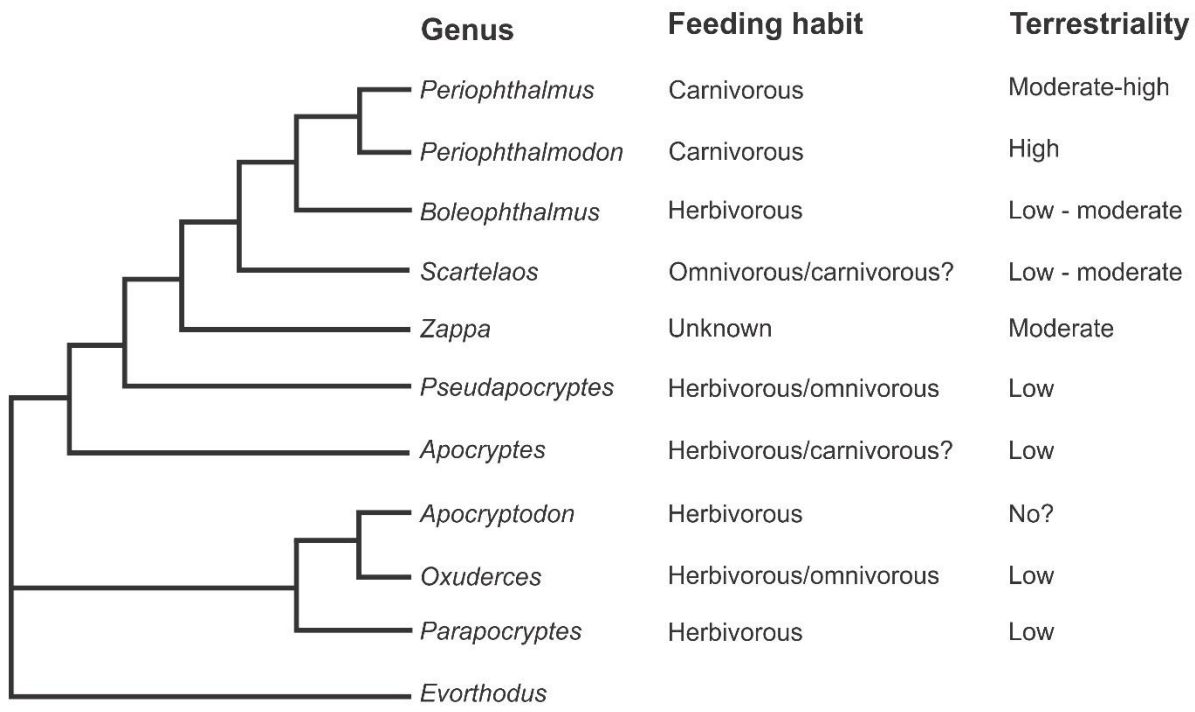

Fig. I-2 Hypothesized relationships of the genera of Oxudercinae, and their terrestriality and feeding habit. The cladogram was modified from Murdy and Jaafar (2017). *Evorthodus* is used as an outgroup. For detailed data of terrestriality and feeding habit, see Table S1

Chapter II

MORPHOLOGY OF THE FEEDING APPARATUS IN THE HERBIVOROUS MUDSKIPPER, *Boleophthalmus pectinitrostris* (Linnaeus, 1758)

I. Introduction

Filter feeding is one of the major feeding strategies in aquatic animals. Animals that filter feed generate a water flow through a filtering structure by swimming or other activities to entrap prey organisms. Filter feeding obviously has a long history in vertebrate evolution and is ubiquitous; it is considered to have been practiced by proto-vertebrates (Mallatt 1984), and is known among both extant non-vertebrate chordates (Wainwright et al. 2015) and a large number of fishes (Lazzaro 1987). Even though the Devonian vertebrates known in the period of transition from aquatic to terrestrial lifestyles are all considered to be macrophagous carnivorous animals (Clack 2012), it seems therefore possible that there have been cases in which plankton-feeding or filter-feeding fishes emerged to exploit terrestrial food resources.

Because of the large difference in physicochemical characteristics of air and water, feeding mechanisms effective in water do not usually work as well in air. For example, suction feeding, which is used by about 60% of extant fish species (Wainwright et al. 2015), does not function effectively in air, because it depends on the much higher density and viscosity of water to entrap prey in the water flow and move it into the buccal cavity. There are fish species that have evolved the capacity to capture prey on land [*Anableps anableps* (Linnaeus, 1758), *Channallabes apus* (Günther, 1873), *Erpetoichthys calabaricus* Smith, 1865, and *Periophthalmus spp*.] and recent papers have demonstrated how they feed on land (Sponder and Lauder 1981; Van

Wassenbergh 2013; Michel et al. 2015a, b; Van Wassenbergh et al. 2017). However, these are all macrophagous, carnivorous species.

A small number of fishes are known to feed on plant matter on land. These include three genera of mudskippers, *Boleophthalmus*, *Pseudapocryptes* and *Scartelaos* of the subfamily Oxudercinae (Clayton 2017), and several amphibious blennies (Rao and Hora 1933; Nursall 1981). The species of these three mudskipper genera graze microalgae, mainly diatoms, growing on the mudflat, while the blennies browse macroalgae, growing on hard substrates. The anatomy of the feeding system of these fishes has been scarcely investigated (Murdy 1989; Clayton 2017). In this study, we examined the morphology of dentition, and the skeletal and muscular systems of the branchial basket of *Boleophthalmus pectinirostris*. *Boleophthalmus pectinirostris* is a herbivorous mudskipper distributed in intertidal mudflats along the coast of the Strait of Malacca (Polgar and Crosa 2009), the East China Sea and the South China Sea (Parenti and Jaafar 2017). The fish grazes and sieves epipelic diatoms with distinct, side-to-side head movements, as in other *Boleophthalmus* species (Clayton 1993).

II. Materials and methods

Sample collection and preservation

A total of 35 individuals (standard length from 81.5 to 180.0 mm) were used in this study. The samples were collected from the Ariake Sea, Saga Prefecture, Japan in October 2016, June 2017 and August 2018 by using pitfall traps inserted into *B. pectinirostris* burrows. They were euthanized by immersing them in a solution of an anesthetic solution, 2-Phenoxyethanol (Wako Pure Chemical Industries, Japan), at a concentration of 100 mL/L and fixed in a 10% neutralized formalin solution for a week. Then, they were rinsed with water overnight and preserved in 75% ethanol.

The gross morphological features of the branchial basket

The branchial baskets were removed under a dissecting microscope (Olympus SZ-STU2, Tokyo, Japan). The number of gill rakers was counted for all gill arches on the left side. The spaces between the gill rakers were measured for the entire length of the first, second, and the anterior row of the third arches. On the other hand, a single determination was made each on the ventral, middle and dorsal segments of the posterior row of the third and both rows of the fourth arches, because preliminary measurements revealed that the space between the gill rakers was highly constant.

To determine the relative size of the pharyngeal plates, the head of the specimens was sectioned through the frontal plane to expose the inside of the oropharyngeal cavity. The dorsal (palatal) and ventral inner surfaces of the oropharyngeal cavity were photographed with a digital camera (Nikon D300, Thailand). Relative size of the pharyngeal plates was calculated as the ratio of the area of the pharyngeal plates to the frontal sectional area of the dorsal or ventral surface of the oropharyngeal cavity. The posterior limit of the oropharyngeal cavity was defined at the level of the esophagus opening. The software ImageJ (version 1.51j8, National Institutes of Health, USA) was used to measure the areas.

To study the skeletal morphology, the dissected branchial baskets were double-stained for cartilages and bones. Cartilages were stained with Alcian Blue 8GX (SIGMA-ALDRICH, Co., India) in a 4:1 solution of 95% ethanol: 99% acetic acid while the bones were stained with Alizarin Red S (Wako Pure Chemical Industries, Ltd., Japan) in a solution of 1% potassium hydroxide (Taylor and Van Dyke 1985). Subsequently, the baskets were cleared by immersion in a solution of 35% borate sodium and trypsin (Dingerkus and Uhler 1977). The cleared specimens were dissected to remove all membranes and soft tissues. The skeleton was photographed and traced with the software Inkscape 0.92.3 (Free Software Foundation, Boston, USA). Disarticulated bones were photographed and measured for the lengths with ImageJ. The measurements were made

following the guidance of Morales and Rosenlund (1979). Due to the bifurcated morphology of the first and third epibranchials, and the L-shape of the fourth epibranchial, their lengths were determined as shown in Fig. 7b. The lever ratio of jaw-closing is calculated by dividing the length of in-lever closing by the length of out-lever (Westneat 2003; Nanami 2016), where the length of in-lever-closing was defined as the distance between the quadrate/articular joint to the distal end of the insertion of the adductor mandibulae A2 on the coronoid process (Fig. II-3b). The length of out-lever was defined as the distance between the quadrate/articular joint to the tip of the lower jaw (Westneat 1994). The specimens used for studying muscular anatomy and dentition were double-stained but not cleared. The opercula were carefully removed to expose the branchial basket and musculature. Both muscular system and dentition were studied by dissection, photographing and tracing.

Scanning electron microscopy

The surface morphology of the pharyngeal plates was studied by scanning electron microscopy (SEM). The dissected pharyngeal plates were dehydrated through a series of ethanol solutions from 50% to 100%, treated with Hexamethyldisilizane (HMDS, Alfa Aesar, Germany) through several steps (a 1:1 solution of HMDS: 100% ethanol; 100% HMDS; and 100% HMDS) for 20 minutes in each step, and dried in a fume hood (Kashi et al. 2014). The dried samples were Palladium coated with an auto fine coater (JFC-1600, JEOL, Tokyo, Japan), and observed with a scanning electron microscope (JSM-6380 LAKII, JEOL, Tokyo, Japan).

Micro-computed tomography scanning

The dissected branchial baskets were stained with a 0.05 mol/L Iodine Solution (FUJIFILM Wako Pure Chemical Corporation, Japan) for about 12 hours and observed with an X-ray CT scanner (ScanXmate B100TSS110, Comscantecno, Kanagawa, Japan) at a tube voltage of 100 kV and a

tube current of 88 μA. Image analysis was done using software Molcer (version 1.3.6.1, WhiteRabbit, Tokyo, Japan). The resolution was 10.127 μm.

Statistical analysis

Numbers of teeth and replacement teeth, tooth length, and tooth width were compared between the premaxilla and dentary using paired t-test. One-way ANOVA was applied to compare the lengths of gill arch bones, followed by post-hoc Tukey test for pairwise comparison. Rstudio version 0.99.903 (Rstudio, Inc) was used for statistical analysis.

III. Results

Dentition

On the premaxilla, there is only a single row of canine teeth, which are directed vertically. Four frontal pairs are larger while the others dwindle posteriorly (Figs. II-1a and II-1c). On the dentary, a single row of teeth is present on the margin, which are directed horizontally. In addition, a pair of fang-like, vertically oriented teeth occur internally to the symphysis of the dentary (Figs. II-1d and II-1f). Five frontal pairs of the marginal teeth on the dentary are canine but slightly blunt while the others are incisors, flattened and enlarged on the cusps (Figs. II-2b and II-2d). The cross-section of the cusps is slightly tilted posteriorly such that the anterior edge of the posteriorly adjacent teeth occasionally overlaps (Figs. II-2b and II-2d). There are approximately 66 teeth on the premaxilla and 75 teeth on the dentary (Table II-1). The tooth attachment is of type 2 as categorized by Fink (1981) with a ring-like structure between the tooth and the attachment bone (Figs. II-2a and II-2b). Number of teeth and replacement teeth, and tooth length are significantly different between the premaxilla and dentary (Table II-1). The replacement begins on the ventral and labial sides of the dentary and the premaxilla, respectively, and moves closer to the functional teeth with growth (Figs. II-2c and II-2d) which is common in teleosts (Trapani 2001).

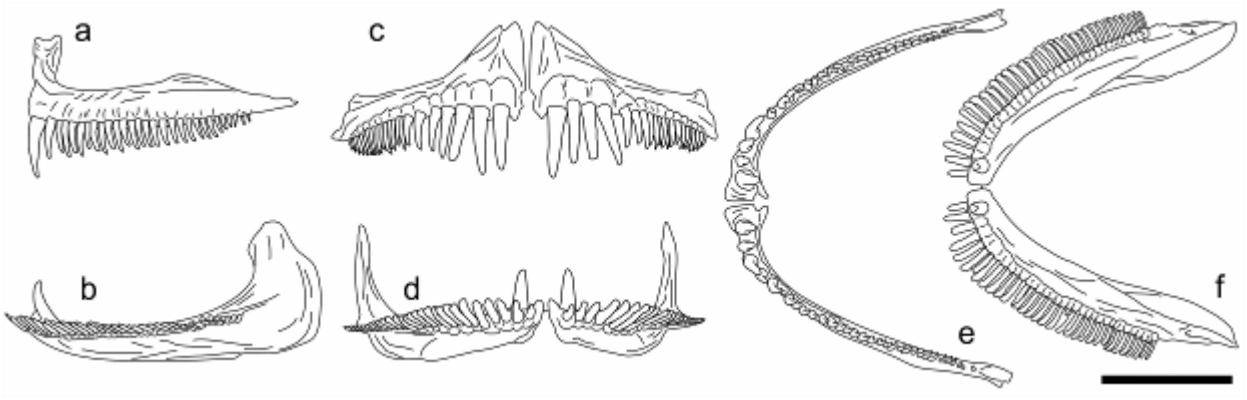

Fig. II-1 Dentition morphology of *Boleophthalmus pectinirostris*. **a** Premaxilla in lateral view. **b** Dentary in lateral view. **c** Premaxilla in frontal view. **d** Dentary in frontal view. **e** Premaxilla in ventral view. **f** Dentary in the dorsal view. Scale bar: 5 mm

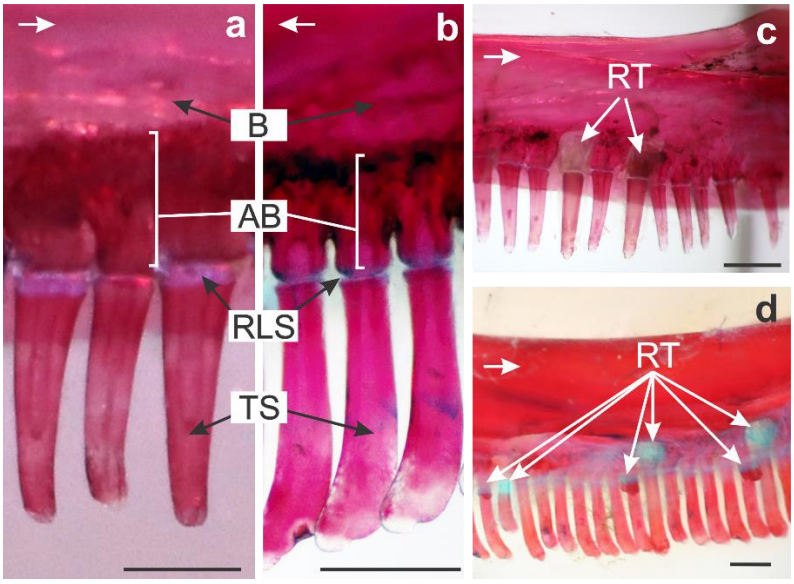

Fig. II-2 Tooth attachment and replacement of *Boleophthalmus pectinirostris*. **a** Tooth attachment on the left side of the premaxilla (lateral view) and **b** dentary (dorsal view). **c** Tooth replacement on the right side of the premaxilla (lateral view) and the dentary **d** (ventral view). Symbols: *B* bone, *AB* attachment bone, *TS* tooth shalf, *RT* replacement tooth, *RLS* ring-like structure. Arrows on the upper left of each photo show the anterior direction. Scale bars: 0.5 mm

Oral jaw bones and muscles

Boleophthalmus pectinirostris possesses the maxilla-mandibular ligament (L1) linking the maxilla with the dentary and the premaxillo-maxillary ligament (L2) linking the premaxilla with the maxilla (Fig. II-3a). The adductors mandibulae A1, A2, and A3 attach onto the maxilla, the coronoid process o the dentary, and the medial side of the dentary, respectively, as in other teleosts (Fig. II-3b). The lever ratio of jaw-closing is 0.3 ± 0.03 (mean ± SD, N = 3).

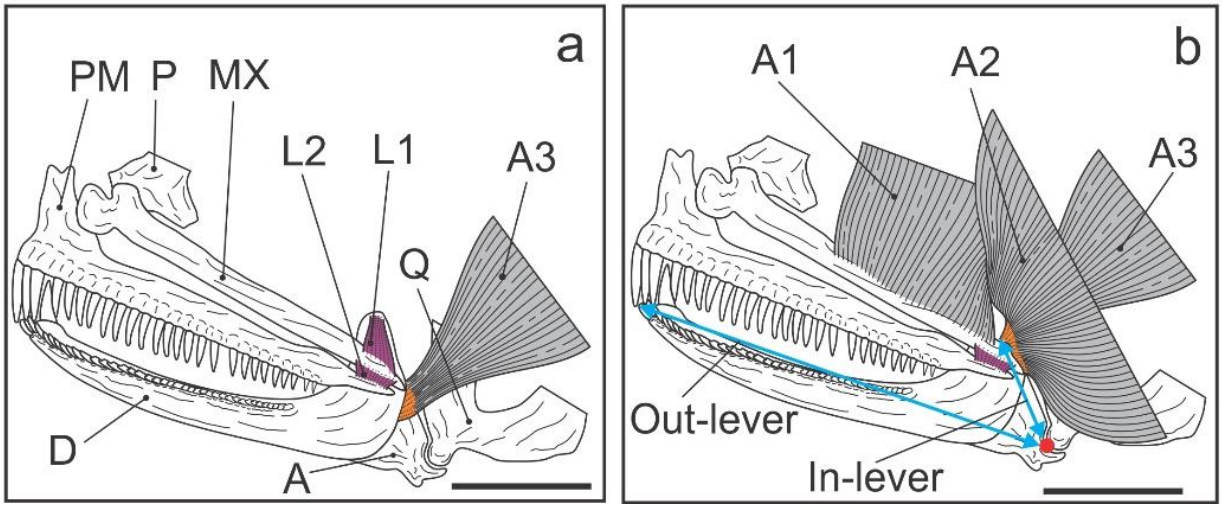

Fig. II-3 Jaw bones (**a**) and muscular system (**b**) of *Boleophthalmus pectinirostris. A* articular, *A1-3* adductor mandibulae 1 to 3, *D* dentary, *L1, 2* ligament 1 and 2, *MX* maxilla, *P* palatine, *PM* premaxilla, *Q* quadrate. Ligaments are shown in purple and tendons are in orange. In **b**, red dot shows the fulcrum, and double arrowheads show the jaw closing lever system. Scale bars: 5 mm

Table II-1 Dentition of *Boleophthalmus pectinirostris*

	Premaxilla	Dentary
Number of teeth	66.4 ± 5.8	74.6 ± 3.2
Number of replacement teeth	2.7 ± 1.1	9.6 ± 2.8
Tooth length (mm)	0.73 ± 0.2	0.96 ± 0.15
Tooth width (at the base) (mm)	0.21 ± 0.04	0.18 ± 0.03
Cusp width (mm)	-	0.26 ± 0.04

The data are significantly different between premaxilla and dentary for number of teeth (p = 0.009), number of replacement teeth (p = 0.001), and tooth length (p = 0.0002, paired t-test). Numbers of teeth represent the values on both sides and replacement teeth are for the left side only. Mean ± SD (N = 7). The data on tooth length and width do not include fangs.

Gill arches

The branchial basket of *B. pectinirostris* comprises four pairs of gill arches with two rows of the gill rakers along each arch. The gill rakers on the first, second and the anterior row of the third arches are short and sparsely spaced. In contrast, the posterior row of the third and the two rows of the fourth arch are comb-like and more densely spaced (Figs. II-4 and II-5a). Accordingly, the spaces between the gill rakers are far smaller on these rows (Fig. II-5b). The gill rakers extend laterally from the inner surface (facing the oropharyngeal cavity) of gill arches along their entire

lengths (Fig. II-4d). Each raker blade has a morphology of a triangular plate, not a filiform morphology as in many filter-feeding fishes. The dorsal sides of the anterior and posterior rows of the fourth arch form a gently curved concave line facing the oropharyngeal cavity (Fig. II-4dIV).

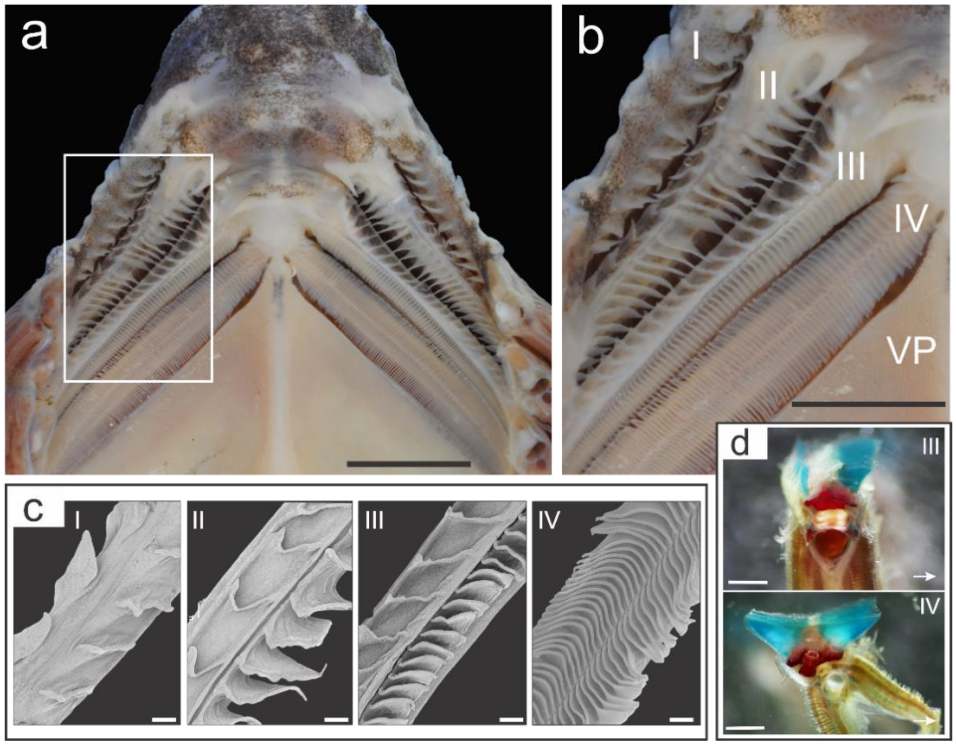

Fig. II-4 The dorsal views of the frontal section of the head of *B. pectinirostris* showing the floor of the oropharyngeal cavity **a**. **b** Enlarged view of the box in **a**. **c** SEM images of each arch. **d** Cross-sectional views of the third and fourth arches, double stained (blue, gill raker blades). Symbols: *I-IV* first to fourth gill arches, *VP* ventral pharyngeal plate. Arrows on the bottom right of photos in **d** show the posteromedial direction. Scale bars: 2 mm for **a**, **b**; 200 μm for **c**; and 500 μm for **d**

Pharyngeal plates

Boleophthalmus pectinirostris possesses a pair of pharyngeal plates on both the dorsal (Fig. II-6a) and ventral (Fig. II-6e) surfaces of the pharynx. The two dorsal pharyngeal plates are convex while the ventral ones are concave (Fig. II-9). The surface areas of the dorsal and ventral pharyngeal plates occupy 19.1 ± 1.5% and 22.8 ± 1.9% (mean ± SD, N = 6) of the dorsal and ventral inner surface areas of the oropharyngeal cavity, respectively. The dorsal pharyngeal plates have a single row of large canine teeth on the anterior margin with the distance of 10-20 μm between them (Fig. II-6b) but are otherwise studded with finer teeth posteriomedially directed, and not arranged in regular rows (Figs. II-6c and II-6d). The teeth on the ventral pharyngeal plates have a large cusp, are hooked and arranged in anteroposteriorly directed rows (Figs. II-6f and II-6g). The teeth densities (numbers/μm^2) were 355 ± 27 and 494 ± 149 (mean ± SD, N = 3) for the dorsal and

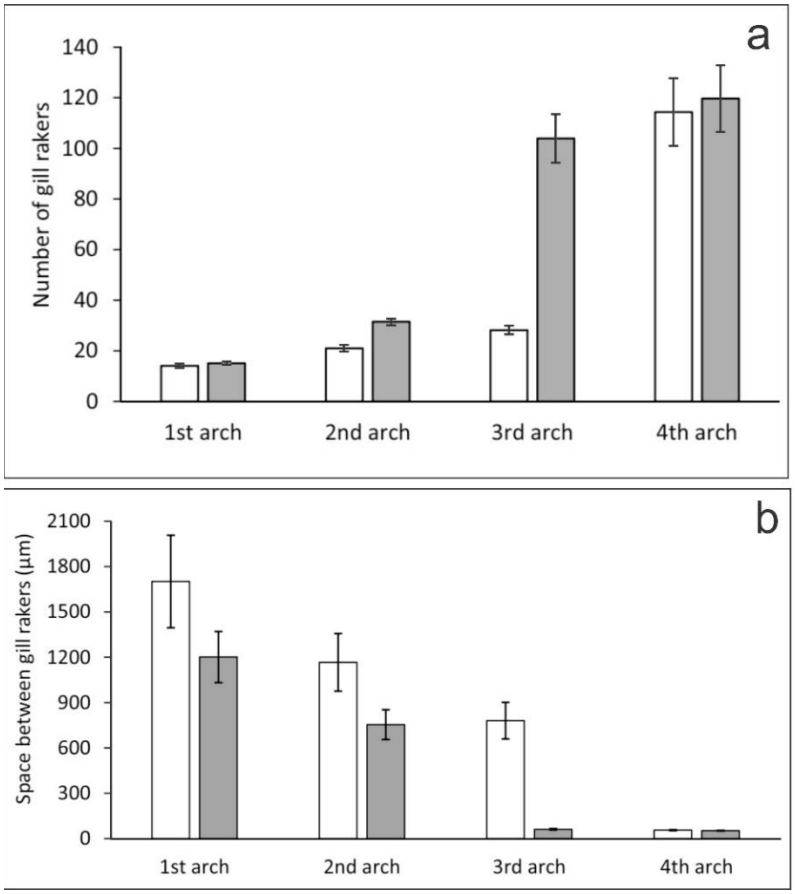

Fig. II-5 Number of gill rakers (mean ± SD, N = 12) (**a**) and average space between them (**b**) (mean ± SD, N = 7) of *Boleophthalmus pectinirostris*. Blank bars show the anterior rows; grey bars show the posterior rows. Size range of fishes: 81.5 - 141.0 mm SL in **a**, and 132.0 - 144.0 mm SL in **b**.

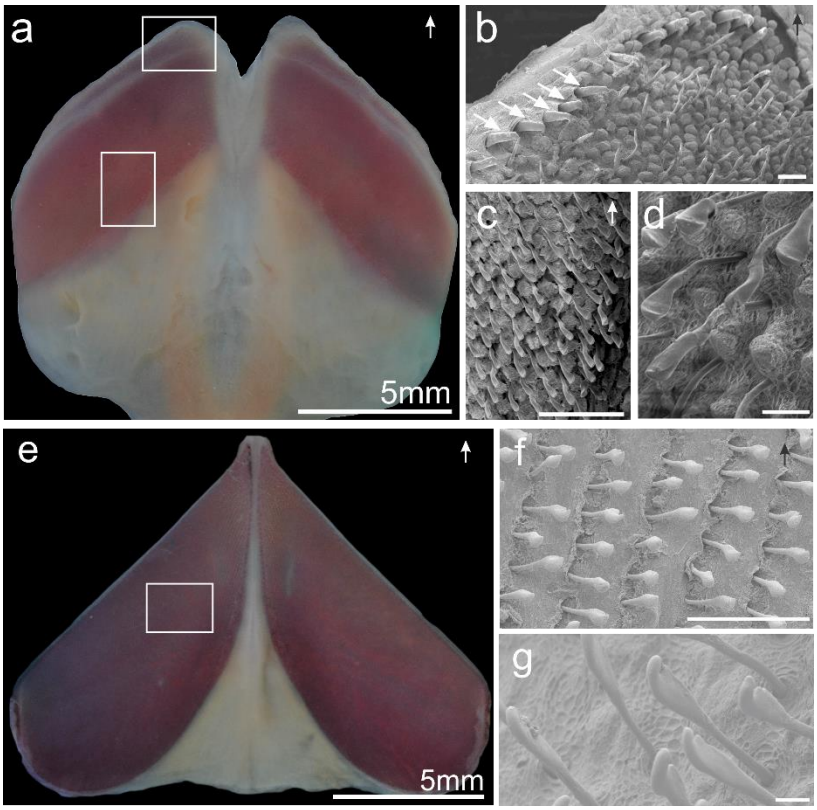

Fig. II-6 Pharyngeal plate morphology of *Boleophthalmus pectinirostris*. Dorsal and ventral pharyngeal plates at different magnifications (**a-d**; **e-f**, respectively). **a** Ventral view of the dorsal pharyngeal plate (stained). **b** Enlarged (SEM) view of the upper box in **a**, showing a line of canine teeth on the marginal edge of the right dorsal pharyngeal plate (white arrows). **c** Enlarged (SEM) view of the lower box in **a**, showing the direction of finer teeth. **d** Tooth-head morphology of the dorsal pharyngeal plate. **e** Dorsal view of the ventral pharyngeal plate (stained). **f** Enlarged (SEM) view of the box in **e**. **g** Tooth-head morphology of the ventral pharyngeal plate. Arrows on the upper right of **a**, **b**, **c**, **e**, and **f** show anterior direction. Scale bars: 100 µm for **b**, **c**, **f**; and 20 µm for **d**, **g**

ventral pharyngeal plates, respectively.

Branchial basket skeleton

The branchial basket skeleton of *B. pectinirostris* comprises five pairs of branchial arches. The first arch consists of the median basibranchial (BB1is not shown in Fig. II-7), the hypobranchial (HB1), the ceratobranchial (CB1) and the epibranchial (EB1). The second and third arches have an additional pharyngobranchial (PB2, PB3) while the fourth arch is formed by basibranchial (BB4), the ceratobranchial (CB4), the epibranchial (EB4) and the pharyngobranchial (PB4) (Fig. II-7). The fifth arch comprises only the ceratobranchial (CB5), i.e. ventral pharyngeal plate. The basihyal (BH) is bifurcated located in anterior of HB1s. The PB 2, 3 and 4 form the dorsal pharyngeal plate; PB2 is slender and lie along the anterior margin of PB3 and PB4, while PB3 and PB4 are broader, overlapped, and in a mediolateral position (Fig. II-7a). The dorsal and ventral pharyngeal plates are curvature and perfectly fit each other (Fig. II-9). EB4 is L-shaped and broad at the medial tip while EB3 is Y-shaped, both articulating with the pharyngobranchials of the same arch, i.e., the dorsal pharyngeal plate. The lengths of HB and CB are significantly different between all arch (Table II-2), while the lengths of EB3 and EB4 are significantly longer than EB1 and EB2, which are not significantly different from each other. As a result, the total length of the fourth arch is significantly longer than the first and third arches.

Branchial basket musculature

The branchial basket musculature of *B. pectinirostris* consists of two main systems. One connects the branchial basket to the surrounding skeletal components. The levatores interni (LI), the levatores externi (LE), and the levator posterior (LP) connect to the neurocranium; the retractor dorsalis (RD) connects to the anterior of the fourth vertebra; the ligament 4 (L4) connect to the post-temporal; the pharyngohyoideus (PH) connects to the urohyal; and the rectus ventrales (RV),

the pharyngocleithralis externus (PHCE), and the pharyngocleithralis internus (PHCI) to the cleithrum (Fig. II-8a). The other system links bones within the branchial basket (Figs. II-8b, II-8c, and II-8d); the transversi dorsales anteriores (TDA), the tranversi dorsales posteriores (TDP), the obliqui dorsales (OD), the ligaments connecting the third and fourth epibranchials (L3-4) and the cartilaginous-cushion-like structure (CC) on the dorsal side (Figs. II-8b, 9II-a, and II-9b); the transversi ventrales (TV), the obliqui ventralises (OV) and the semicular ligament (SL) on the ventral side (Fig. II-8c); and the first to fifth adductors (AD1-5) on the lateral side (Figs. II-8d, II-9c, and II-9d). The most prominent structure in the branchial basket musculature relates to EB4. L4 originates from the corner of the L-shaped EB4 and attaches posteriorly to a post-temporal. LE4 arises from the articulation between EB4 and CB4 and inclines anteriorly, while LP originates in between the attachment of the L4 and LE4. AD5 connects EB4 and CB5 on both dorsal and ventral sides of CB5.

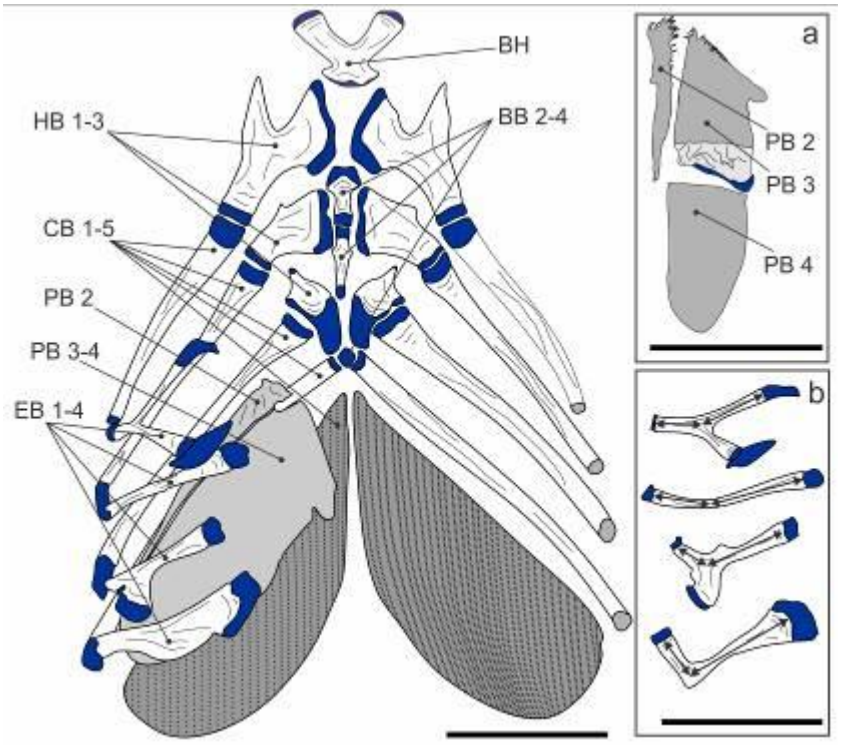

Fig. II-7 Morphology of the branchial basket skeleton (dorsal view) of *B. pectinirostris*. The dorsal pharyngeal plate consists of the second, third and fourth pharyngobranchials; the second pharyngobranchial is separated, and the third and the fourth pharyngobranchials are overlaped. **a** Right dorsal pharyngeal plate with the pharyngobranchials dissected separately; the portion of the third pharyngobranchial covered by the fourth pharyngobranchial is illustrated (light grey). **b** Right epibranchials in ventral view dissected separately. Lengths of epibranchials were determined as shown here. Symbols: *BB 2-4* basibranchials 2 to 4, *BH* basihyal, *CB 1-5* ceratobranchials 1 to 5, *EB 1-4* epibranchials 1 to 4, *HB 1-3* hypobranchials 1 to 3, *PB 2,3,4* pharyngobranchials 2,3,4. BB1 is a small cartilage between the right and left HB1s, therefore not shown. Scale bars: 5 mm

Table II-2 Comparison of the lengths (mean ± SD, mm) of component bones and the total length of the branchial arches in *Boleophthalmus pectinirostris*

Gill arch	Hypobranchial	Ceratobranchial	Epibranchial	Total
Arch 1	5.3 ± 0.4^{a}	9.0 ± 0.8^{a}	5.6 ± 0.4^{a}	19.9 ± 1.4^{a}
Arch 2	3.8 ± 0.3^{b}	10.6 ± 1.0^{b}	5.8 ± 0.4^{a}	20.2 ± 1.6^{ab}
Arch 3	2.5 ± 0.2^{c}	12.3 ± 1.0^{c}	4.9 ± 0.4^{b}	19.4 ± 2.2^{a}
Arch 4	-	15.4 ± 1.2^{d}	7.2 ± 0.5^{c}	22.5 ± 1.7^{b}
One-way ANOVA				
F	136.7	53.3	35.0	4.43
p	<0.001	<0.001	<0.001	0.013

One-way ANOVA was applied to detect significant difference among arches, followed by post-hoc Tukey test for pairwise comparison. The data with different letters in respective columns are significantly different ($p < 0.05$, $N = 7$)

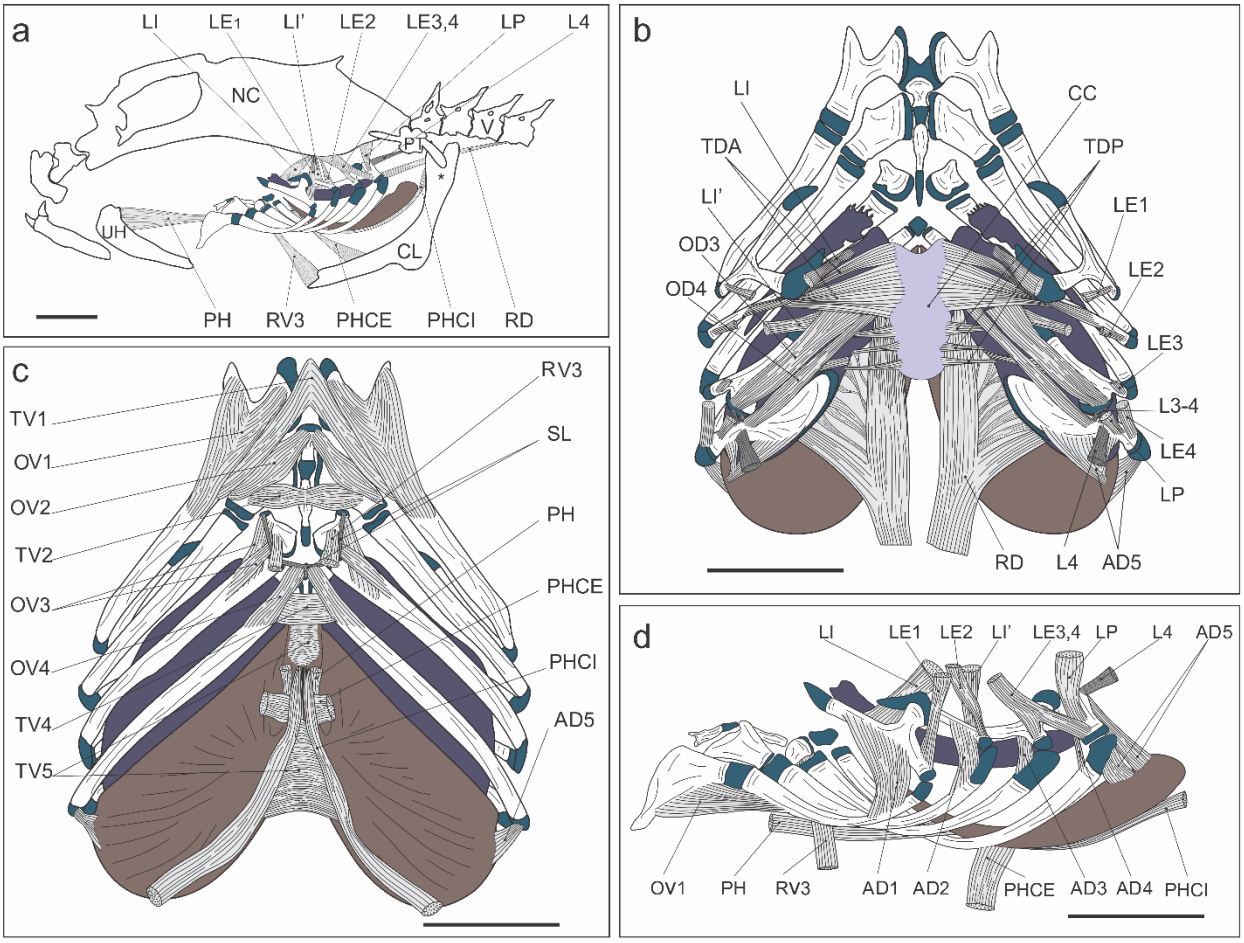

Fig. II-8 Branchial basket musculature of *B. pectinirostris*. **a** Lateral view of external branchial musculature suspending the branchial basket in the oropharyngeal cavity. **b** Dorsal view of the internal musculature of the branchial basket. **c** Ventral view of the internal musculature of the branchial basket. **d** Lateral view of the internal musculature

of the branchial basket. Symbols: *AD1-5* adductors 1 to 5, *CC* cartilaginous cushion, *LE1-4* levatores externi 1 to 4, *LI* levator internus, *LP* levator posterior, *L3-4, 4* ligament 3-4, and ligament 4, *NC* neurocranium, *OD3-4* obliqui dorsales 3 to 4, *OV1-4* obliqui ventrales 1 to 4, *PH* pharyngohyoideus, *PHCE* pharyngocleithralis externus, *PHCI* pharyngocleithralis internus, *PT* post-temporal, *RD* retractor dorsalis, *RV3* rectus ventralis 3, *SL* semicircular ligament, *TDA* transversus dorsalis anterior, *TDP* transversus dorsalis posterior, *TV1, 2, 4, 5* tranversi ventrales 1, 2, 4, and 5, *UH* urohyal, *V* vertebrae, * supracleithrum. Cartilages in blue; dorsal pharyngeal plate in dark purple; ventral pharyngeal plate in brown. Scale bars: 5 mm

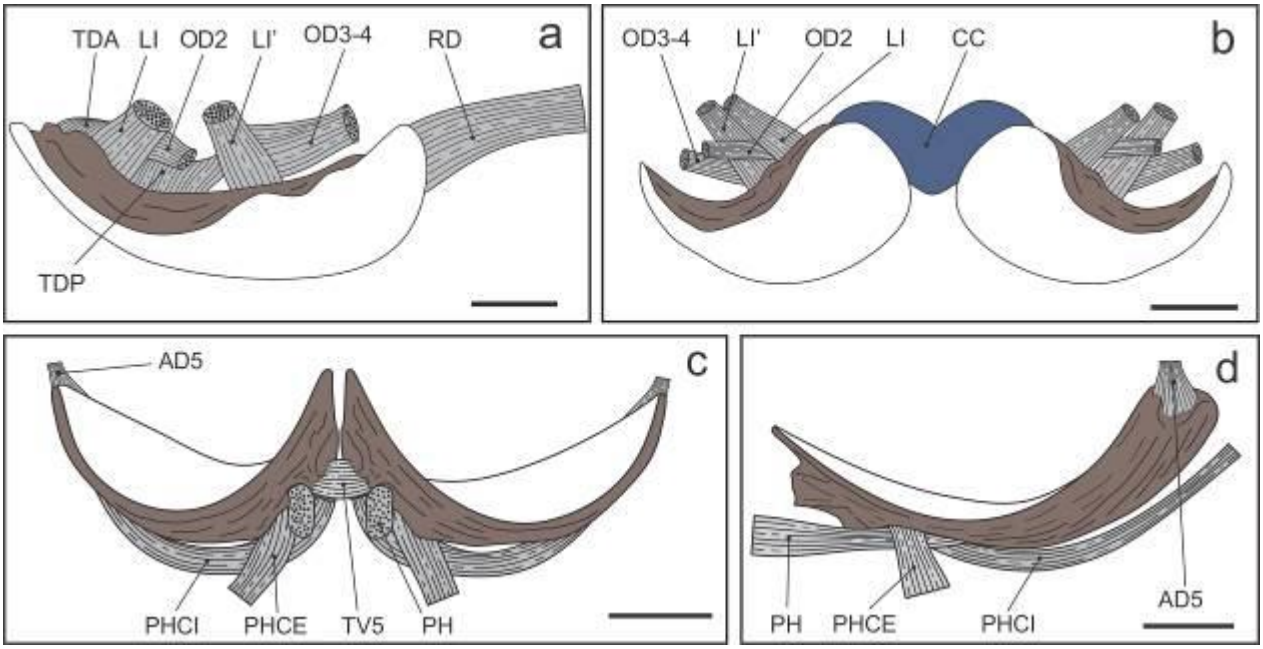

Fig. II-9 Morphology of musculature system attaching to the pharyngeal plates of *B. pectinirostris*. **a** lateral views of the left dorsal pharyngealplate, **b** and **c** frontal views of the dorsal and ventral pharyngeal plates, respectively,and **d** lateral views of the left ventral pharyngeal plate. Symbols are the same as in Fig. 8. The ventral side of the ventral pharyngeal plates and the dorsal side of the dorsal pharyngeal plates are colored in brown. Scale bars: 2 mm

IV. Discussion

The feeding cycle in vertebrates comprises five phases, capture, ingestion, intraoral transport, processing, and swallowing. One or more phases may be skipped or modified (Schwenk and Rubega 2005). A feeding bout of *B. pectinirostris* always starts with sucking a mouthful of water from a burrow or a nearby water pool within its territory (Tran et al., unbpublished observation). Although the fish infrequently fed in shallow water, they mostly fed on the exposed mudflat surface, at least in our study site. As the fish starts grazing, it swings the head from side to side rapidly, stops head swinging, gurgles by rapidly vibrating the buccal and opercular cavities, and finally

expels muddy water through the gill slits and returns to a water source. Since the distribution of epipelic diatoms, the predominant food source of *B. pectinirostris*, is restricted to a thin superficial layer of mud (Aleem 1950; Koh et al. 2006, 2007), the fish needs to skim the very top layer of the sediment to avoid excessive contamination by mud. The fish further needs to effectively separate diatom cells from mud particles. Each feeding bout takes place with a mouthful of water, and therefore somewhat resembles pump filtration of some aquatic fishes in which food particles are ingested sporadically by a series of suction created by expansion of the buccal and opercular cavities while a fish is stationary, but unlike ram filtration, in which a large volume of water continuously passes through the buccal cavity while a fish is swimming with mouth agape and opercles flaring (Gerking 1994).

Functional morphology of the feeding apparatus in *Boleophthalmus pectinirostris*

Our anatomical analysis revealed unique anatomical features of the feeding apparatus in *B. pectinirostris*, which may represent morphological adaptations to terrestrial feeding. Videos of feeding fishes in front view showed that the fish tilted the head by an angle of 17 ± 3.3^0 (N = 88) between the lower jaw and the mud surface (Fig. II-10). This tilting probably aligns the flattened, incised and partly overlapped dentary teeth (Fig. II-1) at a very shallow angle with the mud surface, thus scraping off a thin superficial layer, rich in diatom cells.

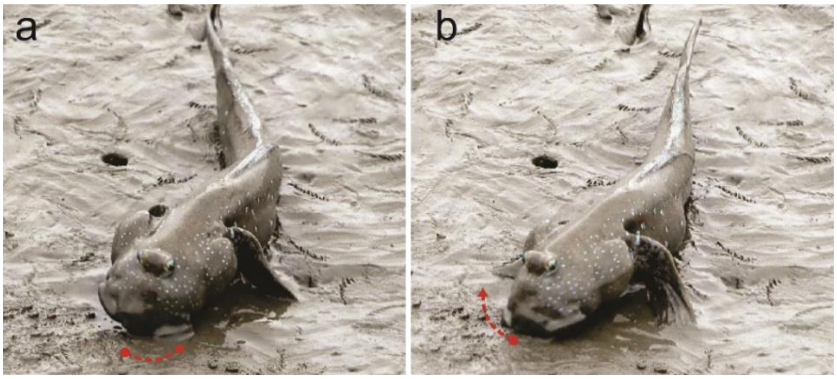

Fig. II-10 Head tilting of *Boleophthalmus pectinirostris* during foraging in their natural habitat (the Ariake Sea, Japan). The head is inclined to the side of the sweeping movement, bringing the dentary teeth of that side in contact with the substrate, thus skimming the mud surface. **a** Head tilting to the left. **b** Head tilting to the right. The dashed line arrow shows the direction of the head sweeping. Images were obtained from a video footage

The gill rakers in pelagic filter-feeding fishes usually extend anteriorly, and are most numerous and longest on the first arch (Iwata 1976; Gibson 1988; Salman et al. 2005); this can be interpreted as an adaptation to trap food particles suspended in water, flowing from the mouth to the gill opening (Berry and Low 1970; Munshi et al. 1984; Cohen and Hernandez 2018). In contrast, the gill rakers of *B. pectinirostris* extend laterally, most evidently on the fourth gill arch (Fig. II-4d), and their density is much higher on the three most posterior rows (Fig. II-5). The lengths of the fourth gill arches are longer than the more anterior ones (Table II-2), which serves for bearing more gill rakers and thereby increasing filtering area. The average space between the gill rakers on the posterior three rows (56.6 ± 3.8 μm) is far smaller than the size of six dominant diatom species recovered from the alimentary tract of *B. pectinirostris* (*Gyrosigma cf. gibbyi*, *G. cf. wansbeckii*, *G. fasciola var. fasciola*, *Navicula sp*., *Nitzschia sp*., and *Pleurosigma sterrenburgii*), whose longer axis length ranges from 189.7 ± 26.2 to 1396.4 ± 408.7 μm (N = 5), and whose shorter axis length (SAL) ranges from 65.3 ± 11.2 to 187.2 ± 14.1 μm, except for *Navicula sp*. (SAL 37.0 ± 10.7 μm) and *Gyrosigma cf. wansbeckii* (SAL 51.0 ± 14.7 μm, N = 5, Tran et al., unpublished data). Towards the end of a feeding bout, muddy water is expelled from the gill opening while the fish is on land. The third and fourth gill arches are located dorsal to the gill opening, possibly forming a device sieving the particles transported by the gravitational flow of exhalant water. The average size of mud particles in the same study area is 7.3 ± 0.5 μm (Ishimatsu et al. 2007), only 13% of the average space between the gill rakers.

The pharyngeal plates are large and bear numerous fine teeth arranging in either posteromedial (dorsal plate) or anteroposterior (ventral plate) directions (Fig. II-6). The resting position of the anterior margin of the dorsal pharyngeal plates aligns with the posterior margin of the third gill arch at its lateral portion (Fig. II-11). In addition, the combination of the L-shape of the shaft and flattened end of the tip of the fourth epibranchial, moved by the levator muscles (LE4,

LP and L4) (Figs. II-7 and II-8) could facilitate anteroposterior and dorsoventral motions of the dorsal pharyngeal plates (Wainwright 2006). We hypothesize that these anatomical arrangements function to transport diatom cells trapped on the gill rakers of the posterior two gill arches to the esophagus. The canine teeth on the anterior margin of the dorsal pharyngeal plates (Fig. II-6b) would help scraping off diatoms trapped on the gill rakers of the three posterior rows. We further hypothesize that the transversi ventrales and the obliqui ventrales 1, 2, and 3 could lift the anterior part of the branchial basket to seal the buccal cavity during gurgling, which might explain the large cross-sectional area of these muscles (Tran et al., personal observation).

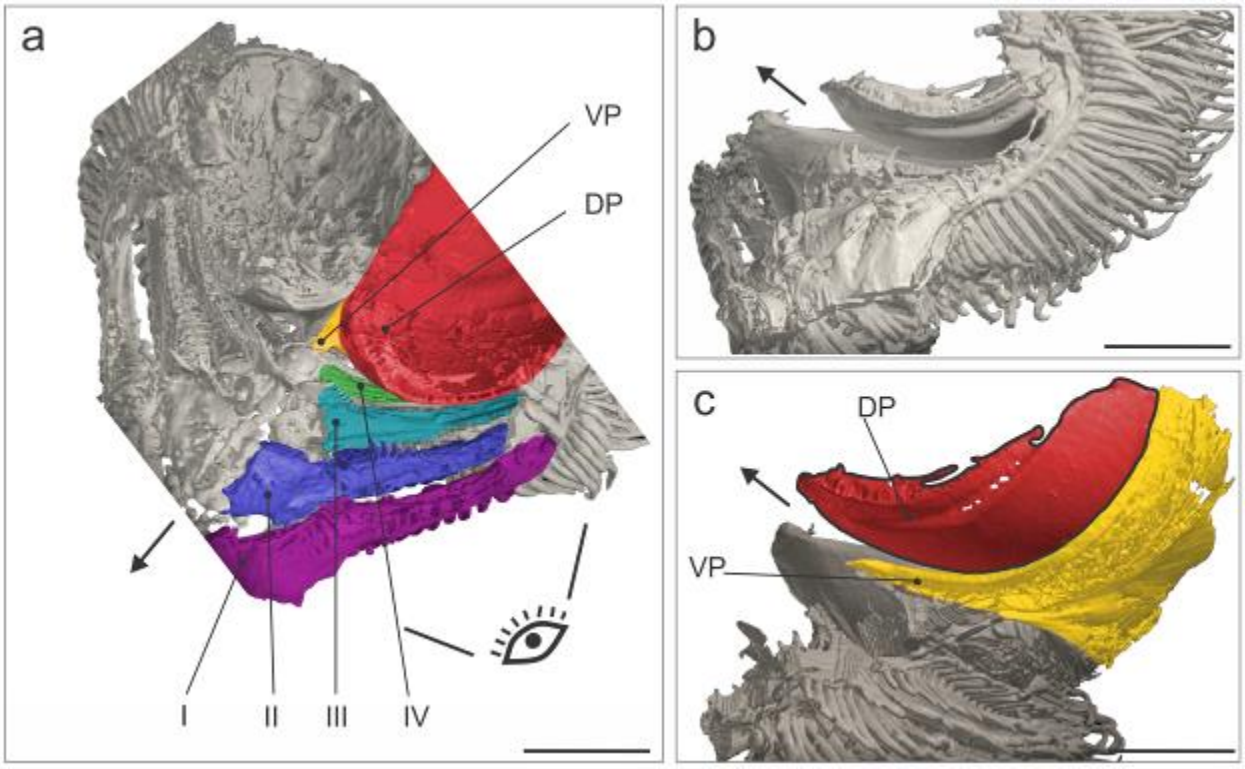

Fig. II-11 Micro-CT scanning images to show the relative position of pharyngeal plates and branchial arches of *Boleophthalmus pectinirostris*. **a** Dorsal view of the branchial basket. **b** The lateroventral view from the anterior left branchial basket (eye view in **a**). **c** The branchial basket in **b** with the left arches removed to expose the portion of the dorsal pharyngeal plate positioned above the left third and fourth arches (red). Arrows shows the head direction. Symbols: *I-IV* first to fourth arches, *DP* dorsal pharyngeal plate, *VP* ventral pharyngeal plate. Scale bars: 5 mm.

Comparison of the feeding apparatus between *B. pectinirostris* and other fishes

Comparisons between the feeding apparatus of *B. pectinirostris* with other teleosts can provide further insight into its morphofunctional characteristics. Both *Plecoglossus altivelis* (Temminck & Schlegel, 1846) (Tachihara and Kimura 1991; Katano et al. 2004), and *Sicyopterus japonicus* (Tanaka, 1909) (Dôtu and Mito 1955; Iida et al. 2010, 2015) are amphidromous species, and when living in rivers, they graze on encrusting algae. *P. altivelis* (Plecoglossidae) possesses groups of diagonally arranged comb-like teeth on the lateral sides of both the premaxilla and dentary (Uehara and Miyoshi 1993). *S. japonicus* (Gobiidae, Sicydiinae) has a single row of tricuspid, shovel-like teeth on the premaxilla, and horizontally directed, rod-shaped teeth along the entire length of the dentary (Mochizuki and Fukui 1983; Sahara et al. 2013; Sakai and Nakamura 1979). Two other sicydiine species, *Lentipes armatus* Sakai and Nakamura, 1979, and *Stiphodon elegans* (Steindachner, 1879), also show a similar dentition, consisting of vertically disposed tricuspid teeth on the premaxilla, and horizontally disposed teeth on the dentary (Sakai and Nakamura 1979). The three sicydiine gobies were all observed to feed on algae growing on the glass wall of aquaria. Therefore, we tentatively conclude that a combination of horizontally disposed teeth on the dentary and vertically disposed teeth on the premaxilla is an adaptation to grazing algae on the substate surface, widespread among oxudercine and sicydiine gobies.

The teeth attachment and replacement patterns are also related to more specific aspects of the feeding habits. In species scraping off encrusting, epilithic algae (growing on stones or rocks), teeth are easily worn so that the frequency of tooth replacement is usually higher compared to species grazing on softer substrates. For example, *S. japonicus*, which feeds on epilithic algae, possesses one functional tooth row and more than 23 rows of replacement teeth which are replaced every 9.2 days (Mochizuki and Fukui 1983). In contrast, there are four to five replacement rows in *P. altivelis* (Howes 1987), and two to four rows in Loricariid fishes (Geerinckx et al. 2007). Mullets

(Mugilidae) show a wide range in the number of replacement teeth from one to more than 30, possibly depending upon different feeding habits (Ebeling 1957). In terms of tooth attachment, teeth attach loosely and are bendable in species scraping on uneven hard surfaces (*S. japonicus*, Sahara et al. 2013; Loricarids, Delariva and Agostinho 2001; Geerinckx et al. 2007) but they attach more firmly in those species grazing on softer surfaces (*Mugil cephalus* Linnaeus, 1758; *Mugil curema* Valenciennes, 1836; Thomson 1954; Ebeling 1957). We found that the teeth attached firmly through a ring-like structure but were yet slightly bendable in *B. pectinirostris*, which could prevent breakage during feeding. The low frequency of tooth replacement on the dentary (Table II-1) may be related to relatively low degrees of wearing while feeding on soft, fine sediments.

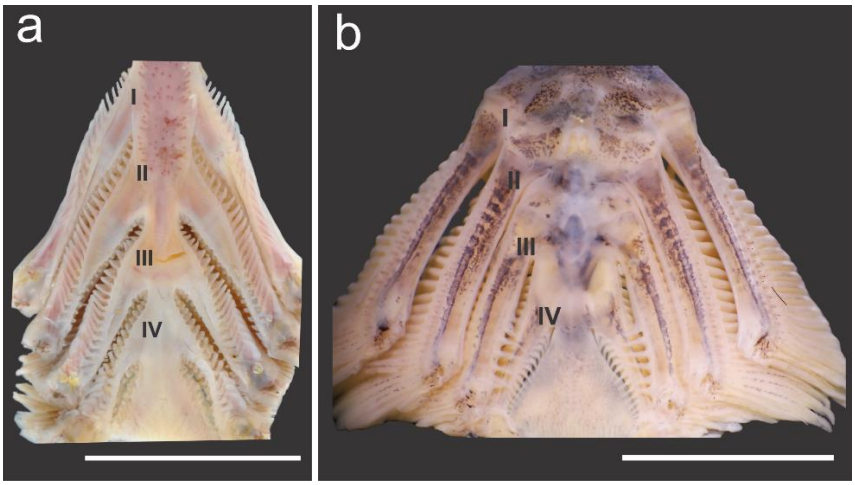

Fig. II-12 Frontal section of the branchial basket of *Plecoglossus altivelis* (**a**) and *Sicyopterus japonicus* (**b**). Symbols: *I-IV* first to fourth gill arches. Scale bars: 5 mm

Compared with *B. pectinirostris*, the gill rakers of *P. altivelis* and *S. japonicus* show a much lesser extent of modification (Fig. II-12). *Plecoglossus altivelis* possesses sparsely spaced, forward facing gill rakers (Fig. II-12a). *Sicyopterus japonicus* has low-density gill rakers, distributed only on the posterior margins of the third and the fourth arches. The first and second gill arches lack gill rakers. The gill rakers on the third and the fourth arches extend laterally from the inner (facing the oropharyngeal cavity) surface of the gill arches but at much lower density than that in *B. pectinirostris* (Fig. II-12b). Both *P. altivelis* and *S. japonicus* feed entirely in water, and they both graze algae off hard substrates. In such conditions, there may be lesser degrees of food

contamination in the oropharyngeal cavity, and therefore less need for separation of food and other particles. To the best of our knowledge, no other fish has gill rakers that have dorsally directed, laterally extending blades, and are most developed on the third and fourth gill arches, as we have found in *B. pectinirostris*. This unique morphology appears to be an adaptation to effectively separate food particles from suspended fine sediments inside the mouth, while the fish feeds out of water.

With respect to the morphology of the pharyngeal plates, *P. altivelis* lacks any teeth on the pharyngobranchials or on the fifth ceratobranchials (Chapman 1941), whereas *S. japonicus* has papiliform teeth on both the dorsal and ventral pharyngeal plates (Tran et al., unpublished observation). The relative surface areas of pharyngeal plates to the dorsal and ventral inner surface areas of the oropharyngeal cavity are much smaller in these two species; the ratios of the dorsal and ventral pharyngeal plates are 4.0 ± 0.4% and 1.3 ± 0.1% respectively (mean ± SD, N = 3) in *P. altivelis*, and 6.3 ± 1.5% and 4.0 ± 0.7% respectively (mean ± SD, N = 4) in *S. japonicus* (Tran et al., unpublished data). The morphology of the gill rakers and pharyngeal plates of several species of Mugilidae (e.g., *M. curema*, *M. cephalus*) shows some similarities with that of *B. pectinirostris*. In these unrelated species, each branchial arch possesses a series of densely packed gill rakers. The gill rakers on the posterior row of the fourth arch form a concave floor, while the prolonged and laterally fused rakers limits the water flow between them. The dorsal pharyngeal plates are covered with a dense arrangement of pharyngeal teeth (Thomson 1954), while the ventral pharyngeal plates are covered with a single series of lamellae, and possess gill rakers on their anterior margins (Günther 1880). Interestingly, these species also share similar feeding behaviors; several mullets (e.g., *M. curema, M. cephalus*) swim with their head down and sweep it from side to side skimming the surface of soft sediment deposits (Jordan 1905; Hiatt 1947).

In conclusion, the feeding apparatus of *B. pectinirostris* is interpreted as an adaptation for grazing on microalgae flourishing on emerged soft sediment deposits. Even though the fish has developed the ability to emerge on land for extended periods (Clayton 1993), the intertidal feeding grounds of *B. pectinirostris* must be in the proximity of the water's edge, due to the need of water during the feeding process.

Chapter III

MORPHOLOGICAL COMPARISION OF THE FEEDING APPARATUS IN THE MUDSKIPPERS: *Boleophthalmus boddarti, Oxuderces nexipinnis, Scartelaos histophorus, Periophthalmus chrysospilos,* AND *Periophthalmodon schlosseri*

1. Introduction

The majority of aquatic vertebrates including fish use suction feeding (Wainwright et al. 2015). In this type of feeding, water and prey are drawn into the mouth cavity by negative pressure generated by the sudden expansion of the cavity. Suction feeding relies on the high density and viscosity of water, and therefore is effective only in water but not on land (Liem 1990; Norton and Brainerd 1993). In contrast, terrestrial vertebrates typically employ teeth on jaws to capture prey and the tongue to transport it into the esophagus (Schwenk and Rubega 2005). As exceptions to this general rule, a small number of fish species have evolved the capacity to capture prey on land. A variety of strategies are used by these fishes to place the oral jaws above prey, a key factor of prey prehension in terrestrial environment (Heiss et al. 2018). For example, *Channallabes apus* (Günther, 1873) and *Erpetoichthys calabaricus* Smith, 1865 lift the anterior part of their elongate body, incline the head downward, and place the mouth on prey (Van Wassenbergh 2013; Van Wassenbergh et al. 2016). *Anableps anableps* (Linnaeus, 1758) and *Periophthalmus barbarus* (Linnaeus, 1766) rotate the dentary to a large angle and protrude the premaxilla for orientating the gape towards the ground (Michel et al. 2014, 2015a, b). The pectoral fins are used to lift the head and anterior trunk in *P. barbarus* enabling the oral jaws to be placed on prey (Sponder and Lauder 1981; Michel et al. 2014). These are macrophagous, carnivorous fishes that are highly adapted to terrestrial environment, and we have little knowledge about how the feeding system of aquatic fish has transitioned during their habitat expansion to land.

Oxudercine gobies show a full spectrum of transition from aquatic to terrestrial mode of life, and include herbivorous, omnivorous, and carnivorous species that feed at the water's

edge and higher in the intertidal zone (Clayton 1993, 2017). In the present study, we chose five mudskippers (*Boleophthalmus boddarti* (Pallas, 1770), *Oxuderces nexipinnis* (Cantor, 1849), *Scartelaos histophorus* (Valenciennes, 1837), *Periophthalmus chrysospilos* Bleeker, 1853, and *Periophthalmodon schlosseri* (Pallas, 1770)) for morphological comparisons of the dentition, the gill rakers, and the skeletal and muscular systems of the branchial basket. These species also represent three types of feeding habits and occur at different microhabitats in the intertidal mudflat. *B. boddarti* and *O. nexipinnis* are herbivorous (but Chaudhuri et al. (2014) reported omnivory in *O. nexipinnis*; note the fish was reported as *O. dentatus* but the study site, India, indicates it is *O. nexipinnis*), *S. histophorus* is omnivorous, and *Ps. chrysospilos* and *Pn. schlosseri* are carnivorous. *O. nexipinnis* spends most of their time in shallow tidal pools, *B. boddarti* and *S. histophorus* inhabits moderately terrestrial environments, and *Ps. chrysospilos* and *Pn. schlosseri* occupy the most terrestrial habitats (Fig. I-1 and Table S1).

2. Materials and methods

Sample collection and preservation

A total of 210 individuals of the five species were collected at Mo O mudflat (9° 26’ 15”N, 106° 10’ 57”E; Tran De District, Soc Trang Province, Vietnam) in September 2017, December 2017 and June 2018 by using traps and by hands. The number and size range of specimens used are shown in Table III-1. The species were sacrificed by immersing in a solution of 2-Phenoxyethanol (Wako Pure Chemical Industries, Japan) at a concentration of 100 mL/L and preserved in 10% neutralized formalin for a week. Then they were rinsed with tap water overnight and preserved in 75% ethanol.

Morphological methods

The methods used in this study were the same as reported in the Chapter 2 with slight modifications accrued from the use of five species with different body size. Tooth length and tooth width were standardized by dividing them by the standard length. The spaces between the gill rakers were measured for the entire length of four arches in *S. histophorus*, *Ps. chrysospilos*,

and *Pn. schlosseri*. In *B. boddarti* and *O. nexipinnis*, the spaces between the gill rakers were measured over the entire length of the arches only for both rows of the first and second arches, and for the anterior row of the third arch. The spaces between the gill rakers of the posterior row of the third arch and both rows of the fourth arch were estimated by measuring five spaces on the ventral, middle and dorsal segments because of the large number of gill rakers in these rows. The relative size of the pharyngeal plates was determined by sectioning the head of the specimens through the frontal plane, and calculated as the ratio of the area of pharyngeal plates to the frontal sectional area of the dorsal or ventral surface of the oropharyngeal cavity. The posterior limit of the oropharyngeal cavity was defined as the level of the esophageal sphincter at the back of the cavity. The skeletal morphology was studied using specimens stained with Alcian Blue for cartilages and with Alizarin Red S for the bones. Subsequently, the branchial baskets were cleared by immersion in a solution of 35% sodium borate and trypsin (Dingerkus and Uhler 1977). The measurements were made following Morales and Rosenlund (1979, see Fig. III-10a2 for the measurement of the length of the epibranchials). We define the arch length as the sum of the lengths of component bones in a gill arch, except basibranchials. The lever ratio of jaw-closing was calculated same as description in the Chapter 2 (Figs. III-2a2 and III-2b2). The adductor mandibulae A2 were dissected from fixed specimens and weighed. The data were standardized as $K = (W/L^3) \times 10^6$ (W, weight of A2 (g); L, standard length (cm)). The specimens used for studying muscular anatomy and dentition were double-stained but not cleared. The opercula were carefully removed to expose the branchial basket and musculature.

The surface morphology of the pharyngeal plates and the gill rakers was observed with a scanning electron microscope (JSM-6380 LAKII, JEOL, Tokyo, Japan) as reported by Tran et al. (2020). The dissected branchial baskets of the five species were stained with a 0.05 mol/L Iodine Solution (FUJIFILM Wako Pure Chemical Corporation, Japan) for about 12 h and observed with an X-ray CT scanner at a tube voltage of 100kV and a tube current of 100 μA. Image analysis was done using software Molcer (version 1.3.6.1, WhiteRabbit, Tokyo, Japan).

The size of food items ingested was measured only for *B. boddarti*, *O. nexipinnis*, and *S. histophorus* to compare with the gill raker space. Ingested food items were recovered from their stomach and observed with a fluorescence microscope (Olympus BX50). The five main food items were determined by frequency occurrence. The longer-axis and shorter-axis lengths of each food item were measured with the software ImageJ (version 1.51J8, National Institutes of Health, USA).

Table III-1 Number and standard length (mm) of the five mudskippers used in this study

Species	Number of fish used for morphological analysis	Number of fish used for stomach content analysis	Standard length
Boleophthalmus boddarti	47	3	92 – 153
Oxuderces nexipinnis	45	3	78 – 116
Scartelaos histophorus	46	3	70 – 104
Periophthalmus chrysospilos	34	–	59 – 96
Periophthalmodon schlosseri	29	–	122 – 226

Statistical analysis

Numbers of teeth, replacement teeth, standardized tooth length, standardized tooth width, the lengths of gill arch bones, and the relative size of the pharyngeal plates were tested for the normality (Shapiro-Wilk test) and the homogeneity of variance (Levene's test). Based on results, one-way ANOVA followed by post-hoc Turkey test (data satisfied normal distribution and equal variance), one-way ANOVA followed by post-hoc Welch test (data satisfied normal distribution but un-equal variance) or Kruskal-Wallis followed by Wilcoxon-Mann-Whitney test (data unsatisfied normal distribution) were performed. All pairwise comparisons were performed with Bonferroni correction of p-value. Principal component analysis (PCA) on correlation was performed for the dentition morphometrics to examine divergence among the species. Rstudio version 0.99.903 (Rstudio, Inc) was used for all statistical analysis.

3. Results

Dentition

Boleophthalmus boddarti, *O. nexipinnis*, *S. histophorus*, and *Ps. chrysospilos* have a single row of vertically oriented canine teeth on the premaxilla (Figs. III-1a, III-1b, III-1c, and III-1d). *Periophthalmodon schlosseri* has an additional row on the premaxilla (Fig. III-1e). Frontal teeth (three pairs in *B. boddarti*, two in *O. nexipinnis*, seven to ten in *S. histophorus* and five in *Pn. schlosseri*) are large and fang-like, while the remaining teeth are smaller and dwindle posteriorly. Teeth in *O. nexipinnis* are sparse. On the dentary, a single row of teeth occurs along the margin in all the species. Dentary teeth extend horizontally in *B. boddarti*, *O. nexipinnis*, and *S. histophorus*, but vertically in *Ps. chrysospilos* and *Pn. schlosseri*. In *B. boddarti*, dentary teeth are incisors, flattened and enlarged on the cusps, but canine in the other species. *B. boddarti* and *S. histophorus* possess a pair of fang-like teeth, medially to the symphysis of the dentaries (Figs. III-1a and III-1c). Cartilaginous finger-like projections extend laterally along the posterior margin of the dentary in *O. nexipinnis* (Fig. III-1b). There are significant differences in the number of teeth, replacement teeth, standardized tooth length and standardized tooth width among species (Table III-2). *B. boddarti* has the highest number of teeth on both the premaxilla and dentary, whereas *O. nexipinnis* has the lowest. In both jaws, the number of replacement teeth is higher in *Ps. chrysospilos* and *Pn. schlosseri* than in the other species, except for the dentary of *B. boddarti*. PCA clearly separates three groups of species in the morphometric multivariate space. The first two components (PC1, PC2) explain 84.6% of total variance (Fig. III-3). Along PC1, *B. boddarti* is separated from the other species by smaller values of standardized tooth length and tooth width on both the premaxilla and the dentary, and a larger number of teeth on the dentary. Along PC2, *Oxuderces nexipinnis* and *S. histophorus* are separated from the other species by smaller numbers of replacement teeth on the premaxilla and the dentary, and by smaller numbers of teeth on the premaxilla (Fig. III-3).

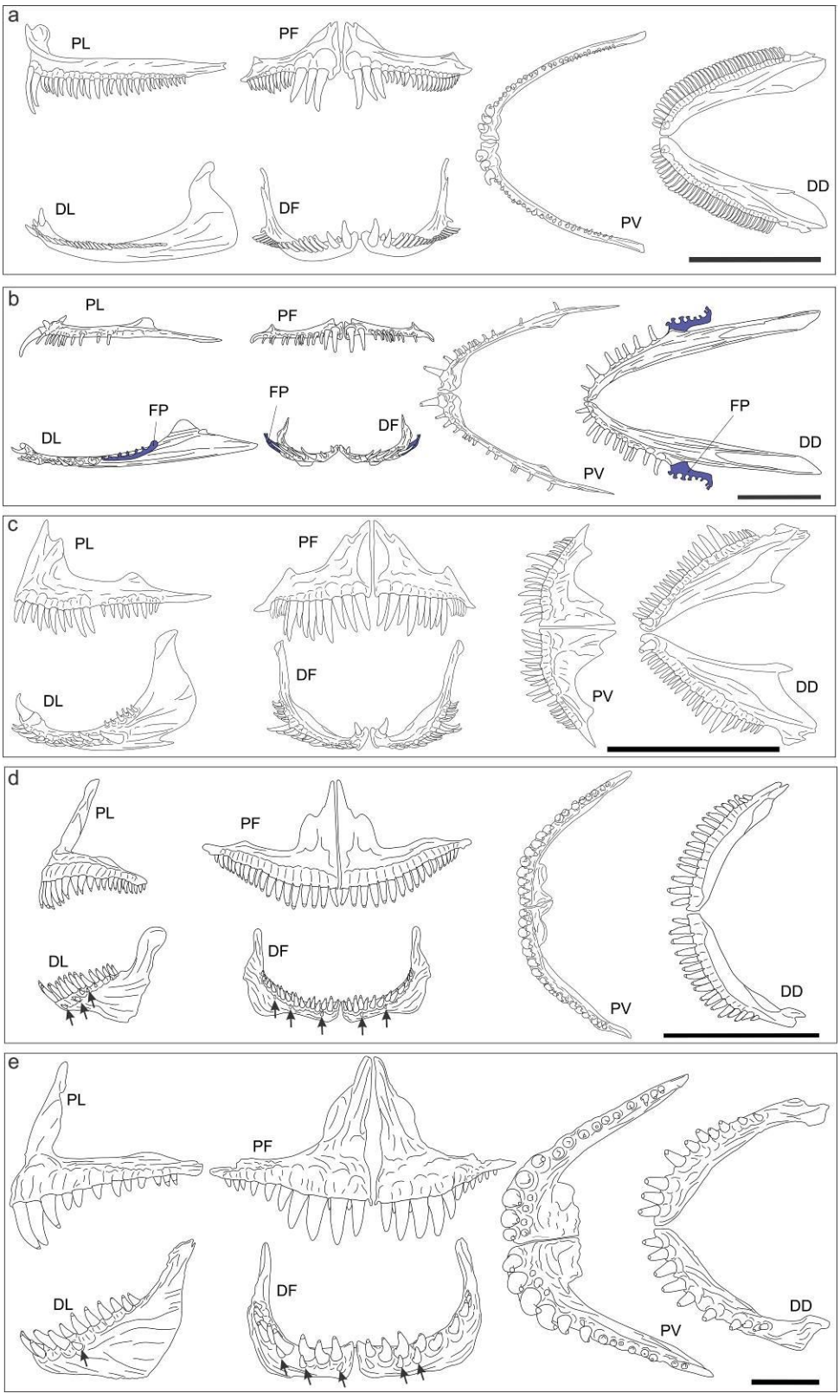

Fig. III-1
Dentition morphology of *Boleophthalmus boddarti* (**a**), *Oxuderces nexipinnis* (**b**), *Scartelaos histophorus* (**c**), *Periophthalmus chrysospilos* (**d**), and *Periophthalmodon schlosseri* (**e**). *DD* dentary in dorsal view, *DF* dentary in frontal view, *DL* dentary in lateral view, *FP* finger-like projection, *PF* premaxilla in frontal view, *PL* premaxilla in lateral view, and *PV* premaxilla in ventral view. Arrows indicate replacement teeth. Scale bars: 5mm

Table III-2 Dentition of the five mudskippers

Species	Premaxilla				Dentary				
	Number of teeth	Number of replacement teeth	Standardized tooth length	Standardized tooth width	Number of teeth	Number of replacement teeth	Standardized tooth length	Standardized tooth width	Cusp width (mm)
Boleophthalmus boddarti	65.6 ± 5.1[a]	3.4 ± 1.7[a]	0.0059 ± 0.0006[a]	0.0020 ± 0.0004[a]	78.8 ± 2.8[a]	6.6 ± 1.1[a]	0.0016 ± 0.0002[a]	0.002 ± 0.0002[a]	0.22 ± 0.02
Oxuderces nexipinnis	26.4 ± 5.8[b]	2.8 ± 0.8[a]	0.0090 ± 0.0008[a]	0.0029 ± 0.0003[b]	25.2 ± 2.3[b]	2.6 ± 0.6[b]	0.0115 ±0.0005[b]	0.0033 ± 0.0004[a]	-
Scartelaos histophorus	29.0 ± 2.9[b]	3.0 ± 0.7[a]	0.0111 ± 0.0007[ab]	0.0030 ± 0.0003[b]	43.2 ± 1.6[c]	3.0 ± 0.7[b]	0.0081 ± 0.0003[b]	0.0024 ± 0.0003[a]	-
Periophthalmus chrysospilos	39.4 ± 3.1[c]	7.6 ± 0.6[b]	0.0093 ± 0.001[ab]	0.0031 ± 0.0005[b]	39.0 ± 4.4[c]	8.8 ± 0.8[ac]	0.01 ± 0.002[b]	0.0031 ± 0.0006[a]	-
Periophthalmodon schlosseri	44.8 ± 2.3[d]	8.6 ± 0.9[b]	0.011 ± 0.003[b]	0.005 ± 0.001[c]	28.6 ± 1.5[b]	7.8 ± 1.3[c]	0.011 ± 0.003[b]	0.005 ± 0.001[b]	-
One-way ANOVA or Kruskal-Wallis									
F or Chi-squared	21.8	18.6	10.4	18.2	21.9	20.2	17.6	20.3	
p	< 0.001	< 0.001	< 0.001	0.0011	< 0.001	< 0.001	0.0015	< 0.001	

Numbers of teeth represent the values of both sides and replacement teeth are for the left side only (Mean ± SD, N = 5). One-way ANOVA followed by post-hoc Tukey test was applied for standardized tooth length on the premaxilla. Kruskal-Wallis followed by Wilcoxon-Mann-Whitney test was applied for the remaining parameters. All pairwise comparisons were performed with Bonferroni correction of p-value. The data with different letters in respective columns are significantly different ($p < 0.05$). The data on tooth length and width do not include fangs. Tooth length and tooth width were standardized by the standard length. Tooth width was measured at the base. Cusp width is defined as the widest distance of the tooth tips from dorsal view.

Oral jaw bones and muscles

The lever ratio of jaw-closing is 0.31 ± 0.01 (mean ± SD, N = 3 for all species) in *B. boddarti*, 0.42 ± 0.01 in *O. nexipinnis*, 0.41 ± 0.01 in *S. histophorus*, 0.50 ± 0.04 in *Ps. chrysospilos*, and 0.58 ± 0.08 in *Pn. schlosseri*. All the five species possess the maxilla-mandibular ligament (L1) linking the maxilla with the dentary and the premaxillo-maxillary ligament (L2) linking the premaxilla with the maxilla (Fig. III-2). The adductores mandibulae A1, A2 and A3 attach onto the maxilla, the coronoid process of the dentary, and the medial side of the dentary, respectively, as in other teleosts. K values were 64.6 ± 11.5 (g cm^{-3} × 10^{-6}, N = 3) in *B. boddarti*, 78.1 ± 15.1 (N = 4) in *O. nexipinnis*, 41.2 ± 10.6 (N = 3) in *S. histophorus*, 126.9 ± 22.5 (N = 3) in *Ps. chrysospilos*, and 93.6 ± 9.3 (N = 2) in *Pn. schlosseri*.

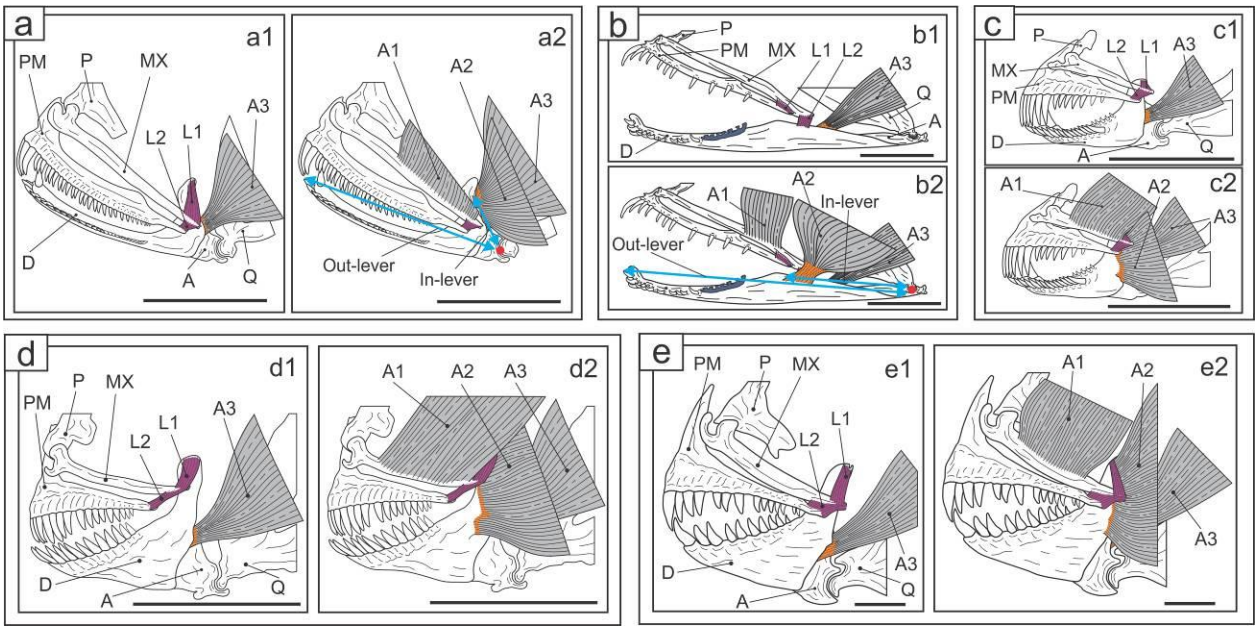

Fig. III-2 Jaw bones and ligaments in *Boleophthalmus boddarti* (**a1**), *Oxuderces nexipinnis* (**b1**), *Scartelaos histophorus* (**c1**), *Periophthalmus chrysospilos* (**d1**), and *Periophthalmodon schlosseri* (**e1**), and adductor mandibulae in *Boleophthalmus boddarti* (**a2**), *Oxuderces nexipinnis* (**b2**), *Scartelaos histophorus* (**c2**), *Periophthalmus chrysospilos* (**d2**), and *Periophthalmodon schlosseri* (**e2**). *A* articular, *A1-3* adductor mandibulae 1 to 3, *D* dentary, *L1, 2* ligament 1 and 2, *MX* maxilla, *P* palatine, *PM* premaxilla, *Q* quadrate. Ligaments are shown in purple and tendons are in orange. In **a2** and **b2**, red dot shows the fulcrum, and double arrowheads show the jaw-closing lever system. Scale bars: 5 mm

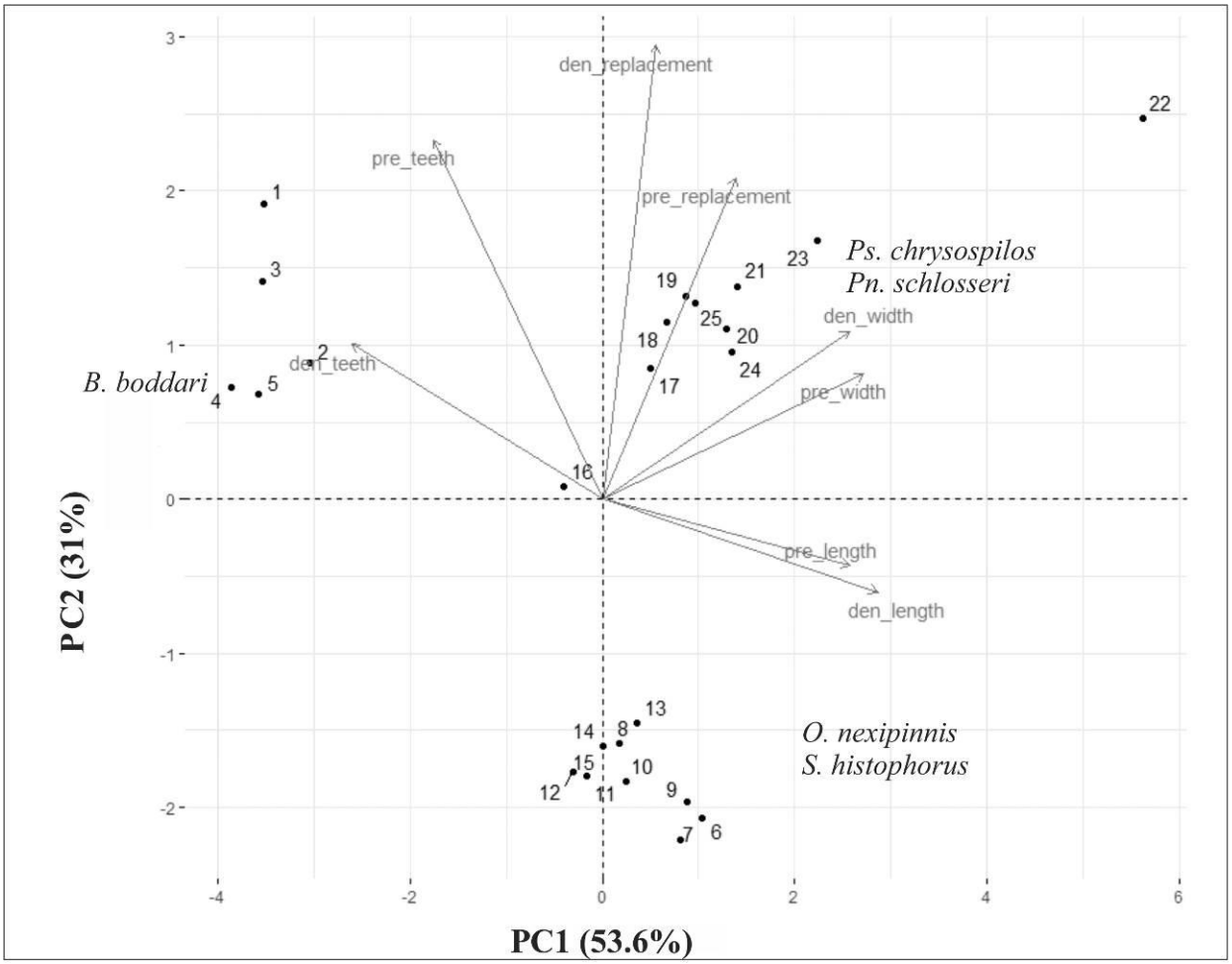

	PC 1	PC 2
pre_teeth	-0.57	0.76
pre_replacement	0.45	0.68
pre_length	0.84	-0.14
pre_width	0.89	0.26
den_teeth	-0.85	0.33
den_replacement	0.18	0.96
den_length	0.94	-0.2
den_width	0.84	0.36

Fig. III-3 PCA biplot of the two principal components (PC1, PC2) showing the multivariate morphometric ordination of the studied taxa (upper box). The morphological variables are represented by vectors; correlated variables have a similar orientation. Loadings of each variable along PC1 and PC2 are shown in the lower table. Symbols: *den_length* standardized tooth length on the dentary, *den_replacement* number of replacement teeth on the dentary, *den_teeth* number of teeth on the dentary, *den_width* standardized tooth width on the dentary, *Dim 1 – Dim 5* dimension 1 to 5, *pre_length* standardized tooth length on the premaxilla, *pre_replacement* number of replacement teeth on the premaxilla, *pre_teeth* number of teeth on the premaxilla, *pre_width* standardized tooth width on the premaxilla. Points 1-5 are the data of *Boleophthalmus boddarti*, 6-10 *Oxuderces nexipinnis*, 11-15 *Scartelaos histophorus*, 16-20 *Periophthalmus chrysospilos*, and 21-25 *Periophthalmodon schlosseri*.

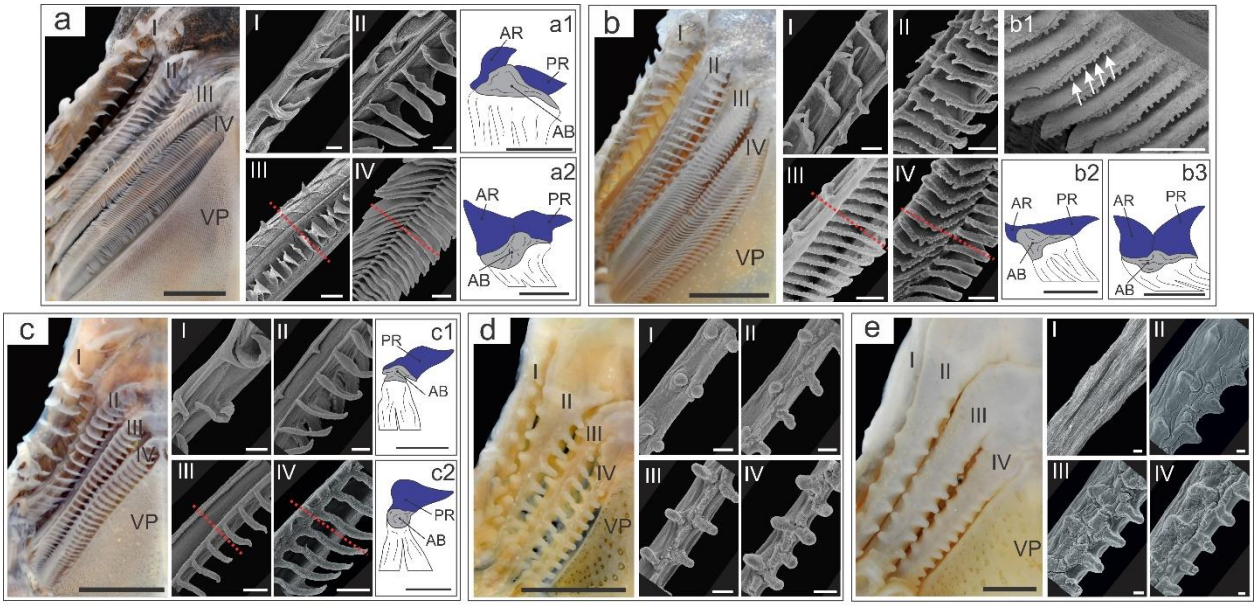

Fig. III-4 Morphology of the gill rakers in *Boleophthalmus boddarti* (**a**), *Oxuderces nexipinnis* (**b**), *Scartelaos histophorus* (**c**), *Periophthalmus chrysospilos* (**d**), and *Periophthalmodon schlosseri* (**e**). In each box, the left photograph shows the dorsal view of the left gill arches, and the right ones are SEM micrographs of each gill arch. The red dashed lines in the SEM micrographs indicate the position of cross-sectioning. The arrows in **b1** indicates the secondary gill rakers. *AB* arch bone, *AR* anterior row, *I-IV* first to fourth gill arches, *PR* posterior row and *VP* ventral pharyngeal plate. Scale bars: 2 mm for the photographs, 200 μm for SEM micrographs, and 0.5 mm for **a1**, **a2**, **b2**, **b3**, **c1**, and **c2**

Gill rakers

All the mudskipper species possess four pairs of gill arches. The disposition of the gill rakers can be classified into three types. In the first type seen in *B. boddarti* and *O. nexipinnis*, the gill rakers are short and sparsely spaced on the first, second and the anterior row of the third arch, while they are comb-like and more densely spaced on the posterior row of the third arch and both rows of the fourth arch (Figs. III-4a, III-4b, III-5, and III-6). The gill rakers extend laterally from the inner surface (facing the oropharyngeal cavity) of gill arches along their entire lengths. Each gill raker blade has a triangular shape in cross-section (Figs. III-4a1, III-4a2, III-4b2, and III-4b3). In the second type observed in *S. histophorus*, the gill rakers are present on the posterior rows of all the gill arches, with an increasingly higher density from the first to fourth arches (Figs. III-4c and III-5), while on the anterior rows the gill rakers are sparse on the first and second arches and absent

on the third and fourth arches (Figs. III-4c, III-5, and III-6). Each gill raker blade on the third and fourth arches has a triangular shape in cross-section (Figs. III-4c1 and III-4c2). In the third type observed in *Ps. chrysospilos* and *Pn. schlosseri*, the gill rakers are short, knob-like, and widely spaced (Figs. III-4d, III-4e, III-5, and III-6). There are no gill rakers on the first arch of *Pn. schlosseri*.

We measured the longer-axis length (LAL) and the shorter-axis length (SAL) of the dominant diatom/amphipod species recovered from the stomachs of *B. boddarti*, *O. nexipinni*s, and *S. histophorus*, and compared them with average space between gill rakers (GRS). The GRS of *B. boddarti* is smaller than the LAL of five dominant diatom species. The GRS is smaller than the SAL of two, nearly equal to the SAL of the other two, and larger than the SAL of the remaining species (Fig. III-7a). The GRS of *O. nexipinnis* is smaller than the LAL but larger than the SAL of four, but smaller than the SAL of the remaining diatom species (Fig. III-7b). The GRS of *S. histophorus* is smaller than the LAL and the SAL of two abundant amphipod species, and smaller than the LAL but larger than the SAL of three diatom species (Fig. III-7c).

Pharyngeal plates

All the five species have a pair of pharyngeal plates on both the dorsal and ventral surfaces of the pharynx, which can also be classified into three types. The first type observed in *B. boddarti* and *O. nexipinnis* is characterized by its large size (Figs. III-8a, III-8b, and III-9) and strong curvature (Figs. III-12a and III-12b). The third and fourth pharyngobranchials (PB3 and PB4) overlap to form one large unit of the dorsal pharyngeal plate (Figs. III-10a1 and III-10b1). Both dorsal and ventral pharyngeal plates bear numerous fine papilliform teeth, being directed posteromedially (Figs. III-8a2, III-8a3, III-8b1, and III-8b3, Table III-3). The teeth on the ventral plates have a large cusp, are arranged in lines, and are hook-like (Figs. III-8a4 and III-8b4). There is a single row of large

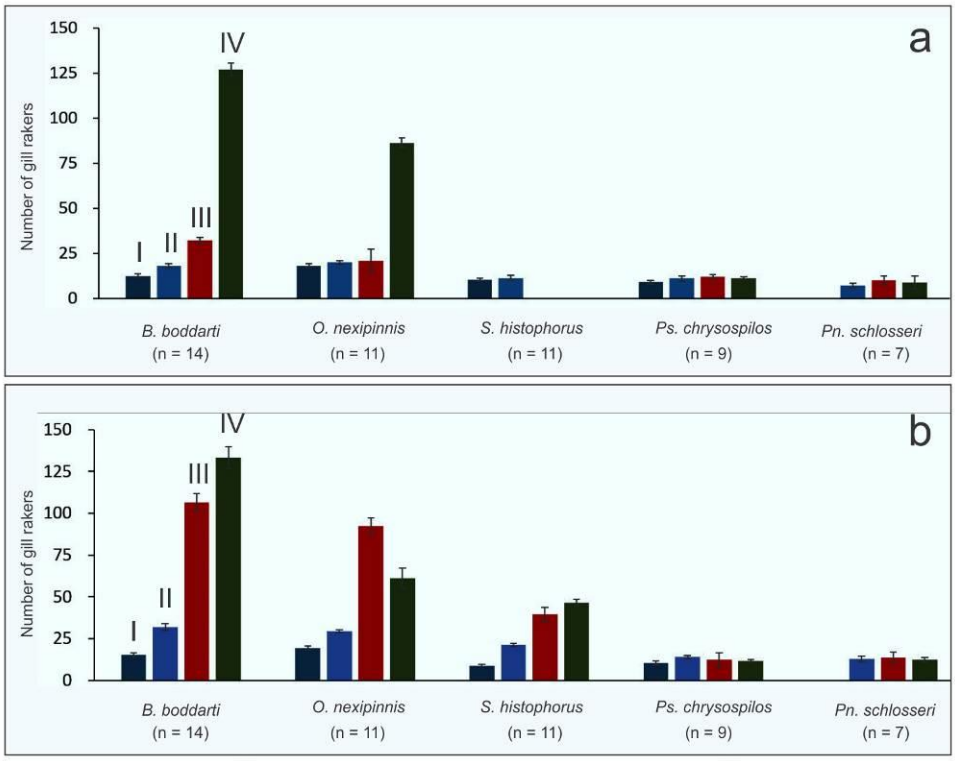

Fig. III-5 Number of gill rakers (mean ± SD) on the anterior (**a**) and posterior (**b**) gill arches of the five species. *I-IV* first to fourth gill arches. Size range of *B. boddarti*: 111-127 mm in standard length (SL), *O. nexipinnis*: 78-91 mm SL, *S. histophorus*: 70-82 mm SL, *Ps. chrysospilos*: 65-83 mm SL, and *Pn. schlosseri*: 122-185 mm SL. The number of individuals used for the measurement is given in the parenthesis

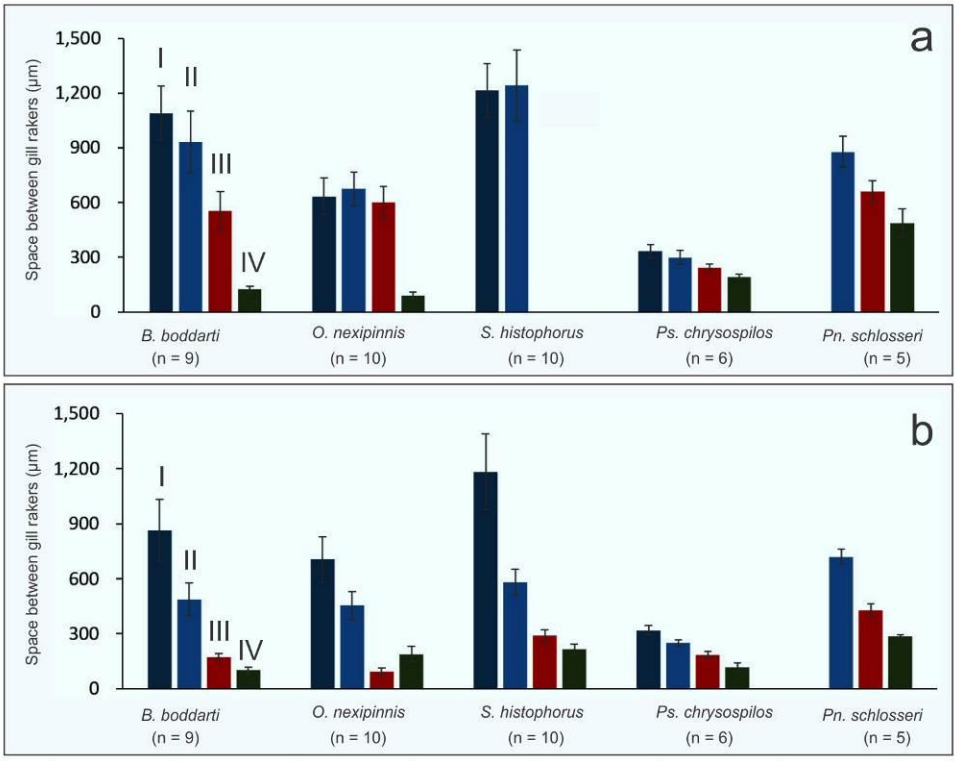

Fig. III-6 Average space between the gill rakers (mean ± SD) on the anterior (**a**) and posterior (**b**) gill arches of the five species. Symbols as the same in Fig. III-5. Size range of *B. boddarti*: 120-125 mm in standard length (SL), *O. nexipinnis*: 78-94 mm SL, *S. histophorus*: 88-104 mm SL, *Ps. chrysospilos*: 65-83 mm SL, and *Pn. schlosseri*: 155-193 mm SL. The number of individuals used for the measurement is given in the parenthesis

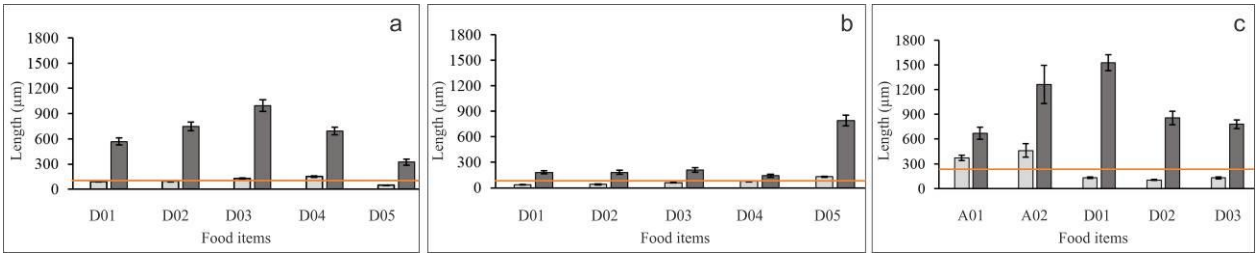

Fig. III-7 Comparison of the average space between gill rakers and the size of main food items (mean ± SD) ingested by *Boleophthalmus boddarti* (**a**), *Oxuderces nexipinnis* (**b**), and *Scartelaos histophorus* (**c**). The average space between gill rakers (horizontal orange line) was calculated for the posterior row of the third arch and both rows of the fourth arch in *B. boddarti* and *O. nexipinnis*, and for the posterior rows of the third and the fourth arches in *S. histophorus*. The longer-axis length (dark-gray bars) and the shorter-axis length (light-gray bars) were measured in 30 specimens of the five main food items found in the stomach contents of each fish species. *D01–05* diatom items 1 to 5 recovered from each mudskipper species, *A01–02* amphipod items 1 to 2 recovered from *S. histophorus*.

canine teeth along the anterior margin of the dorsal pharyngeal plates of *B. boddarti* (distance between adjacent teeth 75-162 μm; Fig. III-8a1). In the second type found in *S. histophorus*, the pharyngeal plates are slightly smaller (Figs. III-8c and III-9) and much flatter (Fig. III-12c),and the overlapping area of PB3 and PB4 (Fig. III-10c1) is smaller than in the first type. There are papilliform and canine teeth on both the dorsal and ventral pharyngeal plates (Table III-3). The papilliform teeth occur in most areas of the pharyngeal plates, while canine teeth are restricted to the medial and anterior margins (Fig. III-8c). The papilliform teeth are hook-like, and arranged in lines on the ventral pharyngeal plates (Figs. III-8c4 and III-8c5). The canine teeth on the dorsal and ventral plates are oriented in opposite directions (Figs. III-8c3 and III-8c6, Table III-3). In the third type observed in *Ps. chrysospilos* and *Pn. schlosseri*, the pharyngeal plates are even smaller and flatter (Figs. III-8d, III-8e, III-9, III-12d, and III-12e). There is a large ventral ridge on the ventral pharyngeal plates (Figs. III-10f4 and III-10f5). Only canine teeth are present on both dorsal and ventral pharyngeal plates (Figs. III-8d and III-8e). Larger teeth are located on the posteromedial edges of both dorsal and ventral pharyngeal plates (Figs. III-8d1, III-8d3, III-8e1, and III-8e3, Table III-3).

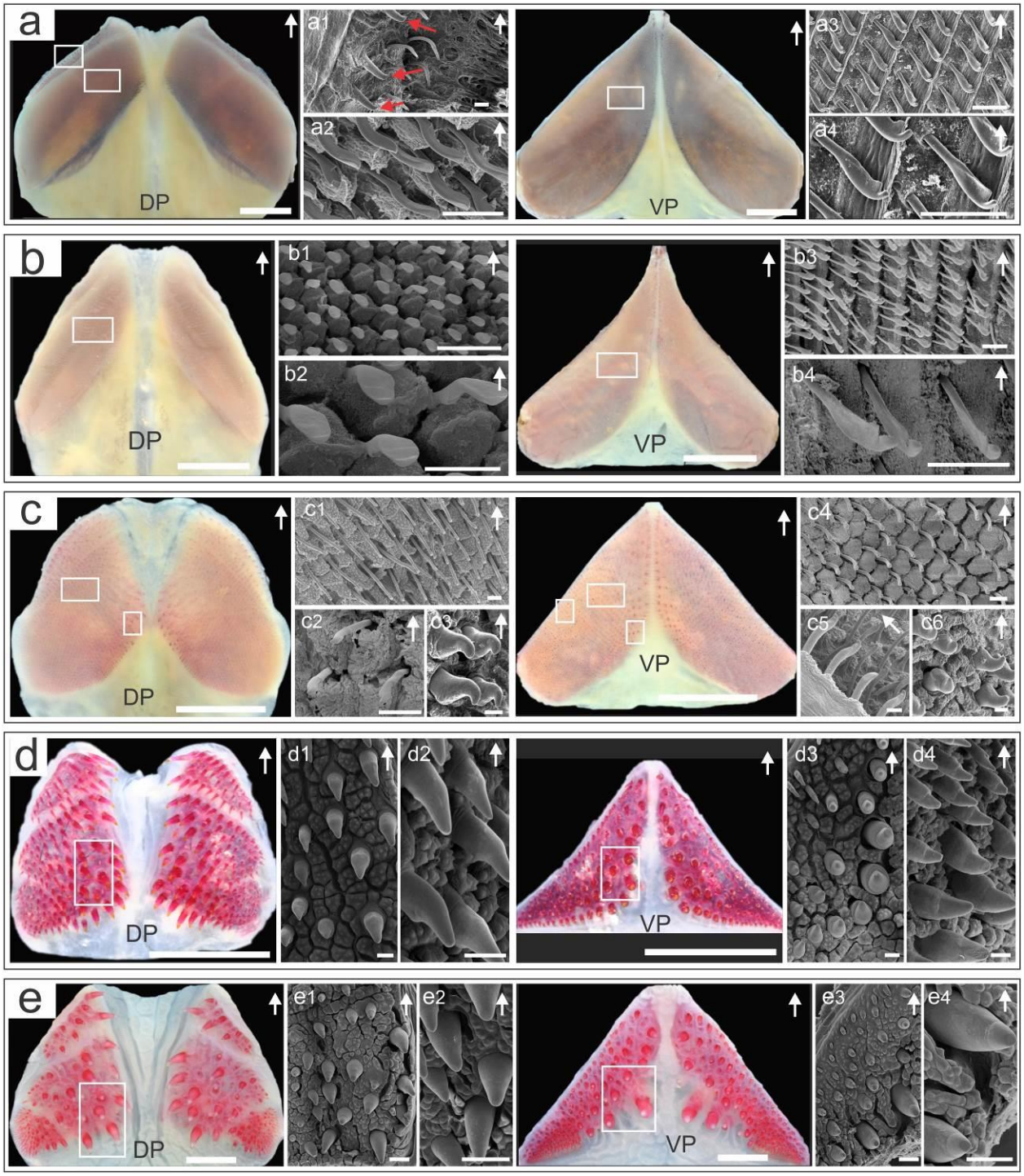

Fig. III-8 Morphology of the pharyngeal plates of *Boleophthalmus boddarti* (**a**), *Oxuderces nexipinnis* (**b**), *Scartelaos histophorus* (**c**), *Periophthalmus chrysospilos* (**d**), and *Periophthalmodon schlosseri* (**e**). Color photographs show surface views of the dorsal (DP) and ventral (VP) pharyngeal plates, accompanied by SEM micrographs. **a1**, **c1** and **a2**, **c3** correspond to the upper and lower boxes in the DP of the same row. **c2** shows the papilliform tooth heads in the upper box at a higher magnification than in **c1**. **c4**, **c5** and **c6** correspond to the upper, lower left and lower right boxes of the VP. Other SEM micrographs show pharyngeal teeth in the corresponding color photographs at different magnifications. Red arrows in **a1** show canine teeth on the marginal edge of the right dorsal pharyngeal plate. White

arrows on the upper right of color photographs and the SEM photos indicate the anterior direction. Scale bars: 2 mm for color photographs, 500 μm for **e1-4**, 100 μm for **d1-4**, 50 μm for **a1-4**, b1, **b3**, **b4**, **c1-4**, and 20 μm for **b2**

Table III-3 Morphology, density, and direction of the teeth on the pharyngeal plates of the five mudskippers

Species	Morphology	Density (number/mm^2)		Direction	
		Dorsal plate	Ventral plate	Dorsal plate	Ventral plate
Boleophthalmus boddarti	papilliform	951.6 ± 313.3	529.5 ± 101.1	PM	PM
	canine*			DV	
Oxuderces nexipinnis	papilliform	2720.2 ± 301.2	700.1 ± 77.9	PM	PM
Scartelaos histophorus	papilliform	146.8 ± 21.0	142.2 ± 37.9	PM	PM
	canine**			posterior	anterior
Periophthalmus chrysospilos	canine	23.1 ± 3.3	34.1 ± 2.6	posterior	anterior
Periophthalmodon schlosseri	canine	6.7 ± 1.1	8.5 ± 0.9	posterior	anterior

*Only along the anterior margin of the dorsal pharyngeal plate. **Along the anterior and medial margins of the dorsal and ventral plates. Mean ± SD. Three individuals were used for each species. DV, dorsoventral; PM, posteromedial.

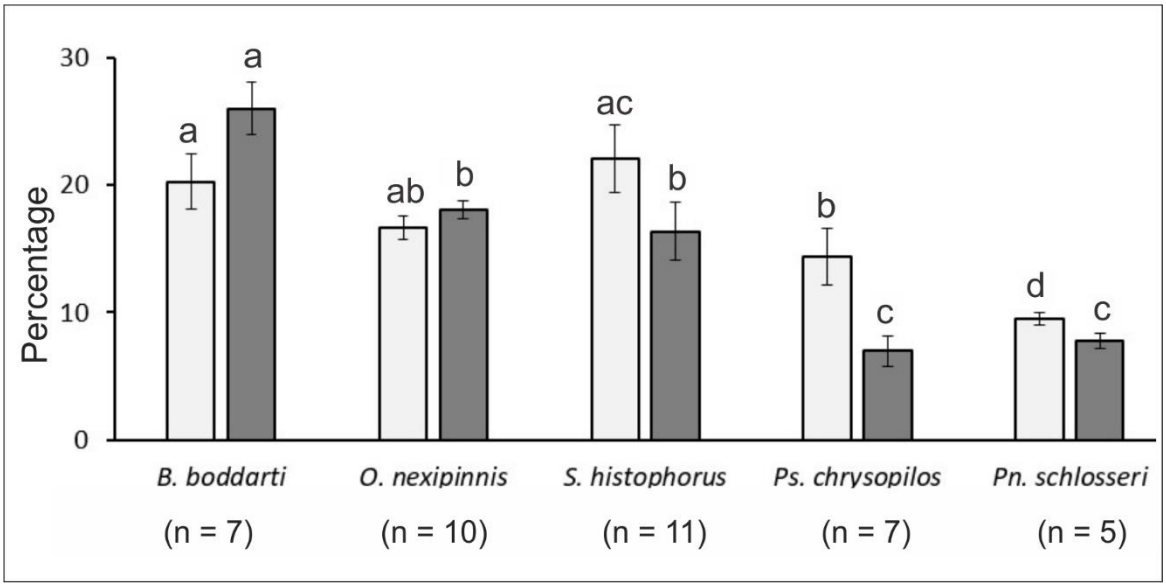

Fig. III-9 The relative size (area of pharyngeal plates/frontal sectional area of the dorsal or ventral surface of the oropharyngeal cavity) (Mean ± SD) of the dorsal (light gray bars) and ventral (dark gray bars) pharyngeal plates. Non-parametric Kruskal-Wallis was performed to detect significant differences among the species, followed by Wilcoxon-Mann-Whitney test. All pairwise comparisons were performed with Bonferroni correction of p-value Data with different letters of the dorsal or ventral pharyngeal plate are significantly different ($p < 0.05$). The number of individuals used for the measurement is given in the parenthesis

Branchial basket skeleton

The ceratobranchials are slender in *B. boddarti* and *O. nexipinnis*, intermediate in *S. histophorus* and robust in *Ps. chrysospilos* and *Pn. schlosseri*. The ratios of length to width of the first to fourth

ceratobranchials (CB1-4, mean ± SD, N = 3) are 13.05 ± 2.14 in *B. boddarti*, 14.17 ± 1.56 in *O. nexipinnis*, 13.37 ± 3.86 in *S. histophorus*, 10.66 ± 2.65 in *Ps. chrysospilos*, and 9.46 ± 1.63 in *Pn. schlosseri*. The basihyal (BH) is bifurcated in *B. boddarti*, and flabelliform in the other species (Fig. III-10). The second pharyngobranchial (PB2) extends along the anterior margin of PB3 and PB4 in *B. boddarti*, *O. nexipinnis*, and *S. histophorus* (Figs. III-10a1, III-10b1, and III-10c1), but lies anteriorly to PB3 in *Ps. chrysospilos* and *Pn. schlosseri* (Figs. III-10d1, and III-10e1), as a consequence of the smaller size of PB4 in these two species. The fourth epibranchial (EB4) is L-shaped in *B. boddarti* (90.7 ± 1.1°, mean ± SD, N = 13, Fig. III-10a2), *O. nexipinnis* (97.9 ± 1.4°, N = 8, Fig. III-10b2), and more obtuse in *S. histophorus* (137.5 ± 1.2°, N = 8, Fig. III-10c2), *Ps. chrysospilos* (141.1 ± 0.7°, N = 7, Fig. III-10d2) and *Pn. schlosseri* (143.7 ± 1.8°, N = 6, Fig. III-10e2). The fourth arch is significantly longer than the other arches in *B. boddarti*, whereas the arch lengths gradually decrease from the first to the fourth arch in *Ps. chrysospilos* and *Pn. schlosseri*. There is no significant difference among the arch lengths of *O. nexipinnis* and *S. histophorus* (Table III-4).

Table III-4 Comparison of the arch lengths (mean ± SD) among the species

	Arch length (mm)						
	N	Arch 1	Arch 2	Arch 3	Arch 4	ANOVA or Kruskal-Wallis	
						F or Chi-squared	*p*
Boleophthalmus boddarti	12	17.6 ± 1.2[a]	18.0 ± 1.2[a]	17.6 ± 1.3[a]	19.6 ± 1.4[b]	6.4	0.001
Oxuderces nexipinnis	10	12.4 ± 2.0[a]	12.7 ± 2.0[a]	12.6 ± 2.1[a]	13.4 ± 2.4[a]	2.5	0.48
Scartelaos histophorus	10	10.2 ± 1.0[a]	9.6 ± 0.9[a]	9.2 ± 0.9[a]	9.6 ± 0.9[a]	1.9	0.15
Periophthalmus chrysospilos	7	11.8 ± 1.2[a]	11.0 ± 1.1[a]	8.9 ± 0.9[b]	8.9 ± 0.8[b]	12.9	< 0.001
Periophthalmodon schlosseri	6	27.1 ± 6.1[a]	24.3 ± 4.9[ab]	19.6 ± 4.0[ab]	18.2 ± 3.9[c]	3.7	0.04

One-way ANOVA followed by post-hoc Tukey test was applied for *B. boddarti*, *S. histophorus*, *Ps. chrysospilos*, and *Pn. schlosseri*. Kruskal-Wallis followed by Wilcoxon-Mann-Whitney test was applied for *O. nexipinnis*. All pairwise comparisons were performed with Bonferroni correction of p-value. The data with different letters in respective rows are significantly different ($p < 0.05$)

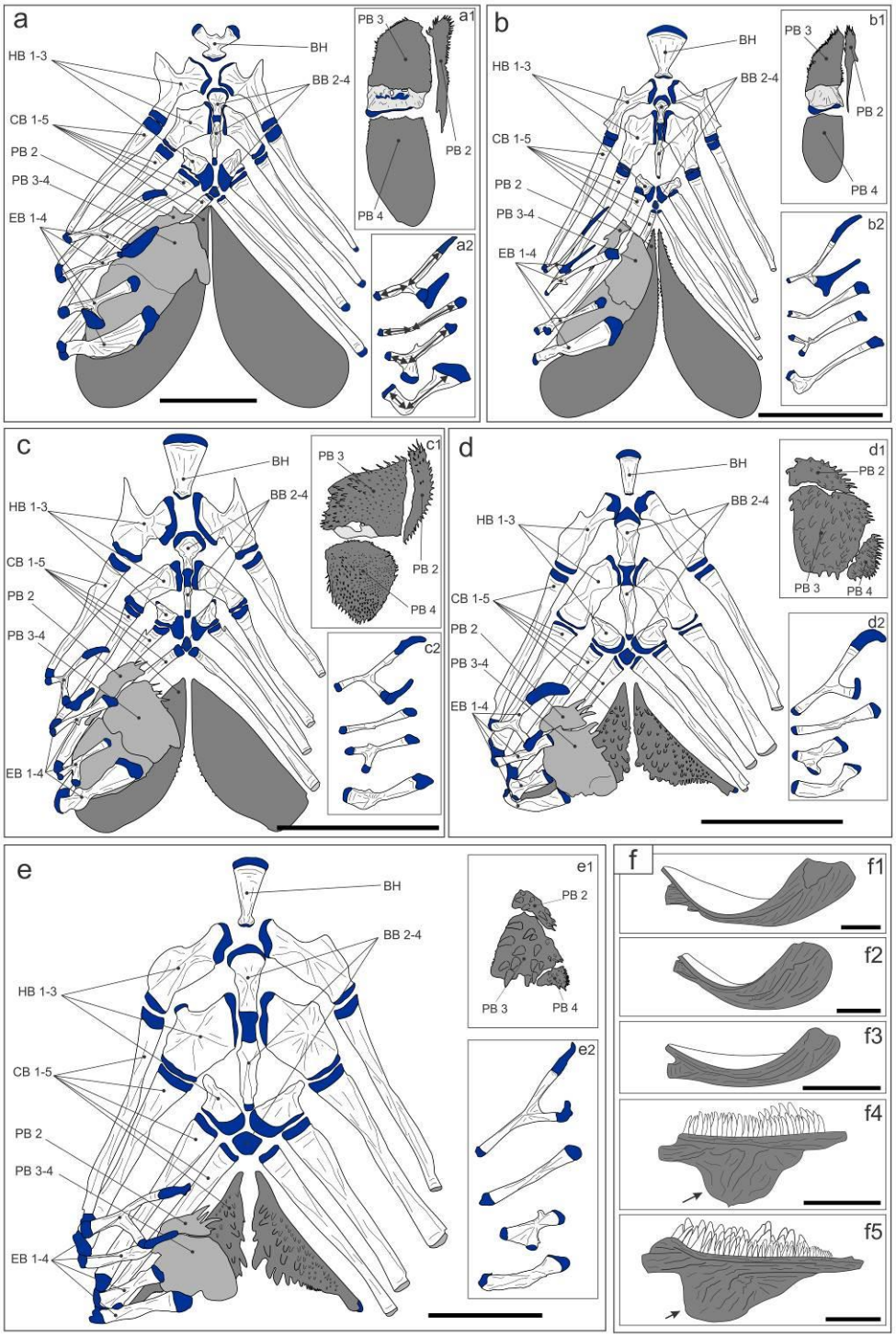

Fig. III-10 Morphology of the branchial basket skeletons (dorsal view) and the left fifth ceratobranchials (lateral view) of *Boleophthalmus boddarti* (**a, f1**), *Oxuderces nexipinnis* (**b, f2**), *Scartelaos histophorus* (**c, f3**), *Periophthalmus chrysospilos* (**d, f4**), *Periophthalmodon schlosseri* (**e, f5**). In each box of **a** to **e**, the whole structure is shown on the left, the left dorsal pharyngeal plate dissected separately is shown in ventral view in **a1- e1**; the right epibranchials dissected separately is shown in ventral view in **a2-e2**. The portion of the third pharyngobranchial covered by the fourth pharyngobranchial is shown in light grey in **a1**, **b1**, and **c1**. Cartilages are in blue. Grey parts in box **f** are the ventral side of the fifth ceratobranchial. Double arrowheads in **a2** show length measurement. Arrows in **f4** and **f5** show ventral ridges. *BB 2–4* basibranchials 2–4, *BH* basihyal, *CB 1–5* ceratobranchials 1–5, *EB 1–4* epibranchials 1–4, *HB*

1–3 hypobranchials 1–3, *PB 2,3,4* pharyngobranchials 2,3,4. BB1 is a small cartilage between the right and left HB1s, and therefore not shown. Scale bars: 5 mm for boxes **a-e**, 2 mm for box **f**

Branchial basket musculature

The branchial basket musculature of the five species consists of four systems. The first system connects the elemental bones of the branchial basket to the surrounding skeletal components; the levatores interni (LI), the levatores externi (LE), the levator posterior (LP), the retractor dorsalis (RD), the pharyngohyoideus (PH), the rectus ventralis (RV), the pharyngocleithralis externus (PHCE), and the pharyngocleithralis internus (PHCI) (Figs. III-11a3, III-11b3, III-11c3, III-11d3, and III-11e3). The second system links the elemental bones dorsally; through the transversi dorsales anteriores (TDA), the transversi dorsales posteriores (TDP), and the obliqui dorsales (OD) (Figs. III-11a1, III-11b1, III-11c1, III-11d1, and III-11e1). A ligament (L3-4) connects the third and fourth epibranchials. In *B. boddarti*, *O. nexipinnis*, and *S. histophorus*, there is a structure that resembles the cartilaginous cushion described by Liem (1973) between the right and left TDA and TDP (CC, Figs. III-11a1, III-11b1, and III-110c1). In *Ps. chrysospilos* and *Pn. schlosseri*, there is only a thin strand of connective tissue in the corresponding position (Figs. III-11d1 and III-11e1). The third system links the elemental bones ventrally; the transversi ventrales (TV), the obliqui ventralises (OV), and the semicircular ligament (SL) (Figs. III-11a2, III-11b2, III-11c2, III-11d2, and III-11e2). The fourth system is made of the adductors connecting the ceratobranchials to the epibranchials (AD, Figs. III-11a3, III-11b3, III-11c3, III-11d3, and III-11e3). The ligament 4 (L4), connecting EB4 to the post-temporal bone, is present only in *B. boddarti* (Figs. III-11a3 and III-11a4); in this species, LE3-4 originates from the articulation between EB4 and CB4 and is directed anteriorly; LP originates between the points of insertion of L4 and LE4 (Fig. III-11a4). RD connects to the posterior portion of the third vertebra and anterior portion of the fourth vertebra in *B. boddarti* (Fig. III-13a); to the dorsal tip of the neural spine of the fourth vertebra in *O. nexipinnis* (Figs. III-13b1 and III-13b2); to the third vertebra in

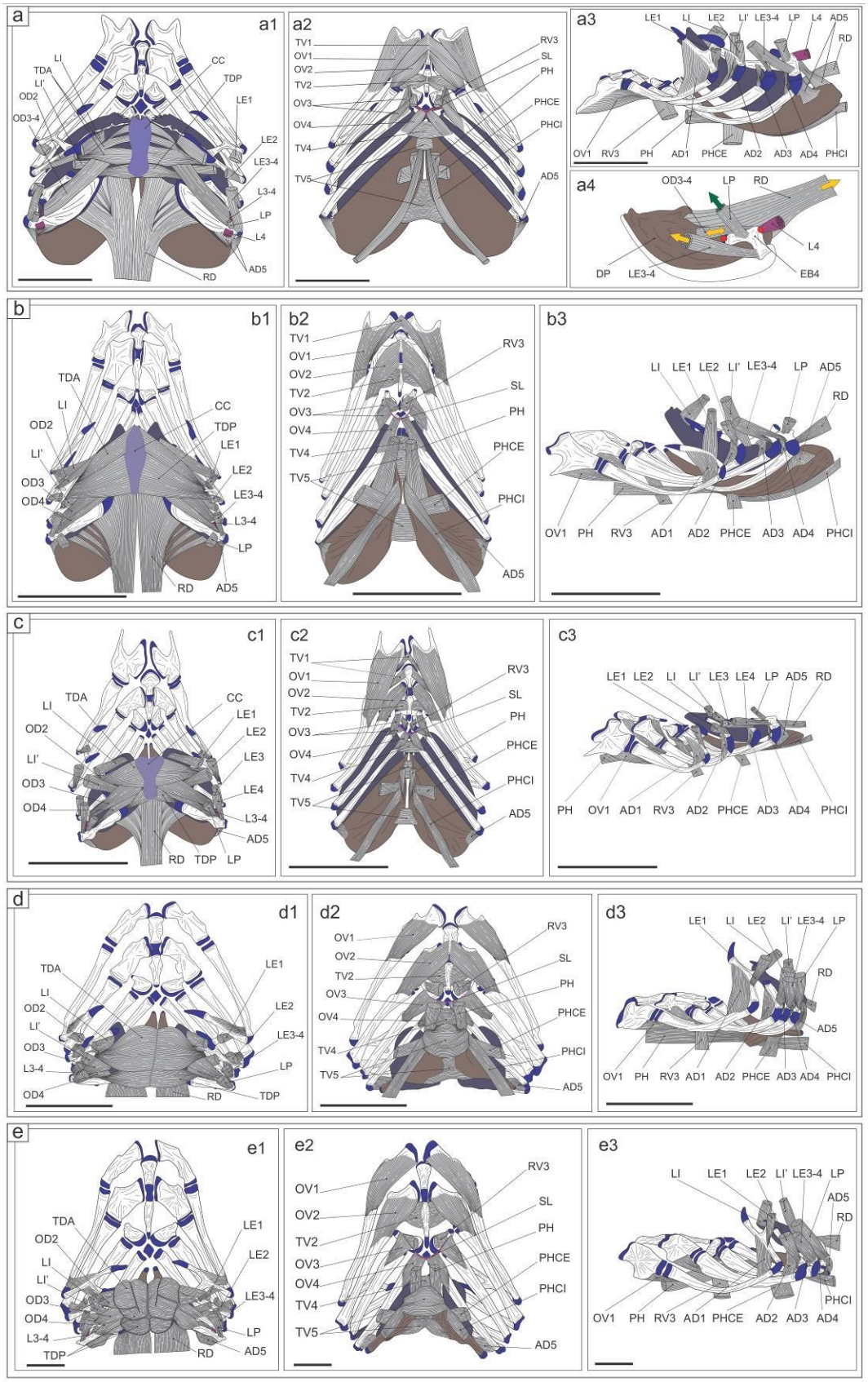

Fig. III-11 Morphology of branchial basket musculature of *Boleophthalmus boddarti* (**a**), *Oxuderces nexipinnis* (**b**), *Scartelaos histophorus* (**c**), *Periophthalmus chrysospilos* (**d**), and *Periophthalmodon schlosseri* (**e**). **a1**–**e1** are dorsal

views, **a2**–**e2** ventral views and **a3**–**e3** lateral views. **a4** a hypothetical mechanism for the movement of the dorsal pharyngeal plates (in dorsolateral view) in *Boleophthalmus boddarti*. In **a4**, red dots show fulcrums, yellow arrows show the direction of force exerted by the contraction of OD3-4, LE3-4, and RD, and the green arrow shows the direction of force by the LP contraction. *AD1–5* adductors 1 to 5, *CC* cartilaginous cushion, *EB4* epibranchial 4, *LE1, 2* levatores externi 1 to 2, *LE3-4* levatores externi 3 and 4 acting on the third and fourth epibranchials, *LI* and *LI'* levatores interni, *LP* levator posterior, *L3–4* ligament 3–4 connecting the third and fourth epibranchials, and *L4* ligament 4 (only in *B. boddarti*), *OD2* obliquus dorsalis 2, *OD3–4* obliqui dorsales 3 to 4, *OV1–4* obliqui ventrales 1 to 4, *PH* pharyngohyoideus, *PHCE* pharyngocleithralis externus, *PHCI* pharyngocleithralis internus, *RD* retractor dorsalis, *RV3* rectus ventralis 3, *SL* semicircular ligament, *TDA* transversus dorsalis anterior, *TDP* transversus dorsalis posterior, *TV1-5* tranversi ventrales 1 to 5. Cartilages in blue; dorsal pharyngeal plate in dark purple; ventral pharyngeal plate in brown. Scale bars: 5 mm

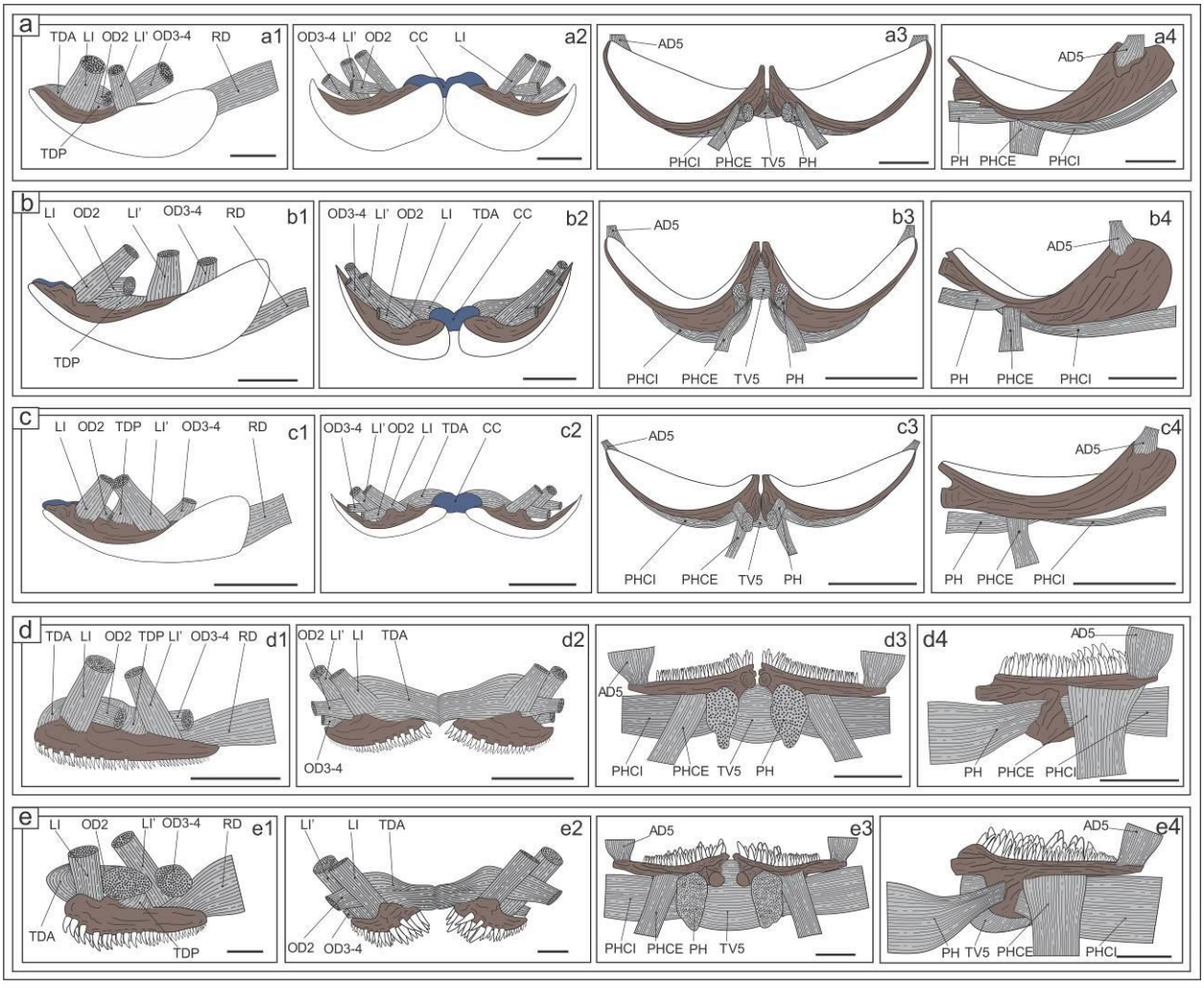

Fig. III-12 Morphology of musculature system attaching to the pharyngeal plates in *Boleophthalmus boddarti* (**a**), *Oxuderces nexipinnis* (**b**), *Scartelaos histophorus* (**c**), *Periophthalmus chrysospilos* (**d**), and *Periophthalmodon schlosseri* (**e**). **a1**–**e1** are lateral views of the left dorsal pharyngeal plate, **a2**–**e2** and **a3**–**e3** frontal views of the dorsal and ventral pharyngeal plates, respectively, and **a4**–**e4** lateral views of the left ventral pharyngeal plate. Symbols are the same as in Fig. III-11. The ventral side of the ventral pharyngeal plates and the dorsal side of the dorsal pharyngeal plates are colored in brown. Scale bars: 2 mm

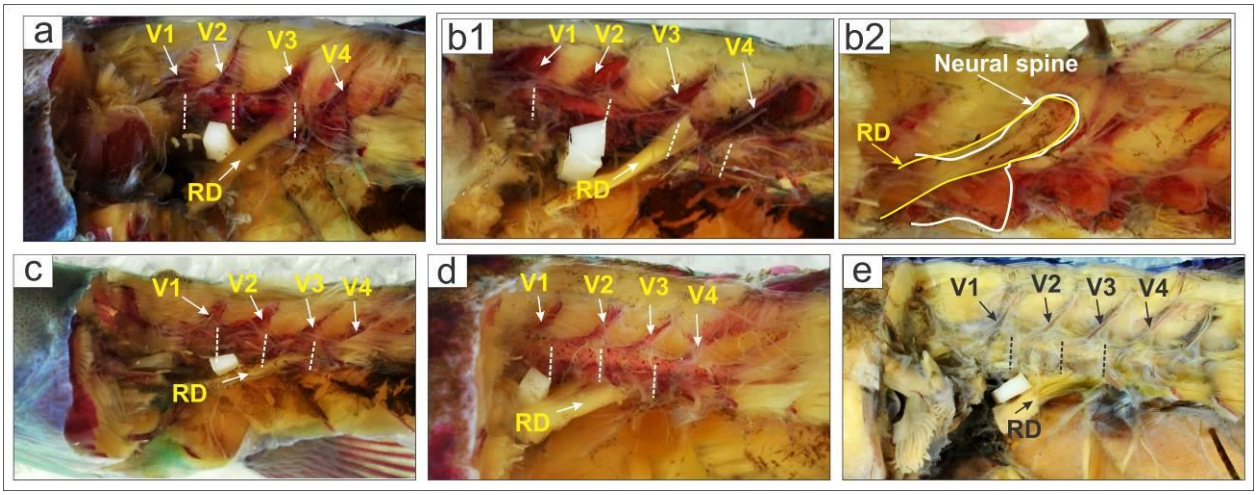

Fig. III-13 Insertion of the retractor dorsalis (RD) to vertebrae in *Boleophthalmus boddarti* (**a**), *Oxuderces nexipinnis* (**b**), *Scartelaos histophorus* (**c**), *Periophthalmus chrysospilos* (**d**), and *Periophthalmodon schlosseri* (**e**). For *O. nexipinnis*, **b1** shows relative position of RD and vertebrae and **b2** shows RD insertion on the neural spine of the fourth vertebra. Symbols: *RD* retractor dorsalis, *V1-V4* neural spines of the first to fourth vertebrae. Dashed lines show joint between vertebrae

S. histophorus (Fig. III-13c); and to the posterior portion of the second vertebra and the anterior portion of the third vertebra in both *Ps. chrysospilos* (Fig. III-13d) and *Pn. schlosseri* (Fig. III-13e).

TV1, connecting to the left and right hypobranchials of the first arch, is present only in *B. boddarti*, *O. nexipinnis*, and *S. histophorus* (Figs. III-11a2, III-11b2, and III-11c2). In contrast, muscles attached to the pharyngeal plates (TDA and TDP) are more developed in *Ps. chrysospilos* (Figs. III-11d1, III-12d1, and III-12d2) and *Pn. schlosseri* (Figs. III-11e1, III-12e1, and III-12e2). PHCI, PHCE, PH, and TV5 are also more developed in *Ps. chrysospilos* (Figs. III-11d2, III-11d3, III-12d3, and III-12d4) and *Pn. schlosseri* (Figs. III-11e2, III-11e3, III-12e3, and III-12e4). PHCI, PH, and TV5 attach to the ventral ridge of CB5 in *Ps. chrysospilos* (Figs. III-10f4, III-12d3, and III-12d4) and *Pn. schlosseri* (Figs. III-10f5, III-12e3, and III-12e4), while these muscles attach to the ventral side of CB5 in *B. boddarti* (Figs. III-12a3 and III-12a4), *O. nexipinnis* (Figs. III-12b3 and III-13b4), and *S. histophorus* (Figs. III-12c3 and III-12c4).

4. Discussion

Fig. I-1 shows generally accepted relationships of oxudercine genera based on 39 morphological characters (Murdy 1989) together with the feeding habit and terrestriality of each genus at an adult stage (see also supplementary Table S1). The data should be regarded as preliminary for the following three reasons. Firstly, the feeding habit has only been anecdotally described for *Apocryptes* (two studies), *Apocryptodon* (one study), *Oxuderces* (one published study and our own data) and *Parapocryptes* (two studies) or totally unknown for *Zappa.* There are also contradictory observations for *Apocryptes*, *Oxuderces*, *Pseudapocryptes*, and *Scartelaos* (Table S1). These discrepancies may be due to local and/or seasonal differences in food availability or some other factors. For example, González-Bergonzoni et al. (2012) reported that omnivory becomes less common with increasing latitudes among fishes in marine, fresh and brackish waters. Secondly, the degree of terrestriality has mostly been reported as amphibious behaviors during low tide, and has rarely been quantified as the percentage of time fish stayed on land and in water (but see Gordon et al. 1969). Furthermore, terrestriality is scarcely studied for several genera (e.g., *Apocryptes*, *Apocryptodon*, and *Parapocryptes*). Thirdly, the tree is inconsistent with several published (though incomplete in terms of taxon sampling) molecular phylogenies (e.g., Agorreta and Rüber 2012; Agorreta et al. 2013). Despite these uncertainties, the overall trend is clear−a transition from herbivory in the more aquatic genera (*Apocryptes*, *Apocryptodon*, *Oxuderces*, *Parapocryptes*, *Pseudapocryptes*), to pure carnivory in the two most terrestrial genera (*Periophthalmus* and *Periophthalmodon*). *Boleophthalmus* may represent a highly specialized stage for algal feeding on land, and *Scartelaos* may be considered as an intermediate stage from herbivory to carnivory. With these reservations in mind, we will attempt to correlate the morphological differences in feeding apparatus revealed in this study with the feeding ecology of the five genera, and discuss a possible scenario of the transition from aquatic to terrestrial habitats among mudskippers, in the following

sections.

Comparison of dentition, jaw structure and gill rakers

Of the five syntopic species of the Mo O mudflat, *Oxuderces nexipinnis* is the least terrestrial, being mostly restricted to shallow waters during low tide. The head of *Oxuderces* species is depressed anteriorly (Murdy 1989), and their oral gape is terminal or slightly superior (Murdy and Jaafar 2017), unlike most other mudskippers in which the gape is subterminal. The head shape, the position of the gape, and the horizontally oriented dentary teeth of *O. nexipinnis* are likely adaptations to graze on diatoms in shallow water (Table S1 and Fig. III-1). Horizontal disposition of the dentary teeth has been reported also for purely aquatic sicydiine gobies *Sicyopterus japonicus* (Tanaka, 1909) (Sakai and Nakamura 1979; Mochizuki and Fukui 1983; Sahara et al. 2013), *Lentipes armatus* Sakai and Nakamura, 1979, and *Stiphodon elegans* (Steindachner, 1879) (Sakai and Nakamura 1979), all of which were observed to feed on algae on the glass wall of aquaria. However, the low number and wide spacing of the dentary teeth of *O. nexipinnis* suggest their limited role in scraping diatoms from the substrate surface in this species. The closely spaced, numerous gill rakers on the posterior row of the third arch and the both rows of the fourth arch in *O. nexipinnis* probably serve for sieving diatoms from the ingested mixture of muddy water and food items.

Scartelaos histophorus is more terrestrial than *O. nexipinnis* and omnivorous, though a congener *S. tenuis* was reported to be carnivorous (supplementary Table S1). *S. histophorus* has horizontally oriented dentary teeth, which are significantly more numerous than in *O. nexipinnis* (Table III-2). *S. histophorus* lacks gill rakers on the anterior rows of the third and fourth gill arches, and lower numbers of gill rakers on their posterior rows, possibly reflecting lower reliance on sieving diatoms and a shift to omnivory. Our analysis of stomach content confirms the omnivory of this species.

Boleophthalmus boddarti shows a higher degree of specialization to grazing on land, as evidenced by the significantly higher number of horizontal dentary teeth, and much closely spaced, higher number of gill rakers located above the gill cleft. The dentary teeth are incisors, flattened and enlarged on the cusps and are lined in a straight, horizontal line. This anatomy allows aligning the entire length of the dentary teeth to skim the top thin layer of the mudflat surface, when the fish swings the head laterally during terrestrial feeding (Tran et al. 2020). The feeding apparatus of *B. pectinirostris*, a temperate species known from the coasts of the East China Sea, has a similar morphology to that of *B. boddarti* (Tran et al. 2020).

Periophthalmus chrysospilos and *Periophthalmodon schlosseri* are the most terrestrial among the five species inhabiting the Mo O mudflat. Similarity of dentition morphometrics of these two species (Fig. III-3), especially the strong canine teeth, are typical of carnivorous fishes. They occasionally capture prey as large as or larger than their gape width, and subdue the prey by repeated biting (AI and LXT, pers. obs.). This must require strong biting force, consistent with the higher jaw-closing lever ratio (0.50 in *Ps. chrysospilos* and 0.58 in *Pn. schlosseri*), and the well-developed adductor mandibulae (K values of 126.9 in *Ps. chrysospilos* and 93.6 in *Pn. schlosseri*) and premaxillo-maxillary plus maxilla-mandibular ligaments (Figs. III-2d and III-2e). The relatively long ascending process of the premaxilla in *Ps. chrysospilos* and *Pn. schlosseri* would permit larger protrusion of the upper jaw and thus help secure crabs and other feed organisms.

Comparison of pharyngeal plates and branchial basket

The pharyngeal plates play an essential role in intraoral transportation in most fishes but they can also be used for crushing and pulverizing prey (Gidmark et al. 2019). The pharyngeal plates of *B. boddarti* and *O. nexipinnis* are larger than those of the other mudskippers, strongly curved ventrally and bearing numerous papilliform teeth. The strong curvature would allow a larger surface area for a given width of the oropharyngeal cavity. The large size of the pharyngeal plate of herbivorous

mudskippers is however unlikely to be an adaptation solely to transporting microalgal cells to the esophagus, because *Si. japonicus* and *Plecoglossus altivelis* (Temminck & Schlegel, 1846), another aquatic algal grazer, have the pharyngeal plates that are much smaller in relative surface area (1–6%, see Tran et al. 2020). The major differences between feeding conditions of mudskippers and *Si. japonicus* and *P. altivelis* are whether feeding occurs on land or in water and whether ingested algal cells co-occur with a quantity of much finer sediment particles or not.

We therefore presume that the large and strongly curved pharyngeal plates bearing numerous teeth directing toward the esophagus opening would facilitate the selective transportation of food particles trapped on the gill rakers of the two posterior gill arches into the esophagus, while minimizing the deglutition of mud particles. The curvature of the dorsal pharyngeal plates perfectly fits the curvatures of both the last two arches, and the ventral pharyngeal plates in *B. boddarti* and *O. nexipinnis* (and also *S. histophorus*). The L-shaped epibranchial 4 (EB4) with a flat tip and muscles inserting to EB4 in *B. boddarti* (levator externus 3 and 4, levator posterior, and obliqui dorsales 3 and 4) could facilitate anteroposterior and dorsoventral motions of the dorsal pharyngeal plates (Wainwright 2006). The resting position of the anterior margin of the dorsal pharyngeal plates is just above the third arch in *B. boddarti*, and the fourth arch in *O. nexipinnis* (Fig. III-14). The intervals between the papilliform teeth of the pharyngeal plates are 20-30 μm, much larger than the average sediment diameter we measured in a habitat of *B. pectinirostris* (7.3 μm, Ishimatsu et al. 2007). The strong muscles transversi ventrales 1 and 2, obliqui ventralises 1 and 2 of *B. boddarti* may seal the buccal cavity, in order to retain water inside during gurgling (see Tran et al. 2020).

The pharyngeal plates of the carnivorous mudskippers, *Ps. chrysospilos* and *Pn. schlosseri*, are much smaller, almost flat, and studded with robust canine teeth, with larger ones distributed

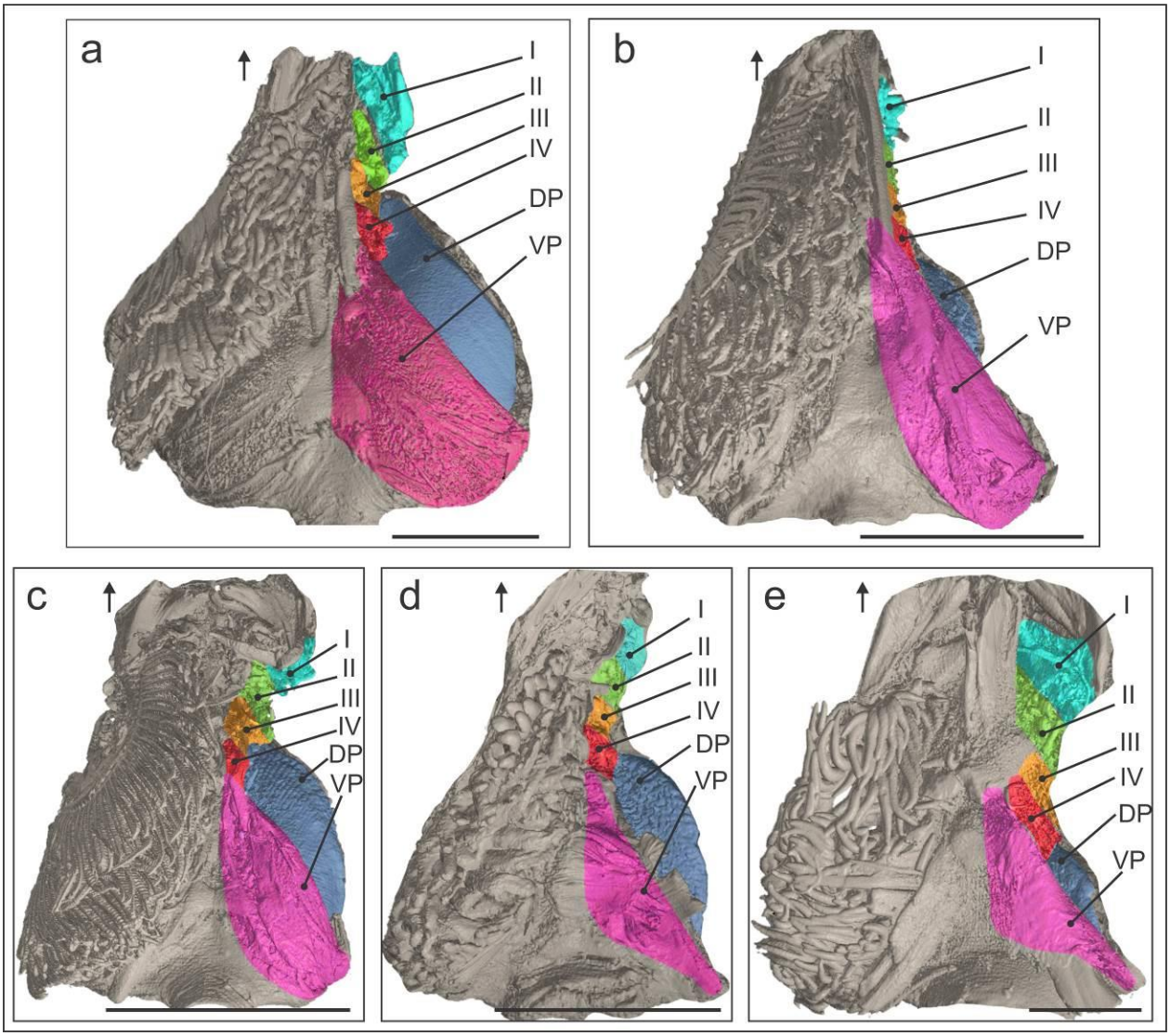

Fig. III-14 Micro-CT scanning images showing the relative position of the dorsal pharyngeal plates (in ventral view with the left arches removed to expose the pharyngeal plates) of *Boleophthalmus boddarti* (**a**), *Oxuderces nexipinnis* (**b**), *Scartelaos histophorus* (**c**), *Periophthalmus chrysospilos* (**d**), and *Periophthalmodon schlosseri* (**e**). Arrows indicate anterior direction. *I-IV* first to fourth gill arches, *DP* dorsal pharyngeal plate, *VP* ventral pharyngeal plate. Scale bars: 5 mm

along the posteromedial margins.The right and left ventral plates each has a ventral ridge, as reported earlier for *Ps. barbarus* by Sponder and Lauder (1981). The pharyngohyoideus (PH) and the pharyngocleithralis (PHCI) connect the ridge to the urohyal and to the dorsal extremity of the cleithrum, respectively. According to Vandewalle et al. (2000), these muscles play an important role for the movement of the ventral pharyngeal plate, even though Sponder and Lauder (1981) found that the ventral plate remained almost stationary during intraoral transport of prey into the

esophagus, while the dorsal pharyngeal plate moved in a much greater anteroposterior excursion. We speculate that the contraction of the transversi dorsales anteriores, adductor 5, and transverse ventrales 5 would hold the prey in position, while the contraction of retractor dorsalis and pharyngohyoideus would pull the dorsal and ventral pharyngeal plates in opposite directions, thus allowing oppositely-directed teeth on the dorsal and ventral plates to penetrate, tear and transport prey into the esophagus (Mihalitsis and Bellwood 2019). The disposition of larger teeth on the posteromedial margins is consistent with the findings by Hulsey et al. (2008) that high stress is concentrated along the posterior midline of the ventral pharyngeal plates during prey processing in cichlids.

The morphology of the pharyngeal plates and related muscular structure of *S. histophorus* shares the configurations of both the herbivorous (ventrally curved pharyngeal plates bearing numerous fine teeth and muscle system) and carnivorous (some canine teeth along the posteromedial margin of the pharyngeal plates) mudskippers.

A hypothesis of mudskipper's feeding habit during transition to land

It is reasonable to assume that the earliest fish that emerged from water had feeding, locomotory, respiratory and sensory mechanisms suited for life in water (Clayton 1993), with limited capacity to detect and capture food on land. If the ecological factor that promoted land invasion was the presence of unexploited trophic resources on land ("the pull hypothesis"), then the food items that "pulled" those transitional animals must have been ubiquitous and easily captured (e.g. epipelic diatoms, biofilms) with little modification of already available aquatic feeding mechanisms (see Sayer and Davenport 1991, Clack 2012, Schoch 2014, and Polgar 2017 for other views). We therefore hypothesize that the first oxudercine gobies that started to expand their niche onto land were semiterrestrial herbivorous or omnivorous grazers. This agrees with the shift of feeding habits observed from extant oxudercine congeners with no to low terrestriality to those of highly

terrestrial congeners (Fig. 1). During the terrestrialization process, oxudercine gobies might have then diverged into more specialized herbivorous species (*Boleophthalmus*) and carnivorous species (*Periophthalmus* and *Periophthalmodon*) through intermediate stages as seen in *Scartelaos* (Table S1). Even though early Devonian transitional vertebrates that evolved into amphibians are thought to have been carnivorous (Clack 2012), there might have also been cases in which herbivorous/omnivorous fishes expanded their habitat beyond the water's edge. It is worth noting that the majority of amphibious blennies are herbivorous (Graham et al. 1985; Nagamoto et al. 2001; Bhikaiee and Green 2002; Shimizu et al. 2006; Hundt et al. 2014), and only a smaller number of them are carnivorous (Nieder 2001).

Chapter IV

MORPHOLOGICAL COMPARISON OF THE FEEDING APPARATUS IN TWO OXUDERCINE GOBIES, *Parapocryptes serperaster* (Richardson 1846), *Pseudapocryptes elongatus* (Cuvier 1816)

1. Introduction

Oxudercine gobies offer a unique window through which we can glimpse how the feeding anatomy, behavior and physiology of aquatic animals may be modified during vertebrate transition from aquatic to terrestrial habitats (Clayton 2017; Tran et al. 2020,2021). This is because these fishes, consisting of 43 species in 10 genera (Murdy and Jaafar 2017), occupy habitats ranging from shallow water through intertidal flats to supralittoral zones, and show all three types of feeding habits, herbivory, omnivory and carnivory (Clayton 1993,2017).

In our preceding paper (Tran et al. 2021), we have compared the morphology of the feeding apparatus of five species of oxudercine gobies (*Boleophthalmus boddarti* (Pallas, 1770), *Oxuderces nexipinnis* (Cantor, 1849), *Scartelaos histophorus* (Valenciennes, 1837), *Periophthalmus chrysospilos* Bleeker, 1853, and *Periophthalmodon schlosseri* (Pallas, 1770)). On the basis of the morphological analyses of dentition, oral jaw, gill rakers and branchial basket, we hypothesized that the earliest oxudercine gobies that started to expand their niche onto land were herbivorous or omnivorous grazers, and that these gobies then diverged into more specialized herbivorous species (*Boleophthalmus*) and carnivorous species (*Periophthalmus* and *Periophthalmodon*) through intermediate stages as seen in *Scartelaos* during the terrestrialization process. At the time of our preceding study, data were lacking for five oxudercine genera, *Apocryptes* Valenciennes in Cuvier and Valenciennes 1837, *Apocryptodon* Bleeker 1874, *Parapocryptes* Bleeker 1874, *Pseudapocryptes* Bleeker 1874, and *Zappa* Murdy 1989. Through further sampling effort, specimens have become available for two species, *Parapocryptes serperaster* (Richardson 1846) and *Pseudapocryptes elongatus* (Cuvier 1816). The present study analyzes the morphology of the feeding apparatus of these fishes.

These two genera show no or the lowest degree of terrestriality (Takita et al. 1999; Dinh et al. 2014; see also Table IV-4) and are therefore at the critical position to understand how initial stages of niche expansion to land could alter the morphology of the feeding apparatus of oxudercine gobies.

2. Materials and methods

Fish collection and preservation

Specimens of *Pa. serperaster* (172–192 mm SL, N = 37) and *Pd. elongatus* (127–185 mm SL, N = 33) were collected at Mo O mudflat (9º 26' 15''N, 106º 10' 57''E, Tran De District, Soc Trang Province, Vietnam) in December 2017 and June 2018 by using bag nets. They were scarified and preserved using the method same as reported by Tran et al. (2020,2021). This study was approved by the Animal Care and Use Committee of the Institute of East China Sea Research, Nagasaki University, Japan (Permit Number #16-01).

Morphological methods

The morphological methods used in this study were the same as reported by Tran et al. (2020,2021). Dentition morphometrics including number of teeth, replacement teeth, tooth length (standardized by standard length), and tooth width (standardized by standard length) of the premaxilla and dentary were examined. The spaces between the gill rakers were measured over entire length for both rows of the first and second arches, and for the anterior row of the third arch. The spaces between the gill rakers of the posterior row of the third arch and both rows of the fourth arch were estimated by measuring five spaces on the ventral, middle and dorsal segments due to the large number of gill rakers on these rows. The relative size of the pharyngeal plates was determined by sectioning the head of the specimens through the frontal plane, and calculated as the ratio of the area of the pharyngeal plates to the frontal sectional area of the dorsal or ventral surface of the oropharyngeal cavity. The specimens used for the skeletal morphology were double-stained for cartilage and bone, and cleared by the method of Dingerkus and Uhler (1977). The measurements were made following Morales and Rosenlund

(1979, see Fig. IV-8a2 for the measurement of the length of the epibranchials). The arch length is defined as the sum of the lengths of component bones in a gill arch, except basibranchials. The lever ratio of jaw-closing was calculated by dividing the length of the in-lever by the length of the out-lever (Westneat 2003; Nanami 2016) with the measurement of the lengths of the in-lever and out-lever same as reported by Tran et al. (2021, see Fig. IV-2a2). The morphology of muscular system was studied using specimens that were double stained but not cleared. The surface morphology of the pharyngeal plates and the gill rakers was observed with a scanning electron microscope (JSM-6380 LAKII, JEOL, Tokyo, Japan). The software ImageJ (version 1.51J8, National Institutes of Health, USA) was used for all measurements.

Statistical analysis

Tests of normality (Shapiro-Wilk test) and homogeneity (Levene's test) were applied for the dentition morphometrics, the lengths of gill arch bones, and relative size of the pharyngeal plates. Based on the results, Student's *t*-test with equal variance (data satisfied normal distribution and equal variance), Student's *t*-test with unequal variance (data satisfied normal distribution but heterogeneous variance) or Wilcoxon test (data unsatisfied normal distribution) were performed for the number of teeth, replacement teeth, standardized tooth length, standardized tooth width, and relative size the pharyngeal plates to compare difference between the two species. One-way ANOVA followed by post-hoc Tukey tests (data satisfied normal distribution and equal variance), one-way ANOVA followed by post-hoc Welch tests (data satisfied normal distribution but heterogeneous variance) or Kruskal-Wallis followed by Wilcoxon-Mann-Whitney tests (data unsatisfied normal distribution) were applied for the lengths of gill arches. Principal component analysis (PCA) based on a correlation matrix of dentition morphometrics was performed for the dentition morphometrics of seven species including five species reported in Tran et al. (2021) (*Boleophthalmus boddarti* (Pallas, 1770), *Oxuderces nexipinnis* (Cantor, 1849), *Scartelaos histophorus* (Valenciennes, 1837), *Periophthalmus chrysospilos* Bleeker, 1853, and *Periophthalmodon schlosseri* (Pallas, 1770))

and the two species in the present study. Rstudio version 0.99.903 (Rstudio, Inc) was used for all statistical analyses.

3. Results

Dentition

Both *Pa. serperaster* and *Pd. elongatus* have a single row of vertical teeth on the premaxilla. Frontal teeth of *Pa. serperaster* (three to four pairs) are large and fang-like (Fig. IV-1a) while more pairs (four to seven) are large with enlarged cusps in *Pd. elongatus* (Fig. IV-1b). The remaining premaxillary teeth of the two species are smaller. Premaxillary teeth in *Pd. elongatus* are sparse. On the dentary, both species have a single row of teeth along the margin extending horizontally and a pair of fang-like teeth located on the medial symphysis. *Pa. serperaster* possesses a cartilaginous finger-like projection extending laterally along the posterior margin of the dentary (Fig. IV-1a). There are significant differences in the number of teeth, standardized tooth length and tooth width between the two species (Table IV-1). Teeth in *Pa. serperaster* are significantly more numerous but smaller as shown by the lower values of standardized tooth length and tooth width on both the premaxilla and dentary. The number of replacement teeth is not significant different between the two species.

Oral jaw bones and muscles

The lever ratio of jaw-closing is 0.42 ± 0.01 (mean ± SD, N = 3) in *Pa. serperaster* and 0.47 ± 0.02 in *Pd. elongatus*. Both species have the maxillo-mandibular ligament (L1) linking the maxilla with the dentary and the premaxillo-maxillary ligament (L2) linking the premaxilla with the maxilla (Fig. IV-2). The adductores mandibulae A1, A2, and A3 attach onto the maxilla, the coronoid process of the dentary, and the medial side of the dentary, respectively.

Table IV-1 Morphological comparison of the oral jaw teeth of *Parapocryptes serperaster* and *Pseudapocryptes elongatus*

Species	Premaxilla				Dentary			
	Number of teeth	Number of replacement teeth	Standardized tooth length ($\times 10^{-3}$)	Standardized tooth width ($\times 10^{-3}$)	Number of teeth	Number of replacement teeth	Standardized tooth length ($\times 10^{-3}$)	Standardized tooth width ($\times 10^{-3}$)
Parapocryptes serperaster	67.6 ± 2.3	8.6 ± 2.3	3.2 ± 0.7	0.9 ± 0.1	53.0 ± 2.7	6.8 ± 2.28	3.2 ± 0.8	0.9 ± 0.1
Pseudapocryptes elongatus	30.3 ± 3.1	7.0 ± 2.0	6.4 ± 1.0	1.8 ± 0.3	20.2 ± 2.9	5.17 ± 0.8	7.1 ± 1.1	1.9 ± 0.4
Student's *t*-test or Wilcoxon test								
T or W values	66[##]	-1.24[#]	5.59[#]	6.45[#]	0.78[##]	7.5[##]	6.48[#]	25[##]
p	0.004	0.25	< 0.001	< 0.001	0.005	0.19	< 0.001	0.008

Numbers of teeth represent the values of both sides and replacement teeth are for the left side only (mean ± SD). Student's t-test or Wilcoxon test were applied for comparison of the parameters with significance of 95%. Tooth length and tooth width were standardized by standard length. Tooth width was measured at the base. The data on tooth length and width do not include fangs. [#] Student's *t*-test, [##] Wilcoxon test. Five individuals were used for both *Pa. serperaster* and *Pd. elongatus*.

Gill rakers

The branchial basket of *Pa. serperaster* and *Pd. elongatus* comprises four pairs of gill arches with two rows of gill rakers along each arch. The morphology of the gill rakers of the two

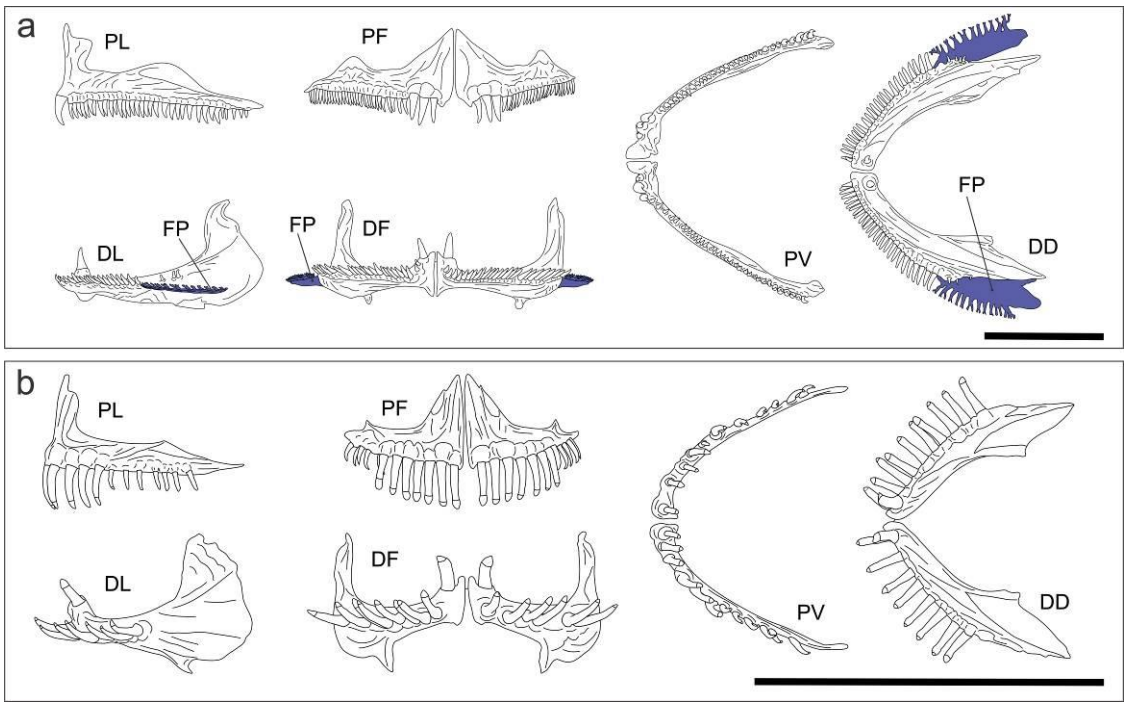

Fig. IV-1 Dention of *Parapocryptes serperaster* (**a**) and *Pseudapocryptes elongatus* (**b**). *DD* dentary in dorsal view, *DF* dentary in frontal view, *DL* dentary in lateral view, *FP* finger-like projection, *PF* premaxilla in frontal view, *PL* premaxilla in lateral view, and *PV* premaxilla in ventral view. Scale bars: 5mm

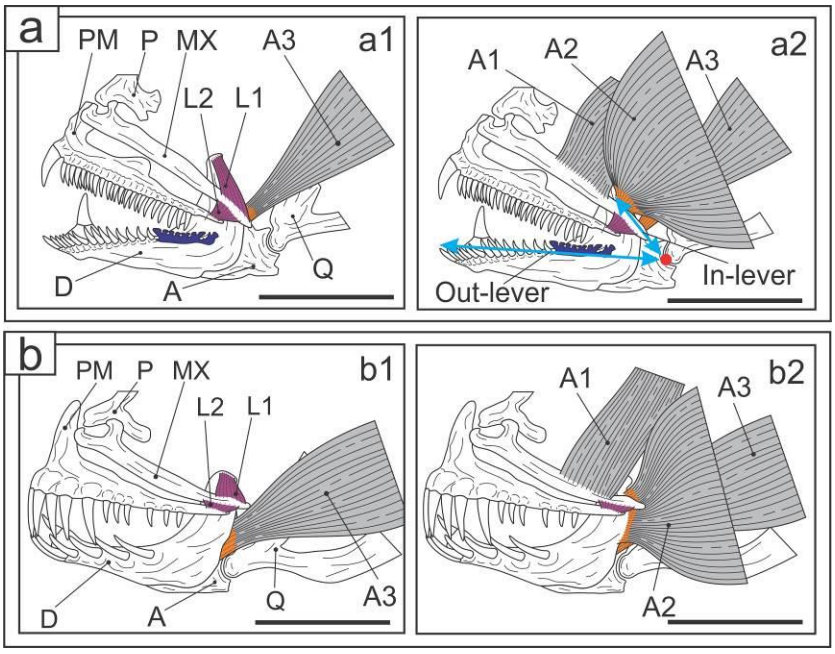

Fig. IV-2 Jaw bones and ligaments in *Parapocryptes serperaster* (**a1**) and *Pseudapocryptes elongatus* (**b1**), and adductores mandibulae in *Parapocryptes serperaster* (**a2**) and *Pseudapocryptes elongatus* (**b2**). *A* articular, *A1–3* adductores mandibulae 1 to 3, *D* dentary, *L1,2* ligaments 1 (maxillo-mandibular ligament) and 2 (premaxillo-maxillary ligament), *MX* maxilla, maxilla, *P* palatine,

PM premaxilla, *Q* quadrate. Ligaments are shown in purple and tendons are in orange. In **a2**, red dot shows the fulcrum, and double headed arrows (blue) show the jaw-closing lever system. Scale bars: 5 mm

species is similar with short and sparsely spaced gill rakers on the first, second and anterior row of the third arch, and comb-like and more densely spaced gill rakers on the posterior row of the third arch and both row of the fourth arch (Figs. IV-3, IV-4, and IV-5). The gill rakers extend laterally from the inner surface (facing the oropharyngeal cavity) of gill arches along their entire lengths. Each gill raker blade has a triangular shape in cross-section both in *Pa. serperaster* (Figs. IV-3a1 and IV-3a2) and *Pd. elongatus* (Figs. IV-3b1 and IV-3b2).

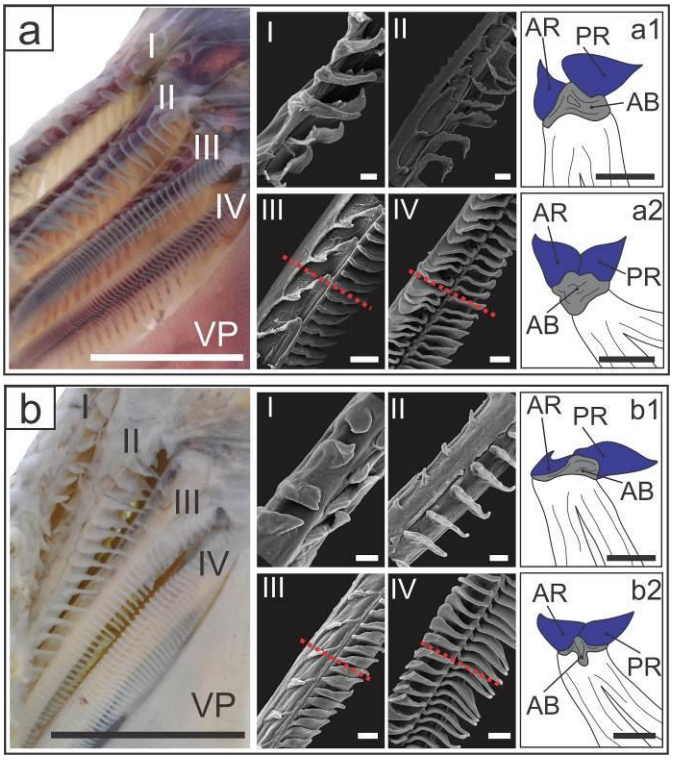

Fig. IV-3 Morphology of the gill rakers in *Parapocryptes serperaster* (**a**) and *Pseudapocryptes elongatus* (**b**). In each box, the left photograph shows the dorsal view of the left gill arches, and the right ones are SEM micrographs of each gill arch. The red dashed lines in the SEM micrographs indicate the position of cross-sectioning. Cross-sectional views of the third and fourth arches are shown in **a1**, **a2**, **b1**, and **b2**. *AB* arch bone, *AR* anterior row, *I–IV* first to fourth gill arches, *PR* posterior row, *VP* ventral pharyngeal plate. Scale bars: 2 mm for the photographs, 200 μm for SEM micrographs, and 0.5 mm for **a1**, **a2**, **b1**, and **b2**

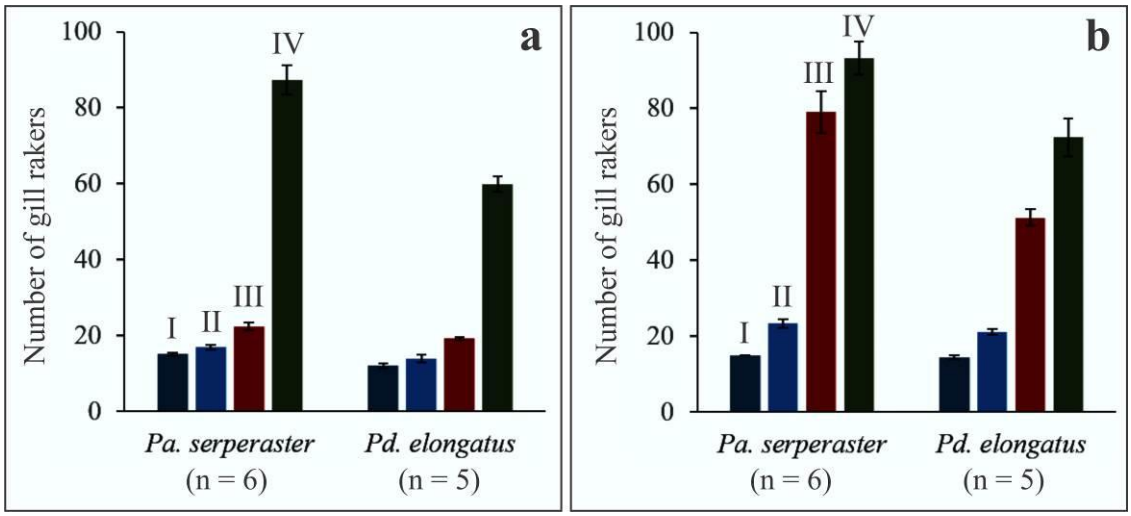

Fig. IV-4 Number of gill rakers (mean ± SD) on the anterior (**a**) and posterior (**b**) gill arches of *Parapocryptes serperaster* and *Pseudapocryptes elongatus*. *I–IV* first to fourth gill arches. Size range of *Parapocryptes serperaster*: 154–186 mm in standard length (SL) and *Pseudapocryptes elongatus*: 150–167 mm SL. The number of individuals used for the measurement is given in parenthesis

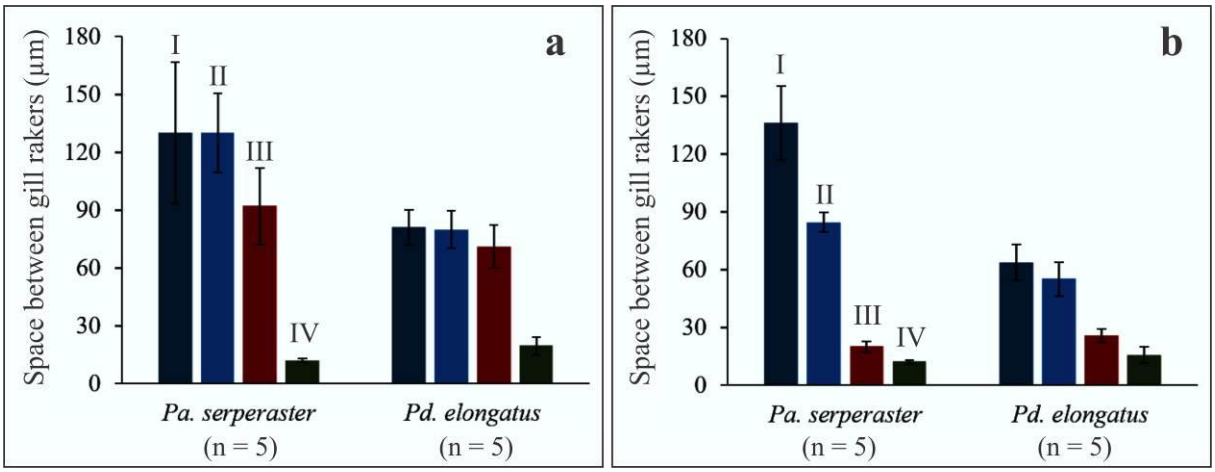

Fig. IV-5 Average space between the gill rakers (mean ± SD) on the anterior (**a**) and posterior (**b**) gill arches of *Parapocryptes serperaster* and *Pseudapocryptes elongatus*. Symbols and size range of fish are the same as in Fig. IV-4. The number of individuals used for the measurement is given in parenthesis

Pharyngeal plates

The pharyngeal plates of the two species show morphological similarities; these include the strong curvature of the plates (Figs. IV-10a and IV-10b), numerous fine papilliform teeth and lesser numbers of canine teeth in both dorsal and ventral pharyngeal plates (Figs. IV-6a and IV-6b, Table IV-2), the distribution of canine teeth (along the anterior and medial margins of both plates), and the overlapping of the third and fourth pharyngobranchials (PB3 and PB4) to form a one large unit of the dorsal pharyngeal plate (Figs. IV-8a and IV-8b). The papilliform teeth on the ventral pharyngeal plates of both species are arranged in lines, and are hook-like (Figs. IV-6a4, IV-6a5, IV-6b4, and IV-6b5). Interspecific differences are the size of the plates (*Pa. serperaster* > *Pd. elongatus*, Fig. IV-7), density and directions of papilliform teeth (dorsal plate only, Table IV-2) and canine teeth (Figs. IV-6a1 and IV-6a2 for *Pa. serperaster*; Figs. IV-6b3 and IV-6b6 for *Pd. elongatus*; see also Table IV-2), and a larger extent of overlapping of PB3 and PB4 in *Pa. serperaster* (Fig. IV-8a1) than in *Pd. elongatus* (Fig. IV-8b1).

Table IV-2 Tooth morphology, density, and direction of the pharyngeal plates of *Parapocryptes serperaster* and *Pseudapocryptes elongatus*

Species	Shape	Density (number/mm^2)		Direction	
		Dorsal plate	Ventral plate	Dorsal plate	Ventral plate
Parapocryptes serperaster	papilliform	515.4 ± 83.4	209.5 ± 33.3	PM	PM
	canine*			DV	DV
Pseudapocryptes elongatus	papilliform	187.3 ± 35.4	149.0 ± 14.3	DV	PM
	canine*			posterior	anterior

* Along the anterior and medial margins of the dorsal and ventral plates. Mean ± SD, N = 3 for *Pa. serperaster*, N = 4 for *Pd. elongatus*. DV, dorsoventral; PM, posteromedial.

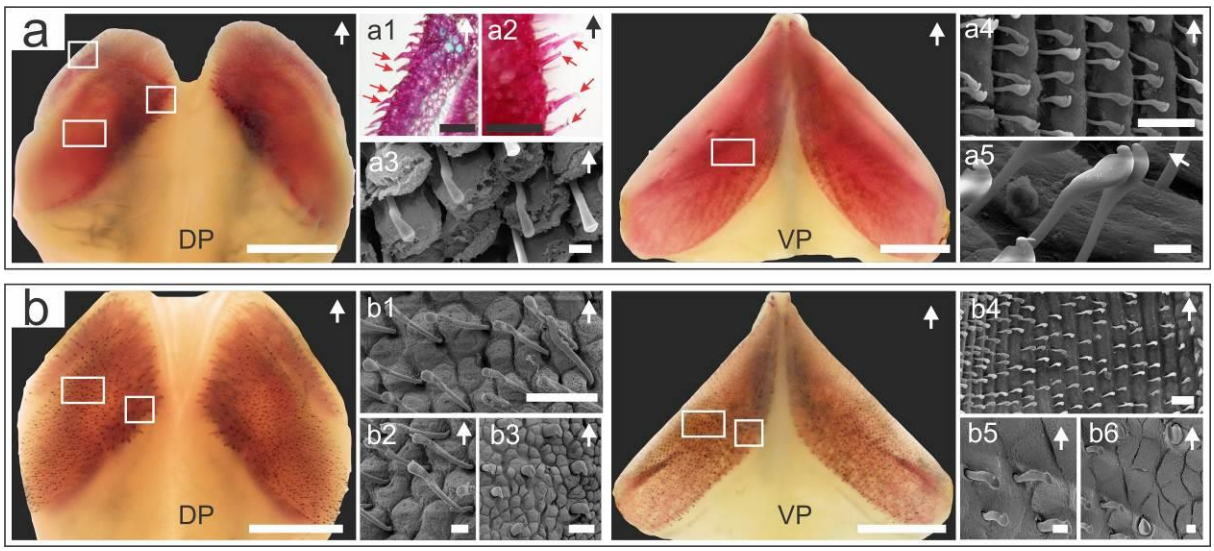

Fig. IV-6 Morphology of the pharyngeal plates of *Parapocryptes serperaster* (**a**) and *Pseudapocryptes elongatus* (**b**). Color photographs show surface views of the dorsal (DP) and ventral (VP) pharyngeal plates, accompanied by SEM and LM micrographs. At the same row, **a1**, **a2**, and **a3** correspond to the upper left, upper right, and lower boxes of the DP, respectively. **a4** corresponds to the box in VP. **b1** and **b3** correspond to the upper and lower boxes of the DP. **b4** and **b6** correspond to the upper and lower boxes of the VP. **a5**, **b2**, and **b5** show pharyngeal teeth in the corresponding color photographs at different magnifications. Red arrows in **a1** and **a2** show canine teeth on the marginal edges of the right dorsal pharyngeal plate. Arrows on the upper right corners of color photographs and the SEM micrographs indicate the anterior direction. Scale bars: 2 mm for color photographs; 500 μm for **a1-2**; 100 μm for **a4**, **b1**, **b3**, **b4**, and 20 μm for **a3**, **a5**, **b2**, **b5,** and **b6**

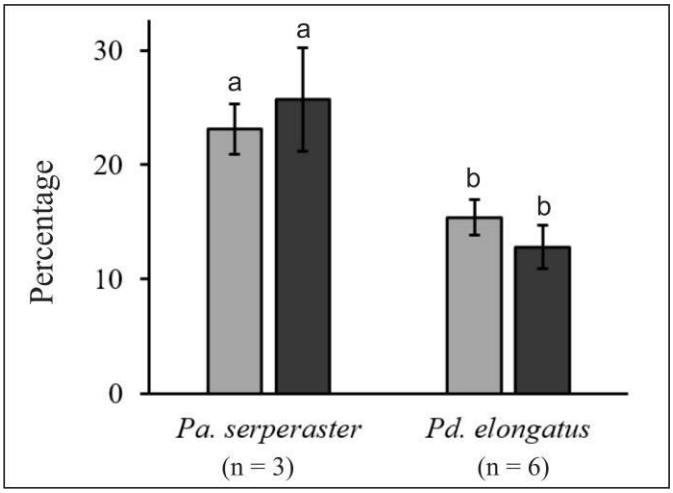

Fig. IV-7 The relative size (area of pharyngeal plates/frontal sectional area of the dorsal or ventral surface of the oropharyngeal cavity) (mean ± SD) of the dorsal (light gray bars) and ventral (dark gray bars) pharyngeal plates. Student's *t*-test and Wilcoxon test were performed to compare the relative size of the dorsal and ventral pharyngeal plates between the two species, respectively. Data with different letters of the dorsal or ventral pharyngeal plate are significantly different ($p < 0.05$). The number of individuals used for the measurement is given in parenthesis

Branchial basket skeleton

The ratios of length to width of the first to fourth ceratobranchials (CB1-4, mean ± SD, N = 3) are 14.96 ± 3.80 in *Pa. serperaster* and 13.48 ± 1.99 in *Pd. elongatus*. The basihyal (BH) is bifurcated in *Pa. serperaster* (Fig. IV-8a) but flabelliform in *Pd. elongatus* (Fig. IV-8b). The

second pharyngobranchial (PB2) extends along the anterior margin of the PB3 and PB4 in both *Pa. serperaster* (Fig. IV-8a1) and *Pd. elongatus* (Fig. IV-8b1). The fourth epibranchial (EB4) is L-shaped in *Pa. serperaster* (91.2 ± 0.8°, mean ± SD, N = 5, Fig. IV-8a2) but more obtuse in *Pd. elongatus* (117.7 ± 1.2°, N = 6, Fig. IV-8b2). There is no significant difference among the arch lengths of the two species (Table IV-3).

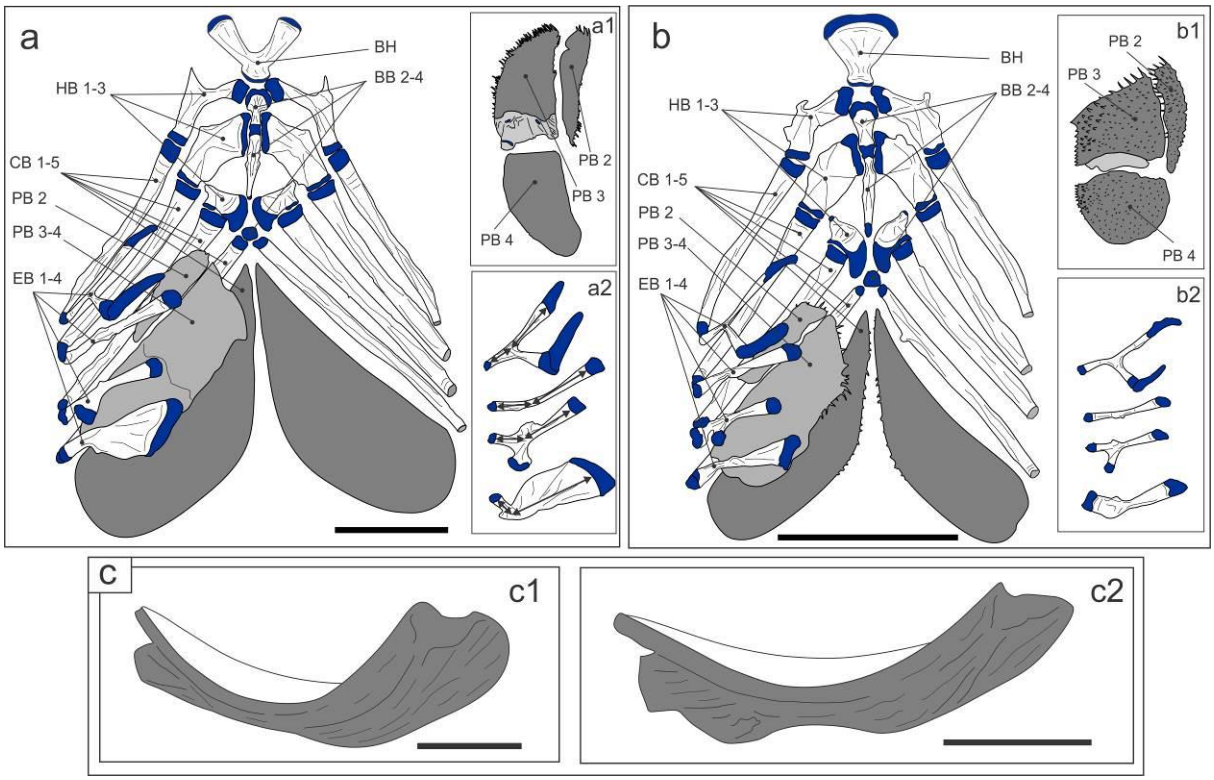

Fig. IV-8 Morphology of the branchial basket skeletons (dorsal view) and the left fifth ceratobranchials (=ventral pharyngeal plate, lateral view) of *Parapocryptes serperaster* (**a**, **c1**) and *Pseudapocryptes elongatus* (**b**, **c2**). In each box of **a** and **b**, the whole structure is shown on the left; the excised left dorsal pharyngeal plate is shown in ventral view in **a1** and **b1**; and the isolated right epibranchials are shown in ventral view in **a2** and **b2**. The portion of the third pharyngobranchial covered by the fourth pharyngobranchial is shown in light grey in **a1** and **b1**. Cartilages are in blue. Grey parts in box **c** are the ventral surface of the fifth ceratobranchial. Double headed arrows in **a2** indicate length measurement. *BB 2–4* basibranchials 2–4, *BH* basihyal, *CB 1–5* ceratobranchials 1–5, *EB 1–4* epibranchials 1–4, *HB 1–3* hypobranchials 1–3, *PB 2,3,4* pharyngobranchials 2,3,4. BB1 is a small cartilage between the right and left HB1s, and therefore not shown. Scale bars: 5 mm for boxes **a** and **b**, 2 mm for box **c**

Table IV-3 Comparison of the arch lengths (mean ± SD) of *Parapocryptes serperaster* and *Pseudapocryptes elongatus*

	Arch length (mm)						
	N	Arch 1	Arch 2	Arch 3	Arch 4	ANOVA	
						F	*p*
Parapocryptes serperaster	6	18.9 ± 2.3[a]	19.8 ± 2.1[a]	19.0 ± .1[a]	20.8 ± 2.0[a]	1.0	0.40
Pseudapocryptes elongatus	7	13.9 ± 1.8[a]	12.9 ± 1.6[a]	12.3 ± 1.6[a]	12.6 ± 1.7[a]	1.1	0.36

No significant difference was detected for the arch length in each species (one-way ANOVA).

Branchial basket musculature

The branchial basket musculature of the two species consists of four systems. The first system connects element bones of the branchial basket to the surrounding skeletal components: the levatores interni (LI, LI'), the levatores externi (LE), the levator posterior (LP), the retractor dorsalis (RD), the pharyngohyoideus (PH), the rectus ventralis (RV), the pharyngocleithralis externus (PHCE), and the pharyngocleithralis internus (PHCI) (Figs. IV-9a3 and IV-9b3). The second system link element bones dorsally: the transversi dorsales anteriores (TDA), the transversi dorsales posteriores (TDP), the obliqui dorsales (OD), a ligament (L3-4) connecting the third and fourth epibranchials, and a structure resembling the cartilaginous cushion (CC) described by Liem (1974) between the left and right TDA and TDP (Figs. IV-9a1 and IV-9b1). The third system links the element bones ventrally: the transversi ventrales (TV), the obliqui ventrales (OV), and the semicircular ligament (SL) of the third system (Figs. IV-9a2 and IV-9b2). The fourth system connects the ceratobranchials to the epibranchials (Figs. IV-9a3 and IV-9b3). RD connects to the anterior portion of the fourth vertebra in both *Pa. serperaster* and *Pd. elongatus* (Fig. IV-11). When viewed dorsally, it is evident that the muscles of the second system are positioned more posteriorly in *Pd. elongatus* then in *Pa. serperaster* (Fig. IV-9).

4. Discussion

The feeding apparatus of *Parapocryptes serperaster* and *Pseudapocryptes elongatus* shares similar morphologies in several respects, but there are also differences. Similarities are heterogeneous development of gill rakers among gill arches, strongly curved pharyngeal plates studded with numerous papilliform teeth and a lesser number of canine teeth, branchial basket skeleton with nearly equal arch length, and branchial basket musculature of similar configuration. The directions of premaxillary (vertical) and dentary (horizontal) teeth are identical in the two species. On the other hand, a closer comparison reveals morphological differences between them. The number of teeth in *Pa. serperaster* is more than double that in

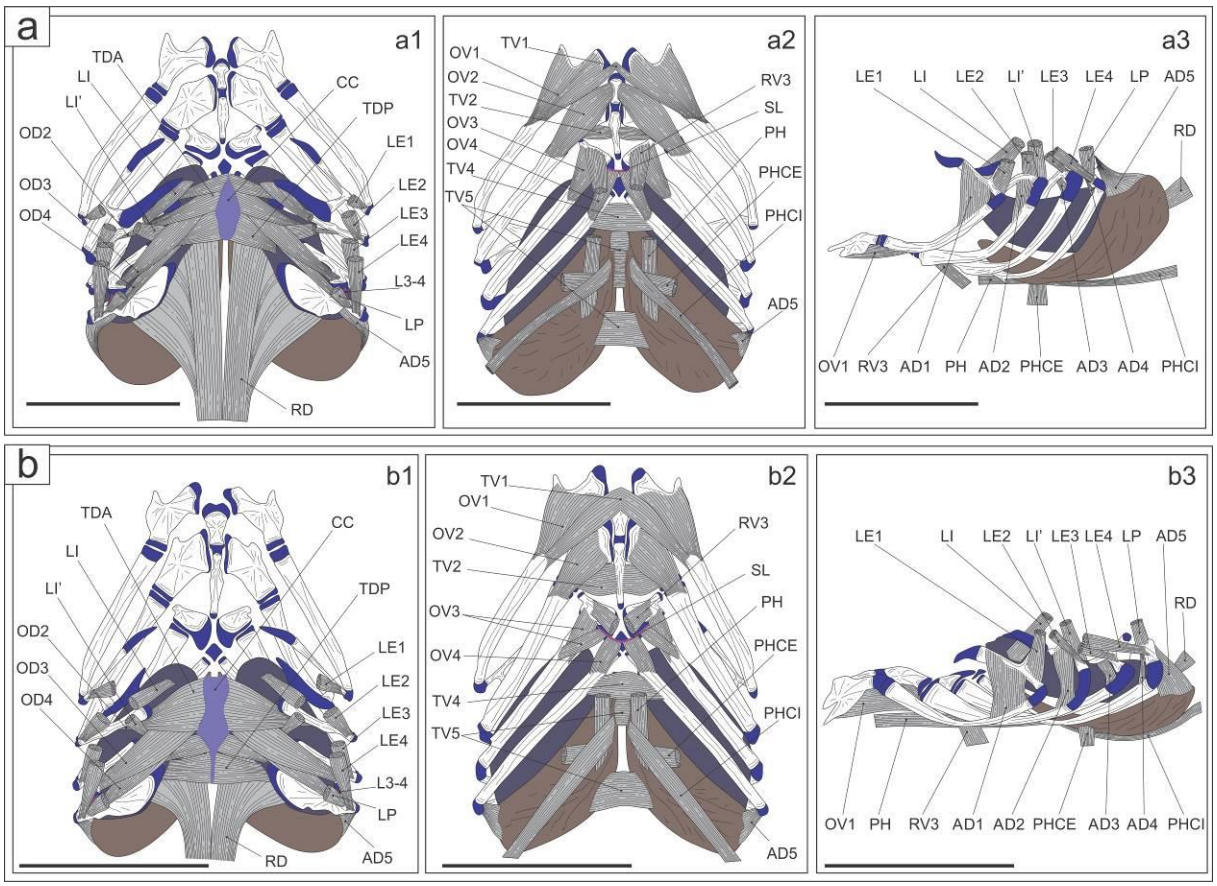

Fig. IV-9 Morphology of branchial basket musculature of *Parapocryptes serperaster* (**a**) and *Pseudapocryptes elongatus* (**b**). **a1** and **b1** are dorsal views, **a2** and **b2** ventral views and **a3** and **b3** lateral views. *AD1–5* adductors 1 to 5, *CC* cartilaginous cushion, *L3–4* ligament 3–4 connecting the third and fourth epibranchials, *LE1, 2* levatores externi 1 to 2, *LE3–4* levatores externi 3 and 4 acting on the third and fourth epibranchials, *LI* and *LI'* levatores interni, *LP* levator posterior, *OD2–4* obliqui dorsales 2 to 4, *OV1–4* obliqui ventrales 1 to 4, *PH* pharyngohyoideus, *PHCE* pharyngocleithralis externus, *PHCI* pharyngocleithralis internus, *RD* retractor dorsalis, *RV3* rectus ventralis 3, *SL* semicircular ligament, *TDA* transversus dorsalis anterior, *TDP* transversus dorsalis posterior, *TV1–5* tranversi ventrales 1 to 5. Cartilages in blue; dorsal pharyngeal plate in dark purple; ventral pharyngeal plate in brown. Scale bars: 5 mm

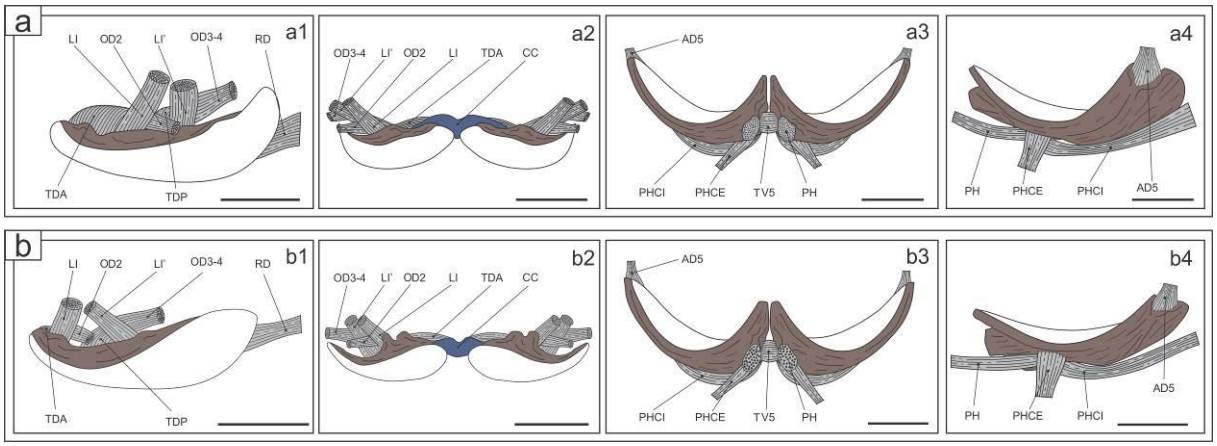

Fig. IV-10 Morphology of musculature system attaching to the pharyngeal plates in *Parapocryptes serperaster* (**a**) and *Pseudapocryptes elongatus* (**b**). **a1**,**b1** are lateral views of the left dorsal pharyngeal plate, **a2**,**b2** and **a3**,**b3**

frontal views of the dorsal and ventral pharyngeal plates, respectively, and **a4**,**b4** lateral views of the left ventral pharyngeal plates. Abbreviations are the same as in Fig. IV-9. The ventral side of the ventral pharyngeal plates and the dorsal side of the dorsal pharyngeal plates are colored in brown. Scale bars: 2 mm

Ps. elongatus for both premaxilla and dentary, while the size of the teeth in *Pa. serperaster* is only half that of *Ps. elongatus* for both length and width (Table IV-1). The size of the pharyngeal plates is larger in *Pa. serperaster* than in *Ps. elongatus* (Fig. IV-7), and the density of papilliform teeth is higher in *Pa. serperaster* than in *Ps. elongatus* (Table IV-2). The contrast between *Pa. serperaster* and *Ps. elongatus* is similar to the morphological differences of the feeding apparatus between *Boleophthalmus boddarti* and *Scartelaos histophorus* reported in our previous paper (Tran et al. 2021): The number of oral jaw teeth was 65.6 (*B. boddarti*) and 29.0 (*S. histophorus*) in the premaxilla and 78.8 (*B. boddarti*) and 43.2 (*S. histophorus*) in the dentary. Standardized tooth length and width of *S. histophorus* are larger than those of *B. boddarti* except tooth width of the dentary. The size of the ventral, but not dorsal, pharyngeal plate is significantly larger in *B. boddarti* than in *S. histophorus*, and the density of papilliform teeth is higher in *B. boddarti* (dorsal plate 950 teeth/mm^2, ventral plate 530) than in *S. histophorus* (dorsal plate 150, ventral plate 140). In fact, the values for *S. histophorus* are quite similar to those in *Pd. elongatus* (Table IV-2).

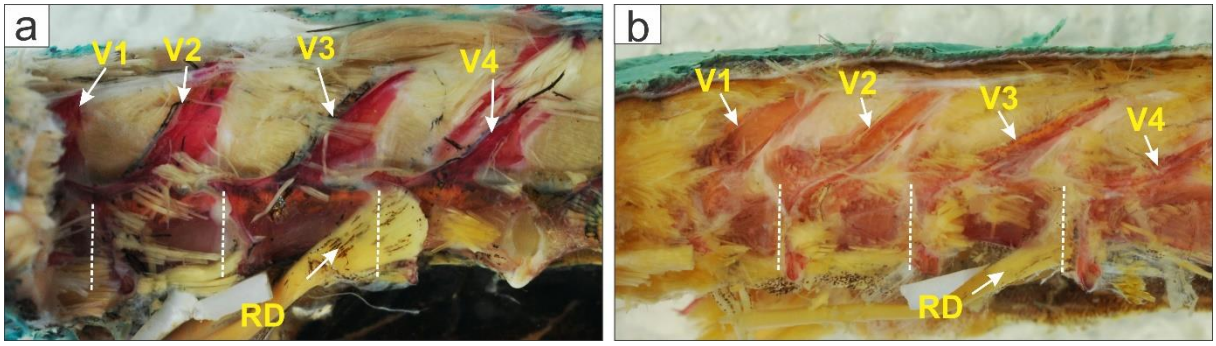

Fig. IV-11 Insertion of the retractor dorsalis to vertebrae in *Parapocryptes serperaster* (**a**) and *Pseudapocryptes elongatus* (**b**). Symbols: *RD* retractor dorsalis, *V1*-*V4* neural spines of the first to fourth vertebrae. Dashed lines show joint between vertebrae

The morphological similarity of *Pa. serperaster* to *B. boddarti* and of *Pd. elongatus* to *S. histophorus* is also supported by the PCA of the oral jaw teeth data (Fig. IV-12). It separates

the seven species of mudskippers (the two species analyzed in this study plus five species reported by Tran et al. 2021; *B. boddarti*, *O. nexipinnis*, *Pn. schlosseri*, *Ps. chrysospilos*, and *S. histophorus*) into three groups in the morphometric multivariate space. The first two components (PC1 and PC2) explain 77.8% of total variance. Along PC1, *Pa. serperaster* and *B. boddarti* are separated from the other species by higher number of teeth, and smaller values of the standardized tooth length and tooth width on both the premaxilla and dentary. Along PC2, *Pa. serperaster* was assigned to the same group with *B. boddarti*, while *Pd. elongatus* belongs to the same group with *O. nexipinnis* and *S. histophorus*. *Ps. chrysospilos* and *Pn. schlosseri*, the two most terrestrial and carnivorous species (Clayton 2017; Tran et al 2021), are separated from the other species by higher number of replacement teeth, and lower number teeth on both the premaxilla and dentary.

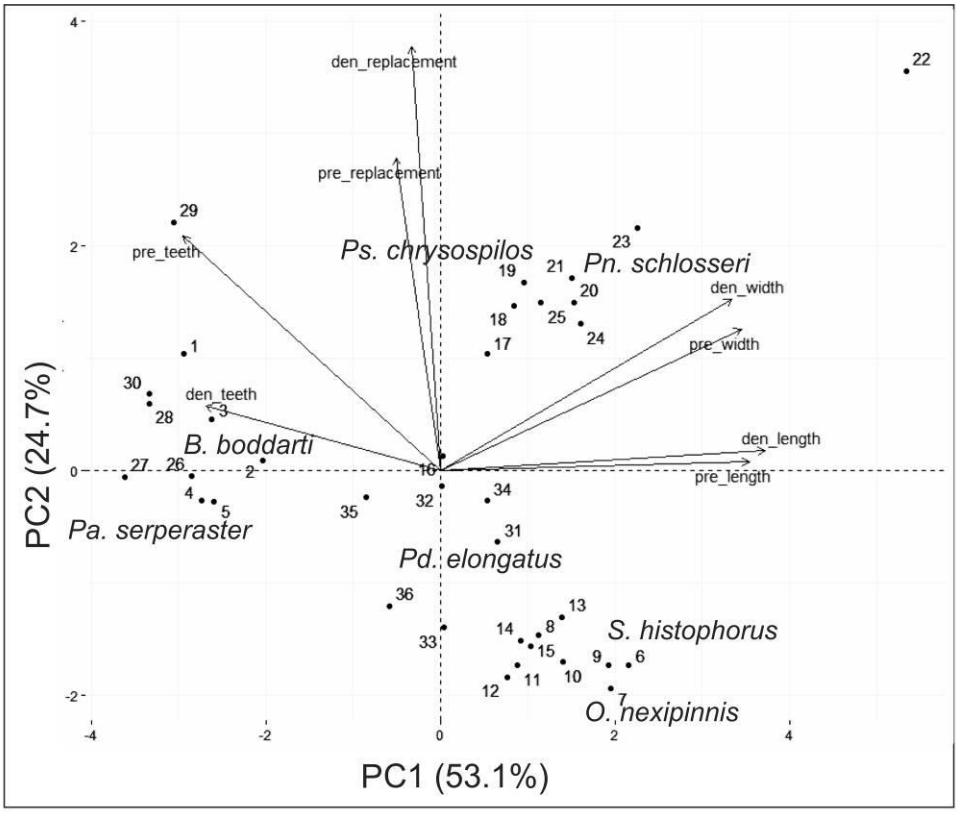

	PC1	PC2
pre_teeth	-0.75	0.53
pre_replacement	-0.13	0.71
pre_length	0.90	0.02
pre_width	0.88	0.32
den_teeth	-0.68	0.15
den_replacement	-0.08	0.96
den_length	0.95	0.04
den_width	0.85	0.39

Fig. IV-12 PCA biplot of the two principal components (PC1, PC2) showing the multivariate morphometric ordination of the studied taxa (upper box). The morphological variables are represented by vectors; correlated variables have a similar orientation. Loadings of each variable along PC1 and PC2 are shown in the lower table. Symbols: *den_length* standardized tooth length on the dentary, *den_replacement* number of replacement teeth on the dentary, *den_teeth* number of teeth on the dentary, *Dim 1 – Dim 5* dimension 1 to 5, *pre_length* standardized tooth length on the premaxilla, *pre_replacement* number of replacement teeth on the premaxilla, *pre_teeth* number of teeth on the premaxilla, *pre_width* standardized tooth width on the premaxilla. Points 1-5 are the data of *Boleophthalmus boddarti*, 6-10 *Oxuderces nexipinnis*, 11-15 *Scartelaos histophorus*, 16-20 *Periophthalmus chrysospilos*, 21-25 *Periophthalmodon schlosseri*, 26-30 *Parapocryptes serperaster*, and 31-36 *Pseudapocryptes elongatus*

Although ecological data are scarce for *Pa. serperaster* and *Pd. elongatus*, the morphological similarity of the feeding apparatus of *Pa. serperaster* to *B. boddarti* and of *Pd. elongatus* to *S. histophorus* might be explained by the feeding habits of these fishes. *Pa. serperaster* was reported to be herbivorous, feeding mainly on both diatoms and detritus (Dinh et al. 2017) or almost exclusively (ca. 90%) on diatoms (Khaironizam and Norma-Rashid 2000). *B. boddarti* (and other *Boleophthalmus* species) is known as purely herbivorous (Yang et al. 2003; Chaudhuri et al. 2014; Tran et al. 2020,2021). There are some discrepancies about the feeding habit of *Pd. elongatus* among papers. Bucholtz et al. (2009) reported pure herbivory (> 90% of gut content was diatoms) of the fish collected in the Mekong Delta, while Chaudhuri et al. (2014) found omnivory (food items consisting of phytoplankton, zooplankton and other animals) of the fish from the Indian Sundarban. Similarly, *S. histophorus* was reported as omnivorous by Chan (1989) and Tran et al. (2021), but a congener, *S. tenuis* was reported as carnivorous by Abidizadegan et al. (2015) and Abdoli et al. (2012). Even though the feeding habits of *Pa. serperaster* and *Pd. elongatus* are obscure to some extent, it may be concluded that the teeth are more numerous and smaller, and the pharyngeal plates are larger and have more papilliform teeth in herbivorous (or more exactly microalgal-feeding) species than in omnivorous species.

On the other hand, we speculate that morphological differences of the feeding apparatus between *Pa. serperaster* and *B. boddarti* and between *Pd. elongatus* and *S.*

histophorus are related to the different terrestriality of these fishes. The morphological differences between *Pa. serperaster* and *B. boddarti* include the number of gill rakers on the posterior row of the third gill arch and the anterior and posterior rows of the fourth gill arch (80-90 in *Pa. serperaster* vs. ca. 130 in *B. boddarti*) and the density of papilliform teeth in the dorsal (515 teeth/mm^2 in *Pa. serperaster* vs. 950 in *B. boddarti*) and ventral (210 in *Pa. serperaster* vs. 530 in *B. boddarti*) pharyngeal plates. More terrestrial *B. boddarti* might need a higher efficiency in separating food items (diatoms) and mud particles than *Pa. serperaster*, because *B. boddarti* probably ingests a higher ratio of mud particles when the fish scrapes the top surface layer of the sediment on the exposed mudflat than when *Pa. serperaster* ingests diatoms in the water bottom (see later). The morphological differences between *Pd. elongatus* and *S. histophorus* include the number of dentary teeth (20 in *Pd. elongatus* vs. 43 in *S. histophorus*) and the density of gill rakers on the anterior row of the third and fourth gill arches (60-70 in *Pd. elongatus* vs. 0 in *S. histophorus*). These differences might stem from a higher reliance of *S. histophorus* on animal foods than *Pd. elongatus*, which appears to feed largely on microalgae and detritus on the water bottom, at least in the population of the Mekong Delta (see Video IV-1). However, there is evidence that *Pd. elongatus* feeds on an exposed mudflat in some other habitat (see Fig. 4.5.5 of Ishimatsu and Gonzales (2011), a photograph taken by the late Professor Toru Takita, showing terrestrial feeding of *Pd. elongatus* in Penang, Malaysia).

In our previous paper (Tran et al. 2021), we hypothesized that the early oxudercine gobies that started to expand their niche onto land were semiterrestrial herbivorous or omnivorous grazers. The hypothesis was based on the data that among the 10 oxudercine genera, those with no (*Apocryptodon*) or the lowest (*Apocryptes*, *Oxuderces*, *Parapocryptes* and *Pseudapocryptes*) degrees of terrestriality are mostly herbivorous or omnivorous, those with moderate degrees of terrestriality are either omnivorous or herbivorous (*Boleophthalmus* and *Scartelaos*), and those with the highest degree of terrestriality are carnivorous (*Periophthalmodon* and *Periophthalmus*). The feeding habit of *Zappa* is currently unknown.

We further speculated that during the terrestrialization process, oxudercine gobies might have diverged into more specialized herbivorous species (*Boleophthalmus*) and carnivorous species (*Periophthalmus* and *Periophthalmodon*) through intermediate stages as seen in *Scartelaos*. Presently, we lack sufficient data for testing the hypothesis, particularly for those mudskipper species with lower degrees of terrestriality (for details, see Table S1 of Tran et al. 2021). There seems to be a large variability in amphibiousness of these fishes even within a species. For example, we observed emersion of *O. nexipinnis* of short (usually less than five seconds) duration, which appears to be for feeding, in a mudflat of Bac Lieu Province in the Mekong Delta (Video IV-2), but we did not observe such behavior for the same species in a mudflat of a neighboring Province, Soc Trang (Ishimatsu et al. unpublished).

Video IV-1 *Pseudapocryptes elongatus* feeding in shallow water. Recorded in a coastal pond in Bac Lieu Province, Vietnam in December 2013.
(Video is available from the author)

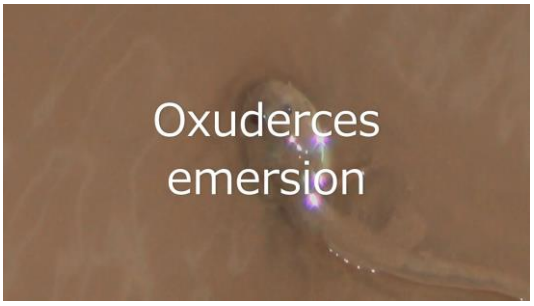

Video IV-2 Emersion of *Oxuderces nexipinnis*. Recorded in a mudflat in Bac Lieu Province, Vietnam in October 2013.
(Video is available from the author)

Table IV-4 summarizes the present knowledge on the emersion behavior, air gulping behavior, and respiratory capillaries in the inner mucosa of the bucco-opercular cavity and the skin, the accessory respiratory organs of mudskippers. It is evident that data are nearly non-existent for five genera, *Apocryptes*, *Apocryptodon*, *Oxuderces*, *Parapocryptes*, and *Zappa*. Filling these knowledge gaps together with better understanding of feeding habits in the 10 genera would help elucidate how the morphology and physiology of feeding system has been modified during the process of terrestrialization in mudskippers.

Table IV-4 Comparison of land emersion and air gulping behaviors and the distribution of respiratory capillaries in the skin and the mucosa of the bucco-opercular cavity in oxudercine gobies

Genus	Land emersion	Air gulping	Capillaries inside the mouth	Capillaries in the skin
Periophthalmus	++ (12,16,17)	+ (7)	+ (6,14)	+ (14,15,19,20)
Periophthalmodon	++ (8,10)	+ (1)	+ (6,14)	+ (14,19)
Boleophthalmus	+ (12,17)	+ (7)	+ (9,14)	+ (9,11,14,18,20)
Scartelaos	+ (17)	+ (7)	+ (14)[a]	+ (2,14,18)
Zappa	+ (13)	?	?	?
Pseudapocryptes	+ (17)	+ (3,7)	+ (14)[b]	+ (14)[b]
Apocryptes	+? (8)	?	?	?
Apocryptodon	-? (5)	?	?	?
Oxuderces	+? (17)[c]	?	?	?
Parapocryptes	-? (4)	?	?	?

[a]Reported as *Boleophthalmus viridis* (see Ishimatsu and Ishimatsu 2021); [b]Reported as *Apocryptes lanceolatus* (see Ishimatsu and Ishimatsu 2021); [c]See Discussion.
References (1) Aguilar et al 2000, (2) Beon et al 2013, (3) Das 1934, (4) Dinh et al 2014, (5) Dôtu 1961, (6) Gonzales et al 2011, (7) Graham et al 2007, (8) Hora 1936, (9) Ishimatsu et al (submitted to J. Morphol.), (10) Mai et al 2019, (11) Park et al 2003, (12) Polgar and Bartolino 2010, (13) Polgar et al 2010, (14) Schöttle 1933, (15) Suzuki 1992, (16) Takeda et al 2012, (17) Takita et al 1999, (18) Zhang et al 2000, (19) Zhang et al 2003, (20) Yokoya and Tamura 1992

Chapter V

MORPHOLOGY OF THE FEEDING APPARATUS IN TWO OXUDERCINE GOBIES, *Periophthalmus modestus* Cantor, 1842 and *Periophthalmodon septemradiatus* (Hamilton, 1822)

1. Introduction

One of major events of vertebrate evolution is the transition from water to land, which is associated with modifications of movement, respiration, reproduction, sensory systems, and feeding (Carroll 2001; Clack 2012). Due to air is much lower density and viscosity compared to water, feeding modes used in aquatic environment, i.e., ram feeding, suction feeding and biting with suction being the most popular, are impractical on land (Wainwright et al. 2015). Therefore, feeding modes must have to modified from suction to prehension as vertebrates invaded land (Schwenk and Rubega 2005; Heiss et al. 2018; Ashley-Ross et al. 2013). Little is known about intermediate steps of the feeding transition.

Oxudercine gobies adapt to live in different degrees of terrestirality and show various feeding habits (Clayton 1993,2017; Tran et al. 2020,2021), and therefore are ideal models for studying feeding transition. In our preceding papers (Tran et al. 2020,2021; unpublished data, manuscript submitted to Zoomorphology), we investigated feeding apparatus of eight oxudercine gobies showing low (*Parapocryptes serperaster* (Richardson, 1864), *Oxuderces nexipinnis* (Cantor, 1849), and *Pseudapocryptes elongatus* (Cuvier, 1816)) to moderate and high terrestriality (*Scartelaos histophorus* (Valenciennes, 1837), *Boleophthalmus boddarti* (Pallas, 1770), *B. pectinirostris* (Linnaeus, 1758), *Periophthalmodon schlosseri* (Pallas, 1770), and *Periophthalmus chrysospilos* Bleeker, 1852) and varying feeding habits. Data suggested that feeding apparatus and feeding habit are modified as fish expanded their niche onto land. We also hypothesized that earliest emerge oxudercine gobies could be semi-terrestrial herbivorous or omnivorous grazers, and they then diverged into specialized herbivores and carnivores during terrestiralization proccess. The present study analyses the feeding apparatus

of two mudskipper species [*Periophthalmodon septemradiatus* (Hamilton, 1822) and *Periophthalmus modestus* Cantor, 1842] and compares to the morphology of the four mudskipper species in the preceding studies, i.e., *B. boddarti, B. pectinirostris, Ps. chrysospilos*, and *Pn. schlosseri* showing moderate and high terrestriality, in order to consolidate the hypothesis and gain more understanding of the feeding transition. Both *Ps. modestus* and *Pn. septemradiatus* show high terrestriality (Table S1) with *Pn. septemradiatus* reported rarely venture into water (Mai et al. 2019).

2. Materials and methods

Fish collection and preservation

A total 68 individuals of the two species were used in this study. *Pn. septemradiatus* (size ranging from 66.0 to 93.0 mm SL) was collected from river banks of a tributary of Hau River (10° 02’ 58”N, 105° 43’ 25”E; Binh Thuy District, Can Tho City, Vietnam) in September 2017, December 2017 and June 2018. *Ps. modestus* (size ranging from 48.0 to 66.5 mm SL)was collected from the Ariake Sea (33° 11’ 45.4”N, 130° 12’ 26.1”E; Saga Prefecture, Japan) in October 2016, June 2017 and August 2018. The methods of sacrifice and preservation were same as reported in Tran et al. (2020,2021).

Morphological methods

The morphological parameters and the methods used to collect data were same as reported by Tran et al. (2020,2021). Dentition morphometrics include number of teeth, replacement teeth, tooth length (standardized by standard length), and tooth width (standardized by standard length) of the premaxilla and dentary. The spaces between the gill rakers were measured for the entire length of four arches. The relative size of the pharyngeal plates, the arch length, the lever ratio of jaw-closing were also determined same as reported in the preceding papers. The methods of double-staining and clearing (Dingerkus and Uhler 1977) were applied for the skeletal (both methods) and the musculature (only double-staining) morphologies. The surface

morphology of the pharyngeal plates and the gill rakers was observed with a scanning electron microscope (JSM-6380 LAKII, JEOL, Tokyo, Japan). The software ImageJ (version 1.51J8, National Institute of Health, USA) was used for all measurements.

Statistical analysis

The morphometrics of the two species in the present study and the four species (*B. boddarti*, *B. pectinirostris*, *Ps. chrysospilos*, and *Pn. schlosseri*) in the preceding studies was statistical analyzed. Tests of normality (Shapiro-Wilk test) and homogeneity (Levene's test) were applied for the dentition morphometrics, the arch lengths and the relative size of the pharyngeal plates. Based on results, One-way ANOVA followed by post-hoc Tukey tests (data satisfied normal distribution and equal variance), one-way ANOVA followed by post-hoc Welch tests (data satisfied normal distribution but heterogeneous variance) or Kruskal-Wallis followed by Wilcoxon-Mann-Whitney tests (data unsatisfied normal distribution) were applied for dentition morphometrics (except standardized cusp width of *B. boddarti* and *B. pectinirostris*). Student's *t*-test with equal variance (data satisfied normal distribution and equal variance), Student's *t*-test with unequal variance (data satisfied normal distribution but heterogeneous variance) or Wilcoxon test (data unsatisfied normal distribution) were performed for standardized cusp width of *B. boddarti* and *B. pectinirostris*. Principal component analysis (PCA) based on a correlation matrix of dentition morphometrics was performed for the dentition morphometrics of six species. Rstudio version 0.99.903 (Rstudio, Inc) was used for all statistical analyses.

3. Results

Dentition

On the premaxilla, *Ps. modestus* possesses a single row of canine teeth (Fig. V-1a), while *Pn. septemradiatus* has an additional row (Fig. V-1b). Frontal teeth of *Pn. septemratiatus* (three pairs) are large and fang-like, while those of *Ps. modestus* are not distinctively large. The remaining teeth dwindle posteriorly in both species. On the dentary, a single row of teeth occurs

along the margin and is directed vertically in both two species. There are significant differences in the number of replacement teeth, tooth width of both the premaxilla and dentary, and number of teeth and tooth length of the dentary between the two species (Table V-1).

PCA clearly separates four groups of species in the morphometric multivariate space. The first two component (PC1, PC2) explain 81.4% of total variance (Fig. V-12). Along PC1, *B. boddarti* and *Ps. modestus* are separated from the other species by smaller values of the standardized tooth length, tooth width on both the premaxilla and dentary, and the number of replacement teeth on the dentary. Along PC2, *B. boddarti* and *B. pectinirostris* are separated from others by higher number of teeth on both the premaxilla and dentary, and smaller number of replacement teeth on the premaxilla.

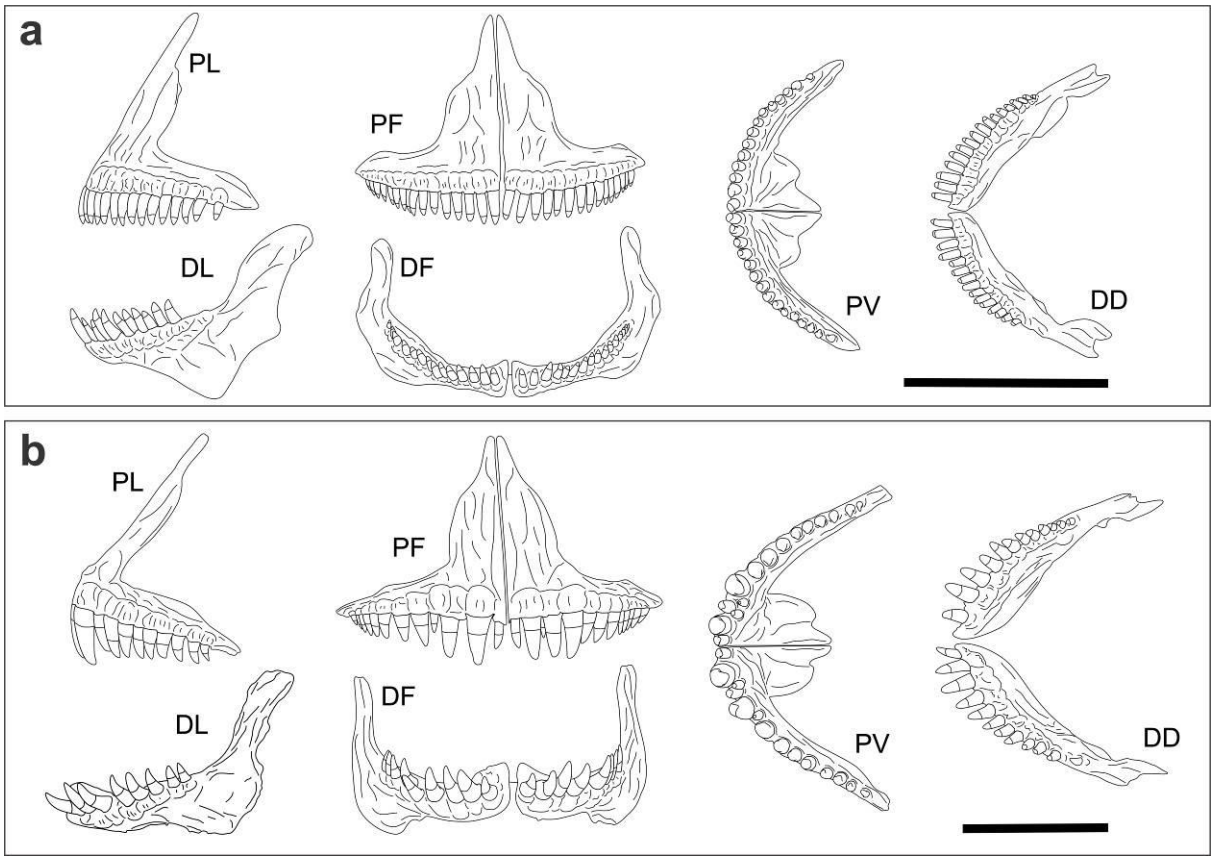

Fig. V-1 Dentition of *Periophthalmus modestus* (**a**) and *Periophthalmodon septemradiatus* (**b**). *DD* dentary in dorsal view, *DF* dentary in frontal view, *DL* dentary in lateral view, *FP* finger-like projection, *PF* premaxilla in frontal view, *PL* premaxilla in lateral view, and *PV* premaxilla in ventral view. Scale bars: 5mm

Table V-1 Dentition of the two mudskippers used in the present study and four species from preceding studies

Species	Premaxilla				Dentary				
	Number of teeth	Number of replacement teeth	Standardized tooth length	Standardized tooth width	Number of teeth	Number of replacement teeth	Standardized tooth length	Standardized tooth width	Standardized cusp width
Boleophthalmus boddarti	65.6 ± 5.1^{a}	3.4 ± 1.7^{a}	$(5.9 \pm 0.6)\times10^{-3\,a}$	$(1.9 \pm 0.4)\times10^{-3\,a}$	78.8 ± 2.8^{a}	6.6 ± 1.1^{ab}	$(7.9 \pm 0.9)\times10^{-3\,a}$	$(1.6 \pm 0.03)\times10^{-3\,a}$	$(2.1 \pm 0.2)\times10^{-3\,a}$
Boleophthalmus pectinirostris	66.4 ± 5.8^{a}	2.7 ± 1.1^{a}	$(13.5 \pm 3.7)\times10^{-3\,b}$	$(3.6 \pm 0.6)\times10^{-3\,b}$	74.6 ± 3.2^{a}	9.57 ± 2.8^{b}	$(17.8 \pm 4.1)\times10^{-3\,b}$	$(3.4 \pm 0.7)\times10^{-3\,bd}$	$(4.0 \pm 1.8)\times10^{-3\,b}$
Periophthalmus chrysopilos	39.4 ± 3.1^{b}	7.6 ± 0.6^{b}	$(9.3 \pm 1.1)\times10^{-3\,bc}$	$(3.1 \pm 0.5)\times10^{-3\,bc}$	39.0 ± 4.4^{c}	8.8 ± 0.8^{b}	$(9.8 \pm 2.3)\times10^{-3\,ac}$	$(3.1 \pm 0.6)\times10^{-3\,bd}$	-
Periophthalmus modestus	32.3 ± 1.7^{b}	4.5 ± 1.3^{a}	$(7.2 \pm 1.1)\times10^{-3\,ac}$	$(2.6 \pm 0.2)\times10^{-3\,ac}$	31.5 ± 2.1^{b}	4.5 ± 1.29^{a}	$(5.6 \pm 0.3)\times10^{-3\,d}$	$(2.4 \pm 0.2)\times10^{-3\,bd}$	-
Periophthalmodon schlosseri	44.8 ± 2.3^{c}	8.6 ± 0.9^{b}	$(10.9 \pm 2.8)\times10^{-3\,cb}$	$(4.6 \pm 1.6)\times10^{-3\,bc}$	28.6 ± 1.5^{c}	7.8 ± 1.3^{b}	$(11.0 \pm 3.2)\times10^{-3\,c}$	$(5.2 \pm 1.5)\times10^{-3\,c}$	-
Periophthalmodon septemdariatus	35.5 ± 4.0^{b}	7.5 ± 1.0^{b}	$(8.6 \pm 1.1)\times10^{-3\,c}$	$(3.9 \pm 0.6)\times10^{-3\,bc}$	25.5 ± 4.4^{d}	8.0 ± 2.16^{b}	$(10.0 \pm 1.1)\times10^{-3\,c}$	$(4.0 \pm 0.8)\times10^{-3\,bc}$	
One-way ANOVA, Kruskal-Wallis or T-test									
F, Chi-squared, or T	$25.9^{\#\#}$	$24.0^{\#\#}$	$22.4^{\#\#}$	$21.4^{\#\#}$	$26.5^{\#\#}$	$5.2^{\#}$	$23.0^{\#\#}$	$22.8^{\#\#}$	$-11.7^{\#\#\#}$
p	< 0.001	< 0.001	< 0.001	< 0.001	< 0.001	0.002	< 0.001	< 0.001	< 0.001

Numbers of teeth represent the values of both sides and replacement teeth are for the left side only (Mean ± SD). One-way ANOVA or Kruskal-Wallis followed by post-hoc Tukey test or Wilcoxon-Mann-Whitney test was applied for comparison of the parameters. The data with different letters in respective columns are significantly different ($p < 0.05$). The data on tooth length and width do not include fangs. Tooth length, tooth width, and cusp width were standardized by standard length. Tooth width was measured at the base. $^{\#}$ ANOVA followed by post-hoc Tukey; $^{\#\#}$ Kruskal-Wallis followed by Wilcoxon-Mann-Whitney, $^{\#\#\#}$T-test. Number of observations: N = 4 for *Ps. modestus* and *Pn. septemradiatus*; N = 5 for *B. boddarti*, *Ps. chrysospilos*, and *Pn. schlosseri*; N = 7 for *B. pectinirostris*.

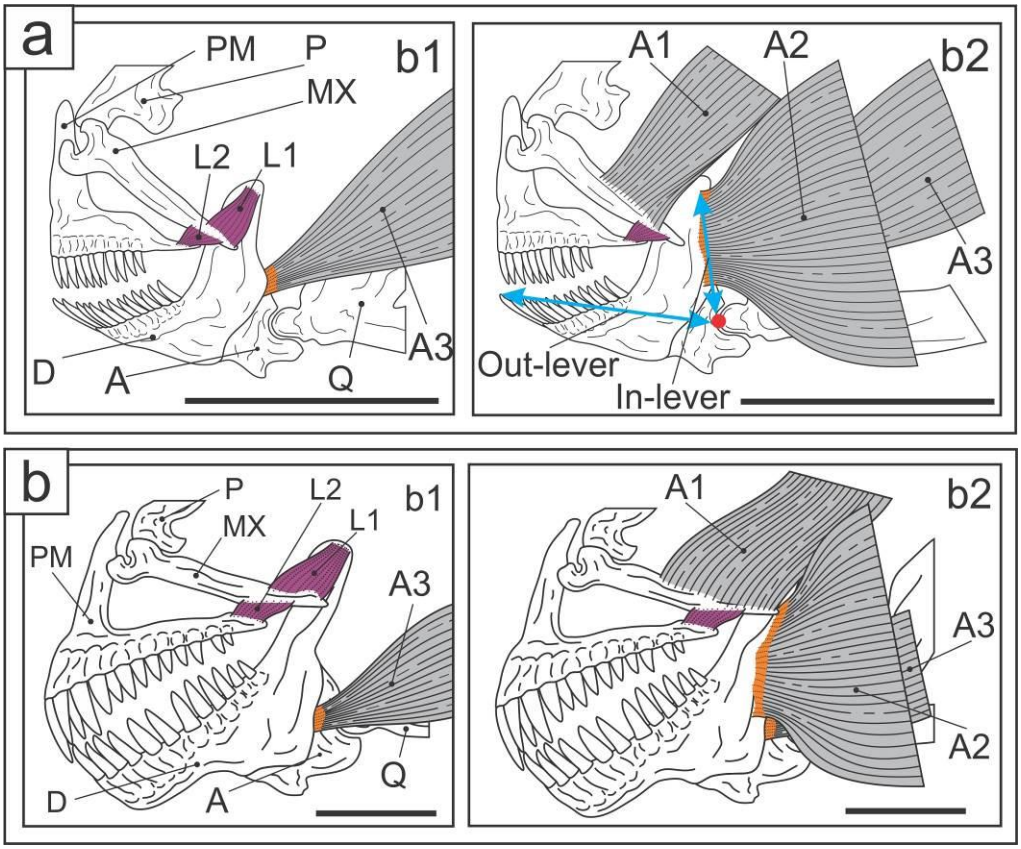

Fig. V-2 Jaw bones and ligaments in *Periophthalmus modestus* (**a1**) and *Periophthalmodon septemradiatus* (**b1**), and adductores mandibulae in *Periophthalmus modestus* (**a2**) and *Periophthalmodon septemradiatus* (**b2**). *A* articular, *A1–3* adductores mandibulae 1 to 3, *D* dentary, *L1,2* ligaments 1 (maxillo-mandibular ligament) and 2 (premaxillo-maxillary ligament), *MX* maxilla, *P* palatine, *PM* premaxilla, *Q* quadrate. Ligaments are shown in purple and tendons are in orange. In **a2**, red dot shows the fulcrum, and double headed arrows (blue) show the jaw-closing lever system. Scale bars: 5 mm

Oral jaw bones and muscles

The lever ratio of jaw-closing is 0.54 ± 0.03 (mean ± SD, N = 3 for the two species) in *Ps. modestus* and 0.56 ± 0.02 in *Pn. septemradiatus*. Both two species possess the the maxilla-mandibular ligament (L1) linking the maxilla with the dentary and the premaxillo-maxillary ligament (L2) linking the premaxilla with the maxilla. The adductores mandibulae A1, A2, and A3 attach onto the maxilla, the coronoid process of the dentary, and the medial side of the dentary, respectively (Fig. V-2). K value is 114.9 ± 10.8 ($gcm^{-3} \times 10^{-6}$, N = 3) in *Ps. modestus* and 148.0 ± 13.0 (N = 3) in *Pn. septemradiatus*.

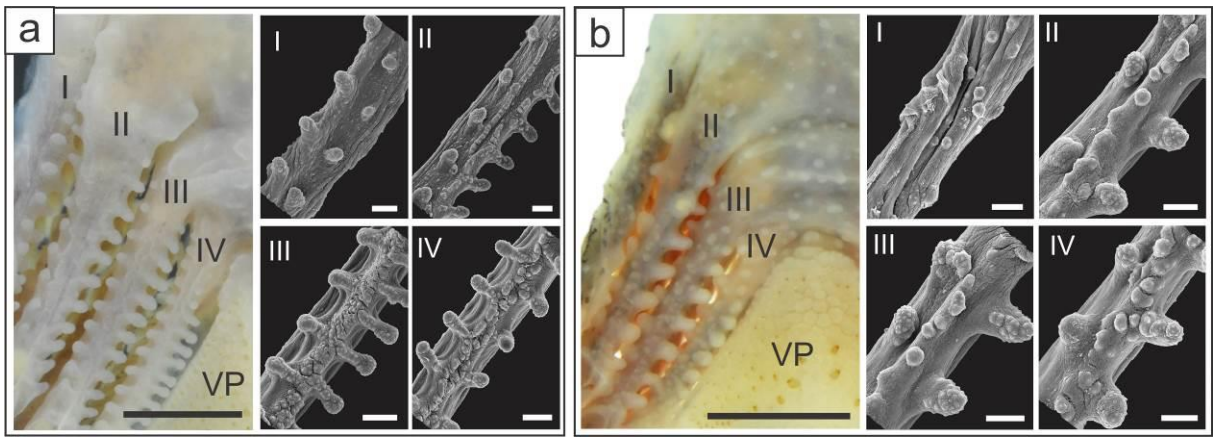

Fig. V-3 Morphology of the gill rakers in *Periophthalmus modestus* (**a**) and *Periophthalmodon septemradiatus* (**b**). In each box, the left photograph shows the dorsal view of the left gill arches, and the right ones are SEM micrographs of each gill arch. *I–IV* first to fourth gill arches, *VP* ventral pharyngeal plate. Scale bars: 2 mm for the photographs, 200 μm for SEM micrographs

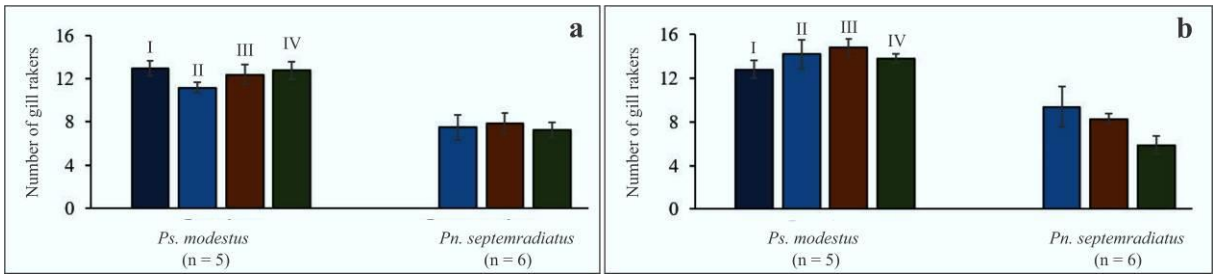

Fig. V-4 Number of gill rakers (mean ± SD) on the anterior (**a**) and posterior (**b**) gill arches of *Periophthalmus modestus* and *Periophthalmodon septemradiatus*. *I–IV* first to fourth gill arches. Size range of *Periophthalmus modestus*: 56–66 mm in standard length (SL) and *Periophthalmodon septemradiatus*: 77–93 mm SL. The number of individuals used for the measurement is given in parenthesis

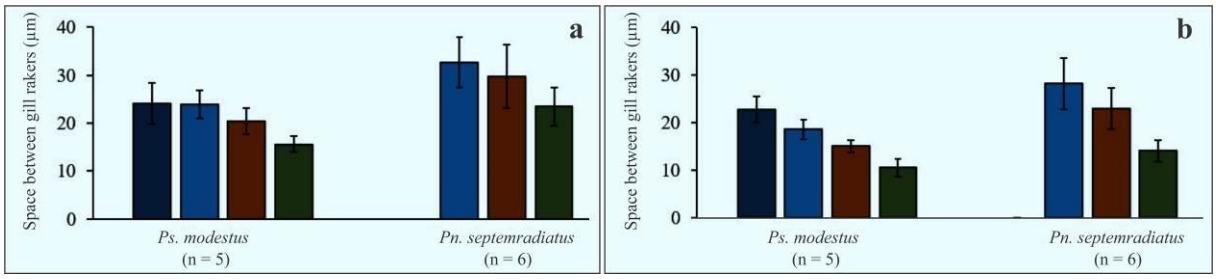

Fig. V-5 Average space between the gill rakers (mean ± SD) on the anterior (**a**) and posterior (**b**) gill arches of *Periophthalmus modestus* and *Periophthalmodon septemradiatus*. Symbols and size range of fish are the same as in Fig. V-4. The number of individuals used for the measurement is given in parenthesis

Table V-2 Tooth morphology, density, and direction of the pharyngeal plates of the two mudskippers in the present study and four species in preceding studies

Species	Shape	Density (number/mm^2)		Direction	
		Dorsal plate	Ventral plate	Dorsal plate	Ventral plate
Boleophthalmus boddarti	papilliform	951.6 ± 313.3	529.5 ± 101.1	PM	PM
	canine*			DV	
Boleophthalmus pectinirostris	papilliform	355.4 ± 27.2	494.2 ± 149.4	PM	AP
	canine*			DV	
Periophthalmus chrysospilos	canine	23.1 ± 3.3	34.1 ± 2.6	posterior	anterior
Periophthalmus modestus	canine	48.3 ± 9.6	52.1 ± 11.3	posterior	anterior
Periophthalmodon schlosseri	canine	6.7 ± 1.1	8.5 ± 0.9	posterior	anterior
Periophthalmodon septemradiatus	canine	13.8 ± 1.2	17.2 ± 2.2	posterior	anterior

*Only along the anterior margin of the dorsal pharyngeal plate. Mean ± SD, N = 3 for the all species. DV, dorsoventral; PM, posteromedial.

Table V-3 Comparison of the arch lengths (mean ± SD) among the species

	Arch length (mm)						
	N	Arch 1	Arch 2	Arch 3	Arch 4	ANOVA or Kruskal-Wallis	
						F or Chi-squared	*p*
Boleophthalmus boddarti	12	17.6 ± 1.2[a]	18.0 ± 1.2[a]	17.6 ± 1.3[a]	19.6 ± 1.4[b]	6.4	0.001
Boleophthalmus pectinirostris	7	19.9 ± 1.4[a]	20.2 ± 1.6[ab]	19.4 ± 2.2[a]	22.5 ± 1.7[b]	4.4	0.01
Periophthalmus chrysospilos	7	11.8 ± 1.2[a]	11.0 ± 1.1[a]	8.9 ± 0.9[b]	8.9 ± 0.8[b]	12.9	< 0.001
Periophthalmus modestus	10	8.9 ± 0.4[a]	8.1 ± 0.3[b]	6.2 ± 0.3[c]	6.1 ± 0.2[c]	32.5	<0.001
Periophthalmodon schlosseri	6	27.1 ± 6.1[a]	24.3 ± 4.9[ab]	19.6 ± 4.0[ab]	18.2 ± 3.9[b]	3.7	0.04
Periophthalmodon septemradiatus	7	13.4 ± 2.0[a]	12.2 ± 1.4[ab]	10.6 ± 1.6[b]	10.5 ± 1.1[b]	4.7	0.02

One-way ANOVA followed by post-hoc Tukey test was applied for *B. boddarti*, *B. pectinirostris*, *Ps. chrysospilos*, *Pn. septemradiatus* and *Pn. schlosseri*. Kruskal-Wallis followed by Wilcoxon-Mann-Whitney test was applied for *Ps. modestus*. The *p*-values of all pairwise comparisons were adjusted using Bonferroni corrections. The data with different letters in respective rows are significantly different ($p < 0.05$)

Gill rakers

The gill rakers of *Ps. modestus* and *Pn. septemradiatus* are short and knob-like (Fig. V-3). There are no gill rakers on the first arch of P. septemradiatus (Fig. V-3b). The average number of gill rakers on each row are nearly doubled in *Ps. modestus* (13.1 ± 1.1, N = 5) compared to those in Pn. septemradiatus (7.7 ± 1.2, N = 6) (Fig. V-4). Consequently, the average space between the gill rakers in *Ps. modestus* (18.9 ± 4.9 μm, N = 5) is smaller than those in *Pn. septemradiatus* (25.2 ± 6.6 μm, N = 6) (Fig. V-5).

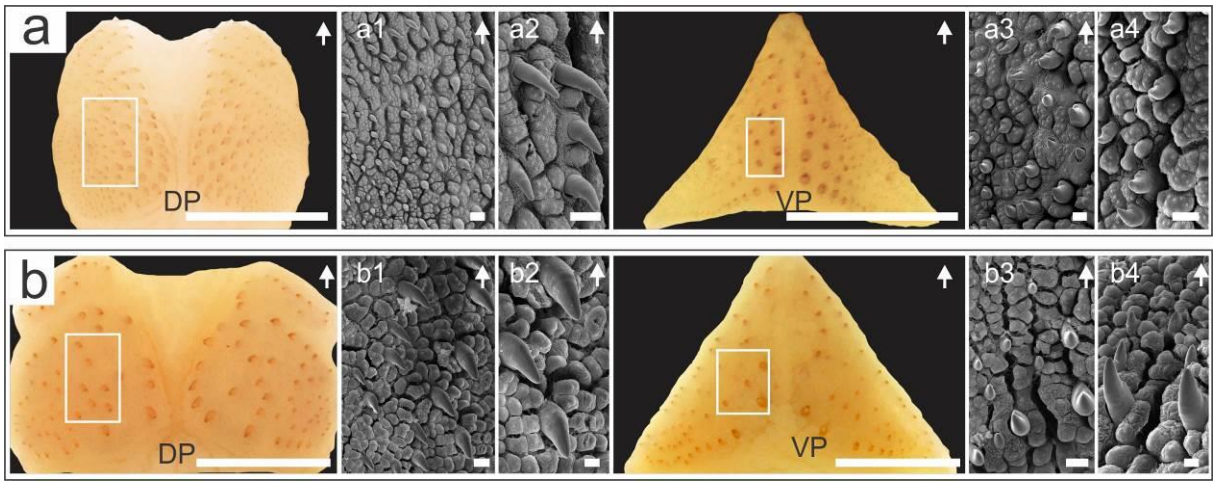

Fig. V-6 Morphology of the pharyngeal plates of *Periophthalmus modestus* (**a**) and *Periophthalmodon septemradiatus* (**b**). Color photographs show surface views of the dorsal (DP) and ventral (VP) pharyngeal plates, accompanied by SEM micrographs. At the same row, **a1**, **a3**, **b1**, and **b3** correspond to the boxes in the DP and VP. **a2**, **a4**, **b2**, and **b4** show pharyngeal teeth in the corresponding color photographs at different magnifications. Arrows on the upper right corners of color photographs and the SEM micrographs indicate the anterior direction. Scale bars: 2 mm for color photographs; 100 μm for the SEM micrographs

Pharyngeal plates

Both dorsal and ventral pharyngeal plates of the two species are flattened and studded with canine teeth with larger ones located on the posteromedial edges (Figs. V-6 and V-8c). The larger teeth in the dorsal pharyngeal plate are directed posteriorly and those on the ventral pharyngeal plate are oriented anteriorly (Fig. V-6a2, V-6a4, V-6b2, and V-6b4). *Ps. modestus* has much higher tooth density on both dorsal and ventral pharyngeal plates compared to those of *Pn. septemradiatus* (Table V-2). The relative size of the ventral pharyngeal plate in *Ps.*

modestus is significantly smaller than that of *Pn. septemradiatus*, while there is no significant difference in the relative size of the dorsal pharyngeal plate between two species (Fig. V-7). The ventral pharyngeal plate has large ventral ridge in both species (Fig. V-8c).

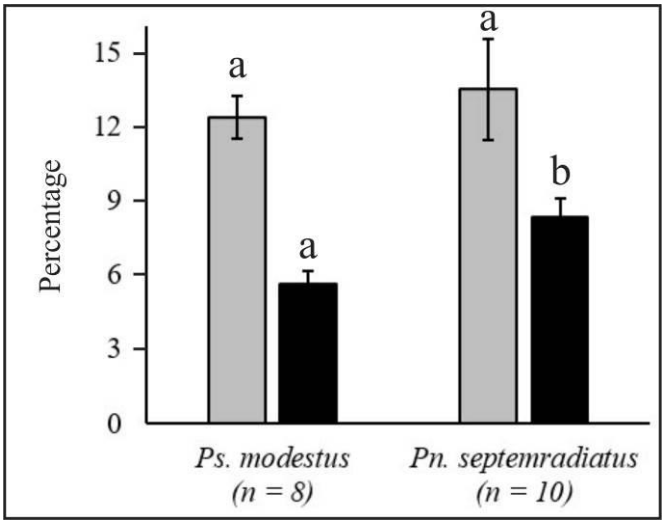

Fig. V-7 The relative size (area of pharyngeal plates/frontal sectional area of the dorsal or ventral surface of the oropharyngeal cavity) (mean ± SD) of the dorsal (light gray bars) and ventral (dark gray bars) pharyngeal plates. Wilcoxon test were performed to compare the relative size of the dorsal and ventral pharyngeal plates between the two species. Data with different letters of the dorsal or ventral pharyngeal plate are significantly different ($p < 0.05$). The number of individuals used for the measurement is given in parenthesis

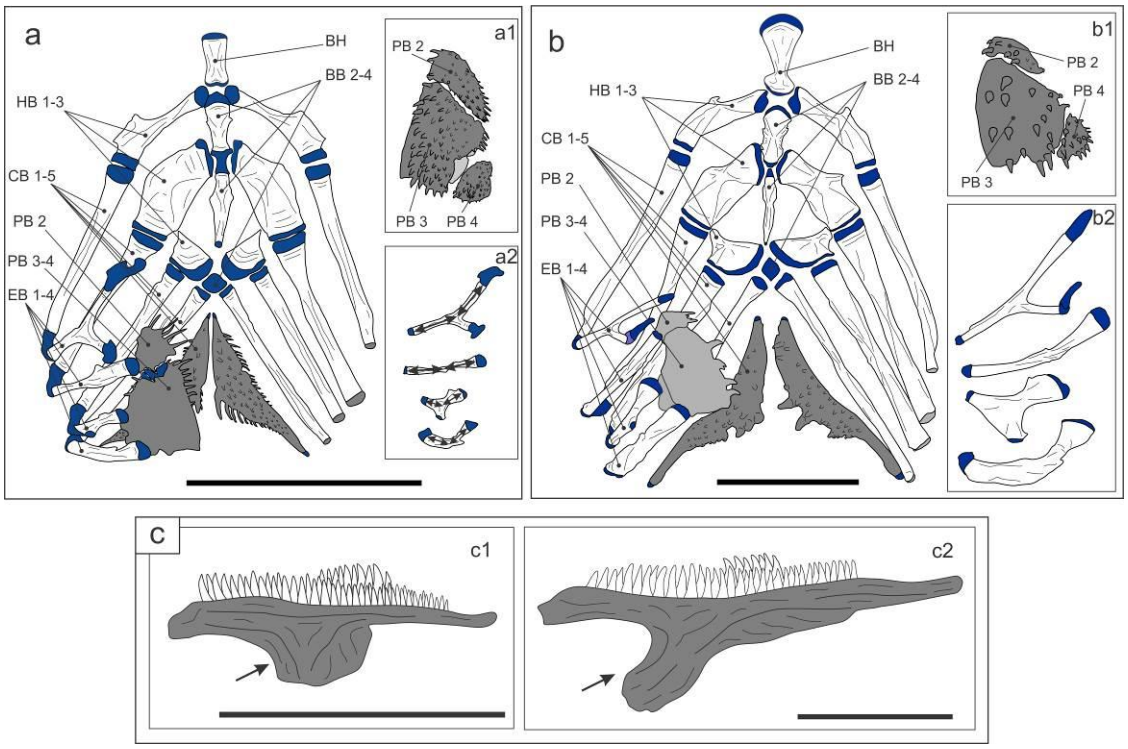

Fig. V-8 Morphology of the branchial basket skeletons (dorsal view) and the left fifth ceratobranchials (=ventral pharyngeal plate, lateral view) of *Periophthalmus modestus* (**a**, **c1**) and *Periophthalmodon septemradiatus* (**b**, **c2**). In each box of **a** and **b**, the whole structure is shown on the left; the excised left dorsal pharyngeal plate is shown in ventral view in **a1** and **b1**; and the isolated right epibranchials are shown in ventral view in **a2** and **b2**. The portion of the third pharyngobranchial covered by the fourth pharyngobranchial is shown in light grey in **a1**. Cartilages are in blue. Grey parts in box **c** are the ventral surface of the fifth ceratobranchial. Double headed arrows

in **a2** indicate length measurement. *BB 2–4* basibranchials 2–4, *BH* basihyal, *CB 1–5* ceratobranchials 1–5, *EB 1–4* epibranchials 1–4, *HB 1–3* hypobranchials 1–3, *PB 2,3,4* pharyngobranchials 2,3,4. BB1 is a small cartilage between the right and left HB1s, and therefore not shown. Scale bars: 5 mm for boxes **a** and **b**, 2 mm for box **c**

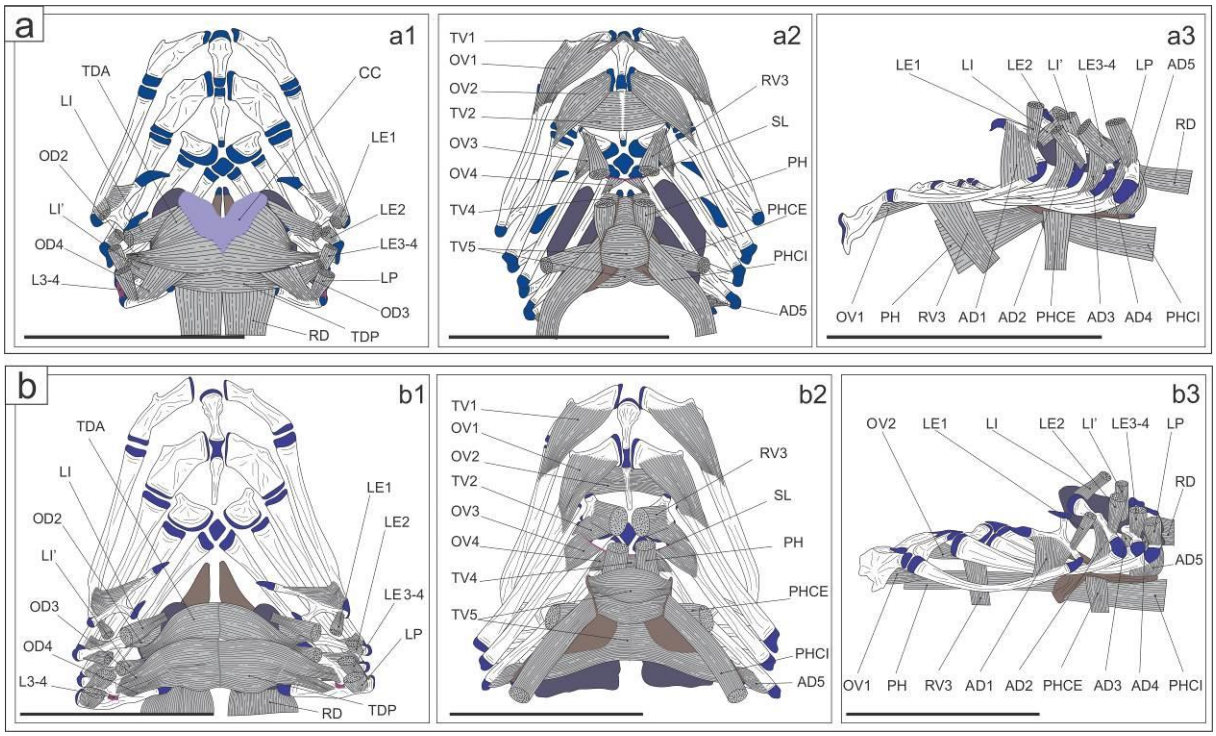

Fig. V-9 Morphology of branchial basket musculature of *Periophthalmus modestus* (**a**) and *Periophthalmodon septemradiatus* (**b**). **a1** and **b1** are dorsal views, **a2** and **b2** ventral views and **a3** and **b3** lateral views. *AD1–5* adductors 1 to 5, *CC* cartilaginous cushion, *L3–4* ligament 3–4 connecting the third and fourth epibranchials, *LE1, 2* levatores externi 1 to 2, *LE3–4* levatores externi 3 and 4 acting on the third and fourth epibranchials, *LI* and *LI'* levatores interni, *LP* levator posterior, *OD2–4* obliqui dorsales 2 to 4, *OV1–4* obliqui ventrales 1 to 4, *PH* pharyngohyoideus, *PHCE* pharyngocleithralis externus, *PHCI* pharyngocleithralis internus, *RD* retractor dorsalis, *RV3* rectus ventralis 3, *SL* semicircular ligament, *TDA* transversus dorsalis anterior, *TDP* transversus dorsalis posterior, *TV1–5* tranversi ventrales 1 to 5. Cartilages in blue; dorsal pharyngeal plate in dark purple; ventral pharyngeal plate in brown. Scale bars: 5 mm

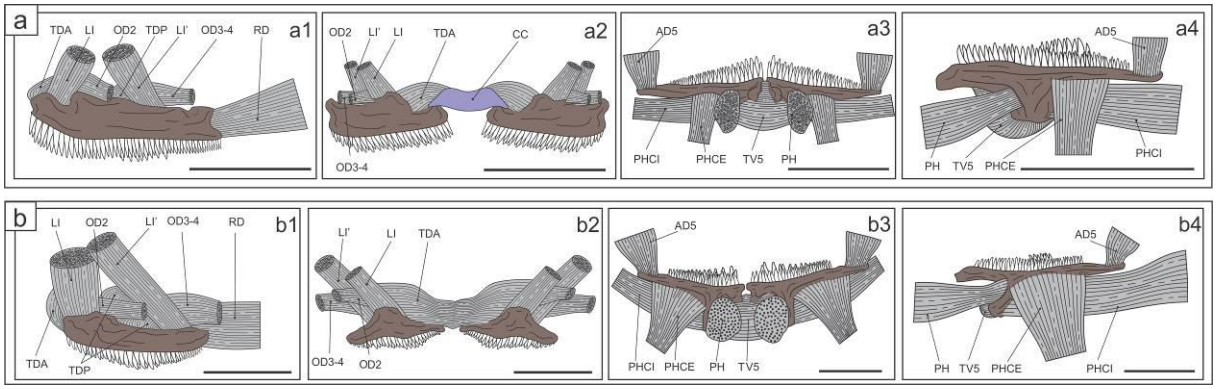

Fig. V-10 Morphology of musculature system attaching to the pharyngeal plates in *Periophthalmus modestus* (**a**) and *Periophthalmodon septemradiatus* (**b**). **a1**,**b1** are lateral views of the left dorsal pharyngeal plate, **a2**,**b2** and **a3**,**b3** frontal views of the dorsal and ventral pharyngeal plates, respectively, and **a4**,**b4** lateral views of the left

ventral pharyngeal plates. Abbreviations are the same as in Fig. V-9. The ventral side of the ventral pharyngeal plates and the dorsal side of the dorsal pharyngeal plates are colored in brown. Scale bars: 2 mm

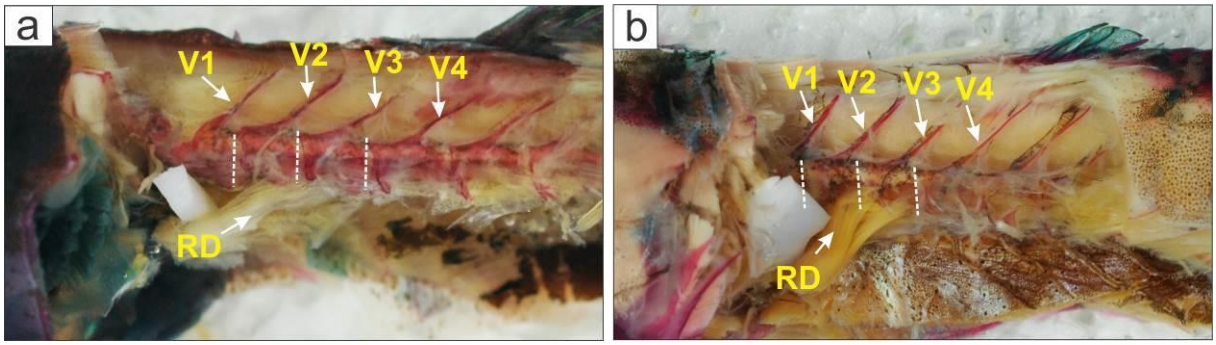

Fig. V-11 Insertion of the retractor dorsalis to vertebrae in *Periophthalmus modestus* (**a**) and *Periophthalmodon septemradiatus* (**b**). Symbols: *RD* retractor dorsalis, *V1-V4* neural spines of the first to fourth vertebrae. Dashed lines show joint between vertebrae

Branchial basket skeleton

The branchial skeleton of the two species shows some morphological similarities including the ratio of the length to width of the first to fourth ceratobranchials (1.08 ± 1.91 in *Ps. modestus*, and 12.49 ± 2.86 in *Pn. septemradiatus*; CB1-4, mean ± SD, N = 3), the flabelliform basihyal (BH), the obtuse fourth epibranchial (EB4, mean ± SD, 139.3 ± 1.2°, N = 9 for *Ps. modestus*, and 140.5 ± 1.7°, N = 8 for *Pn. septemradiatus*), and the gradual decrease in the arch lengths (Fig. V-8, Table V-3). There is a small overlapping area of the third and fourth pharyngobranchials in *Ps. modestus* (Fig. V-8a1), while these two pharyngobranchials are separated in *Pn. septemradiatus* (Fig. V-8b1).

Branchial basket musculature

The morphology of the branchial basket musculature of the two species conforms with those in other oxudercine gobies (Tran et al. 2020,2021), in which the levatores interni (LI), the levatores externi (LE), the levator posterior (LP), the retractor dorsalis (RD), the pharyngohyoideus (PH), the rectus ventralis (RV), the pharyngocleithralis externus (PHCE), and the pharyngocleithralis internus (PHCI) connect to the surrounding skeletal components (Fig. V-9a3 and V-9b3); the transversi dorsales anteriores (TDA), the transversi dorsales

posteriores (TDP), the obliqui dorsales (OD), and the ligament (L3-4) connect the elemental bones dorsally (Fig. V-9a1 and V-9b1); the transversi ventrales (TV), the obliqui ventralises (OV), and the semicircular ligament (SL) connects the elemental bones ventrally (Fig. V-9a2 and V-9b2); and the adductors connecting the ceratobranchials to the epibranchials (Fig. V-9a3 and V-9b3). There is a structure that resembles the cartilaginous cushion described by Liem (1973) between the right and left TDA and TDP in *Ps. modestus* (CC, Figs. V-9a1), whereas there is only a thin strand of connective tissue in the corresponding position in *Pn. septemradiatus* (Figs. V-9b1). TV1, connecting the left and right hypobranchials of the first arch, is present in *Ps. modestus* (Figs. V-9a2) but not in *Pn. septemradiatus* (Figs. V-9b2).

Discussion

Among the oxudercine gobies, genera of *Boleophthalmus*, *Periophthalmodon* and *Periophthalmus* show middle to high terrestriality (Table S1) and spend extensive period of time out of water. *Boleophthalmus boddart*i and *B. pectinirostris* were reported to be specialized herbivores with diatoms, algae, and phytoplankton being dominant food items ingested (Table V-4). They graze for food on the exposed mud surface with side-to-side head movement behavior (Tran et al. 2020,2021). *Periophthalmus modestus*, *Ps. chrysospilos*, *Pn. schlosseri*, and *Pn. septemradiatus* are all carnivores. Dominant food items, i.e., fish eggs, crabs, polychaeta, harpocticoid copepod, ingested by *Ps. modestus* and *Ps. chrysospilos* suggest that their feeding grounds could be in shallow water or near water's edge, whereas *Pn. schlosseri* and *Pn. septemradiatus* could feed in higher terrestrial zones as indicated by the high frequent occurrence of ants, insects, crabs, worms, and fish in their stomachs (Table V-4). Preliminary observations of feeding behavior of *Ps. modestus* show that fish appears to suck mouthful of water before moving to hunt; capture prey with water released from the mouth and suck back prey (producing a large sound and leaving a hole on the mud surface); and gurgling the mouth (Video V-1, Fig. VI-2a), which resembles the feeding behavior of *Ps. barbarus* by using the

hydrodynamic tongue (Michel et al. 2015b). However, they seem to bite mouthful of mud leaving hemispherical depression on the mud surface (Personal observation from Prof. Atsushi Ishimatsu). Note that fish could ingest large amount of mud (hemispherical marks) and therefore medium of water and the action of mouth gurgling could be useful to retain less admixture of mud before swallowing. These raise the question: what type of feeding mechanism *Ps. modestus* employ (hydrodynamic tongue or biting or switching between the two types)? Further investigation on feeding behavior and gut analysis could clarify the feeding mechanism of this species. *Ps. chrysospilos* and *Pn. schlosseri* were observed to strike prey by jumping forward with the mouth opened (Fig. VI-2b and VI-2c). Feeding behavior of *Pn. septemradiatus* is little known, but from our preliminary observations, they also hunt by striking like observed in *Ps. chrysospilos* and *Pn. schlosseri*. Below, we will compare and discuss the morphology of feeding apparatus among the six species to gain understanding of the feeding mechanism as they feed on land.

Video V-1 Feeding behavior of *Periophthalmus modestus*. Video footage includes two individuals: suction behavior (1–12s); and prey striking with water released and the mouth gurgling (13–49s). Recorded in a mudflat in the Ariake Sea, Saga Prefecture, Japan in June 2017
(Video is available from the author)

Comparison of the dentition, jaw structure and gill rakers

The function of dentition and feeding habit can be inferred from morphological features of the dentition. For instance, comb-like teeth in *Plecoglossu altivelis* (Tachihara and Kimura 1991; Uehara and Miyoshi 1993; Katano et al. 2004), Sicydiinae species (Sakai and Nakamura 1979; Mochizuki and Fukui 1983; Sahara et al. 2013), and Acanthurid species (Fishelson and Delarea 2014) serve encrust algae off hard surfaces, whereas canine teeth arranging in a single- or multi-

rows function to capture evasive prey (Grubich et al. 2008; Mihalitsis and Bellwood 2019), or molar teeth arranging in pads are employed to crush hard prey (Cataldi et al. 1987; Elgendy et

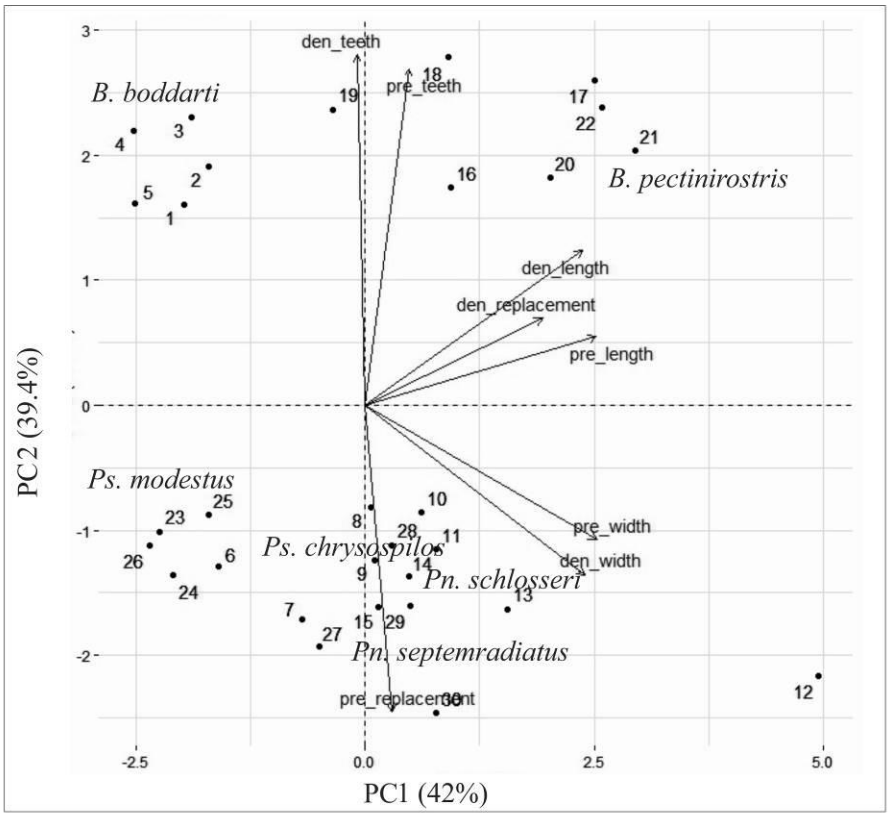

	PC1	PC2
pre_teeth	0.17	0.93
pre_replacement	0.10	-0.85
pre_length	0.87	0.19
pre_width	0.87	-0.37
den_teeth	-0.03	0.97
den_replacement	0.67	0.24
den_length	0.82	0.43
den_width	0.83	-0.47

Fig. V-12 PCA biplot of the two principal components (PC1, PC2) showing the multivariate morphometric ordination of the studied taxa (upper box). The morphological variables are represented by vectors; correlated variables have a similar orientation. Loadings of each variable along PC1 and PC2 are shown in the lower table. Symbols: *den_length* standardized tooth length on the dentary, *den_replacement* number of replacement teeth on the dentary, *den_teeth* number of teeth on the dentary, *Dim 1 – Dim 5* dimension 1 to 5, *pre_length* standardized tooth length on the premaxilla, *pre_replacement* number of replacement teeth on the premaxilla, *pre_teeth* number of teeth on the premaxilla, *pre_width* standardized tooth width on the premaxilla. Points 1–5 are the data of *Boleophthalmus boddarti*, 6–10 *Periophthalmus chrysospilos*, 11–15 *Periophthalmodon schlosseri*, 16–22 *Boleophthalmus pectinrostris*, 23–26 *Periophthalmus modestus*, and 27–30 *Periophthalmodon septemradiatus*

al. 2016). In *B. boddarti* and *B. pectinirostris*, dentary teeth are incisor, flattened and enlarged cusps, and oriented horizontally, which could serve skimming thin layer of mud surface (Tran

et al. 2020,2021). Canine teeth are present in *Ps. modestus*, *Ps. chrysospilos*, *Pn. schlosseri*, and *Pn. septemradiatus* but frontal fang-like teeth only occur in the later three species, which suggest the requirement of handling durable and/or evasive prey. This agrees with prey items ingested by these species (Table V-4). The PCA of dentition morphometrics among the six species clearly separates into four groups (Fig. V-12). The dentition of *B. boddarti* is different from these of *B. pectinirostris* by having smaller values of standardized tooth length, standardized tooth width on both the premaxilla and dentary, smaller number of replacement teeth on the dentary, and lower value of standardized cusp width (Table V-1). The morphological differences between *B. boddarti* and *B. pectinirostris* could be because the later grazes in higher terrestriality with harder mud surface, which could be verified by investigation of their feeding environment. Dentition morphometrics of *Ps. modestus* are separated from *Ps. chrysospilos*, *Pn. schlosseri*, and *Pn. septemradiatus* by having smaller values of replacement teeth, standardized tooth length, standardized tooth width on both the premaxilla and dentary (Table V-1), which suggest the *Ps. modestus* could handle less durable and evasive prey (Table V-4).

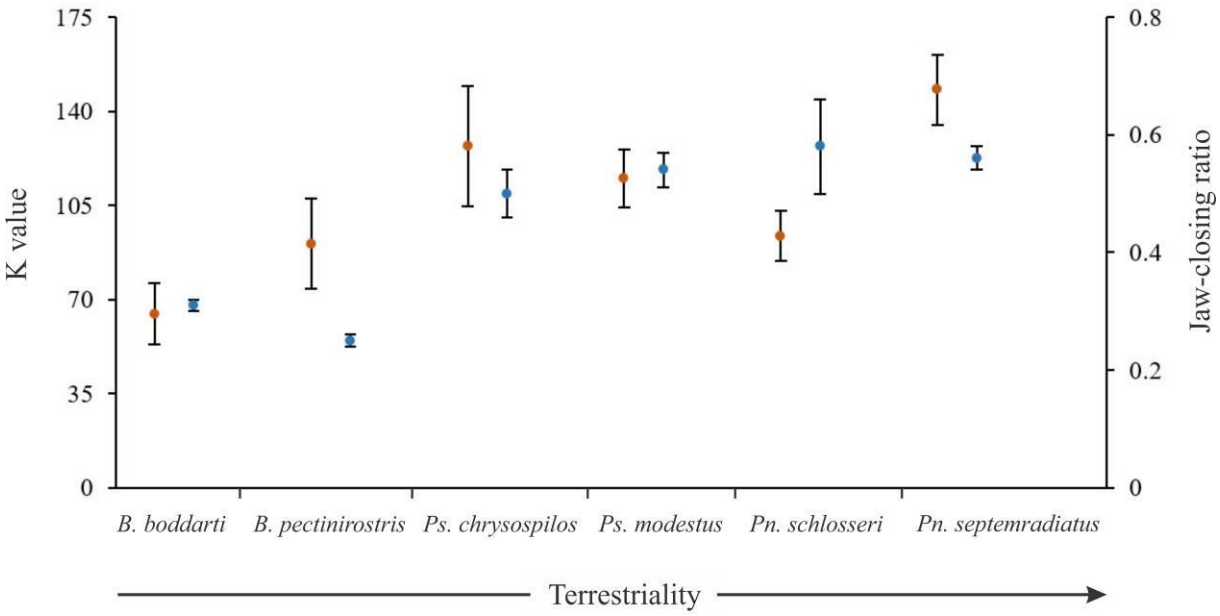

Fig. V-13 Plotting K values (red dots, mean ± SD) and jaw-closing ratios (blue dots, mean ± SD) among the six species. Number of observations are three for each species, except N = 2 for K value in *Pn. schlosseri*

Fish feeding on evasive prey usually have the jaw-closing value higher than 0.4 (or jaw-closing displacement advantage ratio higher than 2.51), which produce strong biting force (Westneat 1995; Wainwright et al. 2004). Among the six mudskipper species, *B. boddari* (0.31 ± 0.01 of jaw-closing ratio) and *B. pectinirostris* (0.25 ± 0.01) have the jaw-closing values smaller than 0.4, whereas the values are higher in *Ps. chrysospilos* (0.5 ± 0.04), *Ps. modestus* (0.54 ± 0.03), *Pn. schlosseri* (0.58 ± 0.08), and *Pn. septemradiatus* (0.56 ± 0.02). The adductor mandibulae 2 is more developed in *Ps. chrysospilos*, *Ps. modestus*, *Pn. schlosseri*, and *Pn. septemradiatus* compared to *B. boddarti* and *B. pectinirostris* (Fig. V-13). These morphological features could be because skimming for the mud surface in *B. boddarti* and *B. pectinirostris* does not require much force as handling durable prey as in the other carnivorous species. Differences in the jaw-closing values and K values among the species could be also related to burrow excavation. Note that digging deep burrows requires strong biting force. Currently, inadequate data of burrow volume and variations of hardness of sediment among the species limit our attempt to correlate between the morphology and burrow excavation.

The gill rakers usually take a role of food retention and are most developed, numerous and filamentous in shape in typical planktivrous fishes (Friedland et al. 2006; Collard et al. 2017; Storm et al. 2020). The gill rakers in *B. boddarti* and *B. pectinirostris* are most numerous and developed on the last three rows, upward facing and in triangular shape, which could serve sieving diatoms on land (Tran et al. 2020,2021). The gill rakers of *Ps. chrysospilos*, *Ps. modestus*, *Pn. schlosseri*, and *Pn. septemradiatus* are short and knob-like, with the later two species having rudiment gill rakers on the first arch, which suggest that the role of gill rakers is less important as feeding on land.

Comparison of pharyngeal plates and branchial basket

Typically, fish employ the pharyngeal plates for prey processing, and therefore, configurations of the pharyngeal plates, e.g., shape, size, and tooth bearing, could suggest their roles (Gidmark

et al. 2019). For example, the pharyngeal plates of mollusk feeders are relatively large, suturing the left and right sides of the ventral pharyngeal plates, and studded with molar teeth, while those of piscivorous fishes seem smaller and are borne with canine teeth (Hulsey 2006; Grubich 2003; Burress 2015), and those of herbivorous and omnivorous species are borne papilliform teeth (Burress 2015, 2016). Among the six species, the pharyngeal plates of *B. boddarti* and *B. pectinirostris* are distinct with large relative size (20.3–26.0 % of the former, and 19.1–22.8 of the later), bearing numerous papilliform teeth (529–951 teeth/mm^2 of the former and 355–494 teeth/mm^2 of the latter), and strong curvature (Tran et al. 2020,2021). Difference in tooth density between the two species could be related to the size of food items ingested (see Fig. S2 in Tran et al. 2021). The pharyngeal plate morphology of *Ps. modestus*, *Ps. chrysospilos*, *Pn. schlosseri*, and *Pn. septemradiatus* conforms with typical carnivorous fishes but there are some differences among the species. Tooth density varies among the four species with *Ps. modestus* having the highest density (48.3 and 52.1 teeth/mm^2 of the dorsal and ventral pharyngeal plates, respectively), lower in *Ps. chrysospilos* (23.1 and 34.1 teeth/mm^2), and lowest in *Pn. septemradiatus* (13.8 and 17.2 teeth/mm^2) and *Pn. schlosseri* (6.7 and 8.5 teeth/mm^2). These variations could be because of processing different types of prey. For example, *Ps. modestus* ingested relative small and soft prey (Table V-4) whereas *Pn. schlosseri* is usually observed handling large, evasive prey. The musculoskeletal system of the branchial basket of the fourth carnivorous species shares similarities by having the arch lengths decreasing posteriorly, large ventral ridges on the ventral side of the ventral pharyngeal plates, and well developed muscles attaching on the pharyngeal plates, but *Ps. modestus* show distinct morphological features from the three carnivorous species with the third and fourth pharyngobranchials overlapping, possession of the TV1 and CC (Figs. V-8a1, V-9a1, and V-9a2). The distinct morphological configurations of *Ps. modestus* resembles those of *Boleophthalmus*. Further comparison of feeding mechanism among these species could clarify the linkage between morphological features and functions. Note that *Ps. modestus* show feeding behavior different from the three

carnivorous species but share some similarities (sucking water and mouth gurgling) to *B. boddarti* and *B. pectinirostris*.

Intraoral processing in mudskippers is little known. Currently, there are only two studies of how *Ps. barbarus* swallow prey (Michel et al. 2015b; Sponder and Lauder 1981, reported as *Ps. koelreuteri*) but they suggested different mechanisms of prey swallowing. Michel et al. (2015b) suggested the hydrodynamic tongue plays the role of swallowing on land, whereas Sponder and Lauder (1981) indicated that the pharyngeal plates were employed for the intraoral transport. Both studies show limitations of using immobilized and soft prey, and achieving the experiments in the laboratory conditions, i.e., uniform terrain. In reality, carnivorous mudskippers hunt various types of prey (Table V-4) in various conditions of terrain. In many cases, they strike by jumping forward with mouth opened, and the hydrodynamic tongue appears impractical. Sponder and Lauder (1981) show the dorsal pharyngeal plates moved at large distance whereas the ventral pharyngeal plates were stable. However, we found that the pharyngohyoideus (PH), pharyngocleithralis (PHCI), and pharyngocleithralis externus (PHCE) attaching on the large ventral ridge of the ventral pharyngeal plates are well developed in the carnivorous mudskippers, which suggest their large distance movement.

Table V-4 Comparison of feeding habit among the six mudskipper species

Species	Major food items	References
Boleophthalmus boddarti	[#] Phytoplankton (76.0%), detritus (24.0%)	Chaudhuri et al. 2014
B. pectinirostris	Diatoms (exclusive)	Yang et al. 2003
Periophthalmus chrysospilos	[##] Fish eggs (8057), crabs (1935)	Ridho et al. 2019
Ps. modestus	[#] Polychaeta (52.4%), harpocticoid copepod (35.0%)	Baeck et al. 2013
Periophthalmodon schlosseri	[#] Crabs (55.7%), fish (32.8%)	Zulkifli et al. 2012
	[###] Crabs (55.7%), insects (23.0%), worms (21.2%)	Ghaffar et al. 2006
Pn. septemradiatus	[#]Ants (60.2%), detritus (26.6%)	Dinh et al. 2019

[#] Frequency of occurrence; [##] index of relative important; [###] Frequency of prey chosen

The large ventral ridge was also reported in *Pogonias cromis* with the proximal edge of the ventral ridge contacting the cleithrum. As the protractor pectoralis contraction, the cleithrum is

lift up causing the ventral pharyngeal plates raising up against the dorsal pharyngeal plate, which facilitates grinding hard prey (Grubich 2005). This is not the case of the carnivorous mudskippers because the ventral ridge is not contacting the cleithrum, but just give more space for muscles (PH, PHCI, PHCE) attaching on. In addition, the relative short of the epibranchials could restrict the anteroposterior movement of the dorsal pharyngeal plates. Therefore, we speculate that flexible movement of the whole branchial baskets, especially the ventral pharyngeal plates could facilitate prey swallowing on land in carnivorous mudskippers. Further investigation by tracking movement of the whole branchial basket using electromyography or cineradiography could elucidate how they swallow prey on land.

The flexible movement of the branchial basket, especially the basihyal, was well reported in the tongue-bite apparatus of the salmonid *Salvelinus fontinalis*, the rainbow trout *Oncorhynchus mykiss*, Australian arowanas *Scleropages jardinii*, or osteoglossomorph *Chitala ornate* (Konow and Sanford 2008a,b; Camp et al. 2009). These species employ tongue-bite mechanism to reduce and immobilize prey due to their prey are usually large and alive. The movement of the branchial basket, especially the basihyal, is mainly endowed by well developed muscles of adductor mandibularis, epaxialis, hypaxialis, and protractor hyoideus. Contraction and protraction of these muscles cause the dorsoventral and anterioposterior movement of the pharyngeal plates, especially the anterior part.

Chapter VI

GENERAL DISCUSSION AND FUTURE DIRECTION

Evolution of feeding apparatus during land invasion of vertebrates

The suction-to-biting transition of feeding mode is thought to have happened around the time when vertebrates were shifting their life from aquatic to terrestrial environment (Clack 2012; Lemberg et al. 2021). In order to generate suction force, the oral-opercular cavities must be rapidly expanded, which is endowed by loosely connection of element bones of the skull. On the other hand, biting requires force and pressure to exert on prey, which is enabled by rigidity of the feeding structure (Schwenk and Rubega 2005). Therefore, the basic differences between the two feeding modes lie in the degrees of flexibility of the skull structure including the opercular series, the branchial system, the lower jaw, and the skull roof. In addition, teeth are also modified to meet the requirement of handling different prey types, and thus their morphological features could be used as indicators of feeding habits. Tracing the evolution of the feeding structures in stem species, e.g., primitive fish (*Polyterus endlicherii*), Devonian (*Eusthenopterop*, *Tiktaalik*, *Ichthyostega*, and *Acanthostega*), and Permian (*Phonerpeton*) tetrapod species, could reveal how the feeding modes were transitioned (Long and Gordon 2004; Clack 2012). The followings will discuss the modifications of the feeding structures in stem species and compare to those of mudskippers in order to gain more understanding of the feeding transition.

Prominent function of the branchial system and the opercular series is to pump water through the mouth and thus serves respiratory ventilation and suction feeding in fish, which is enabled by the expanding and reducing rhythm of the oral and opercular cavities. During land invasion, vertebrates became less reliance on the pumping mechanism, and instead they used the jaw prehension for feeding and lung for respiration. Consequently, the opercular series including the gill openings were lost or modified to form stapes, and the branchial system was

reduced and modified to form a tongue serving prey swallowing in tetrapods (Clack 2012). These modifications are found in *Eusthenopteron* and *Panderichthys* by possessing ossified operculum, and in the later emerge tetrapods, Dendrerpeton, by loss of the operculogular plates (Ahlberge and Clack 1998; Clack 2012). Recent findings suggested that even though possessing the elongate jaws and loss of the suspensoria, *Tiktaalik roseae* could still employ suction feeding (Lemberg et al. 2021). In mudskippers, the branchial system and the opercular series mainly share the morphological features of typical fish but show some modifications facilitating feeding in shallow pools and upper intertidal zone. The branchial system is well developed showing unique morphology in the herbivorous and omnivorous species. For example, the arch lengths increase posteriorly with the fourth arch being longest allowing more gill rakers bearing, and the pharyngeal plates are large and strong curve, which could serve sieving and transport diatoms as feeding in semi-terrestrial environment. The branchial system of the carnivorous species shows the typical morphology of carnivorous fishes but the pharyngeal plates are studded with strong canine teeth and have well developed muscle system, which could function for processing prey and intraoral transport. Regarding the opercular series, mudskippers still possess this structure (Murdy 1989) but show some modifications facilitating feeding and respiration on land. Their opercular cavities are large with the relative small gill openings, which could serve retaining water for feeding and respiration on land (Murdy 1989; Clayton 1993). Species of *Boleophthalmus* genus were found to suck mouthful of water for suspending food particles and sieving (Tran et al. 2020, 2021), while *Ps. barbarus* use hydrodynamic tongue aiding prey capture and swallowing (Michel et al. 2015b). Comparison of feeding mechanism and respiration among mudskippers shows the trend of less reliance on pumping mechanism in the higher terrestrial species. For instance, species of genera *Parapocryptes*, *Oxuderces*, *Apocryptodon*, *Apocryptes*, and *Pseudapocryptes* show no/low terrestriality with some species appear to show mouth gurgling as feeding (preliminary observations and need further investigations, Fig. VI-1a and VI-1b). Given living mainly in aquatic environment,

oxygen uptake should be from water, and therefore pumping mechanism could mainly employed by these species. Species of genera *Scartelaos*, and *Boleophthalmus* show higher terrestriality but they still stick to water for feeding and respiration (Fig. VI-1c). Species of genera *Periophthalmodon* and *Periophthalmus* show highest terrestriality and feed on land. They possess capability of respiration through skin and buccal cavity (Clayton 1993, see Table IV-4), and show the capability of feeding without using water such as *Ps. kalolo* (Sponder and Lauder 1981). Note that mudskippers show air gulping for burrow-dwelling and embryos developing (Ishimatsu et al. 1998,2007), which is endowed by possessing the opercular series.

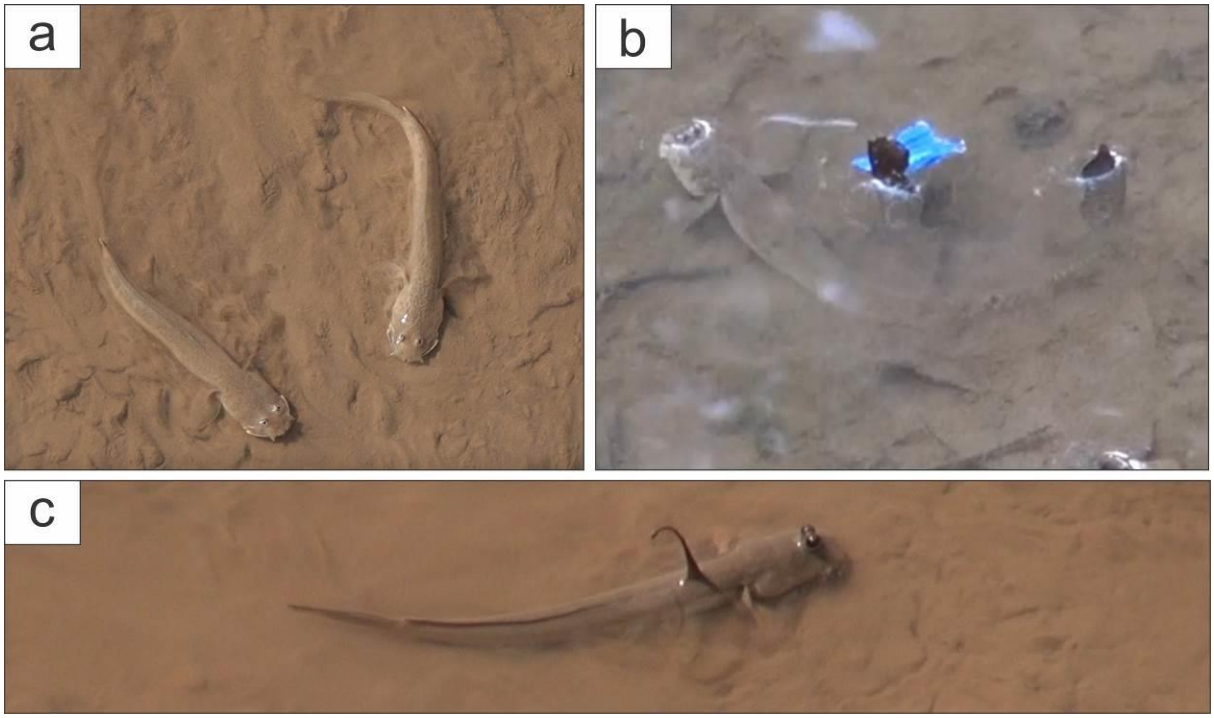

Fig VI-1 Feeding behavior of *Oxuderces nexipinnis* (**a**), *Pseudapocryptes elongatus* (**b**), and *Scartelaos histophorus* (**c**) in shallow pools. Photos were taken from video footages recorded in Mo O mudflat (**a**, **c**), Soc Trang Province, and in a mudflat in (**b**) Bac Lieu Province, Vietnam.

Due to taking the role of gape widening and/or prey handling, and being well preserved in fossil deposits, the lower jaw and its' dentition are commonly used in tracing feeding transition. In suction feeding, the gape needs to be widened, which is partly endowed by the kinetic of the lower jaw, i.e., formed from loosely connections of the dentary, the cartilage Meckelian, the angular, and the quadrate (Westneat 2006). As shifting the biting, the lower jaw becomes strengthened, more rigid and tubular, which are resulted from fused element bones,

reduction of the coronoid, and loss of the Meckelian (Ahlberge and Clack 1998; Long and Gardon 2004). In addition, dentition at anterior end of the jaw becomes double, parasymphysial fangs are lost, and dentary fangs are reduced (Ahlberge and Clack 1998). *Panderichthys* and *Elpistostege* show these modifications and are thought to feed in shallow water (Ahlberg and Milner 1994; Ahlberge and Clack 1998) and therefore, the suction-to-biting transition is thought to have already occurred in aquatic environment and early tetrapods were all carnivorous (Clack 2012). Further evolution of the prehension was traced in a divergence of the lower jaws enable to generate different types of jaw-closing, i.e., a kinetic inertial system and a static pressure system. The emergence of the later system and the appearance of molar teeth allow tetrapods grind plant materials, which suggest the later emergence of the herbivores in the late Mississippian or Pennsylvanian (Anderson et al. 2013). By possession of the dentary, the articular, and the Meckelian cartilage, the lower jaw of mudskippers shares the morphology of typical fish. However, the structure appears rigid, which could be because many of them use the oral jaws for excavating deep burrows. Note that some mudskippers (*B. boddarti* and *B. pectinirostris*, Tran et al. 2020,2021; *Ps. barbarus*, Michel et al. 2015b) show suction behavior but the slow-kinematic suction is mainly facilitated by the expansion of the oral-opercular cavities rather than the fast protrusion of the oral jaws in typical suction feeders. Mudskippers show some modifications allowing them exploit food resources on land. For example, the lower jaw of the herbivorous mudskippers is elongate and borne with numerous incisor teeth directed horizontally. These features could serve skimming thin layer of mud surface with high density of food particles. On the other hand, the lower jaw in the carnivorous mudskippers is relative short with the long coronoid process, which allows the dentary rotate at large angle and produces strong biting. The premaxilla has the long ascending facilitating long protrusion. Strong canine teeth present on the both jaws. These morphological features allow them capture and handle durable prey. The morphological configurations of the omnivorous species are intermediate between the herbivorous and carnivorous species.

The basic difference in skull morphology of suction-based and biting-based modes lies in a cranial kinesis of the former and a rigidity of the later (Clack 2012). In modern fish, the skull consists of at least 20 independent moveable bones with separation of the premaxilla and the maxilla, and consequently, the framework is flexible facilitating suction mechanism (Westneat 2006). The skull roof in lobe-finned fishes, Sarcopterygii, possesses an intracranial articulation allowing dorsoventral movement of the snout (Thomson 1967; Thomson 1969). The intracranial hinge becomes sutured (Ahlberge and Milner 1994), and other element bones, e.g., the premaxilla, the maxilla, and other skull roof bones, are tightly fused together in order to accommodate higher strain from biting in later true terrestrial tetrapods (Long and Gordon 2004). Therefore, sutural morphology could suggest types of strain exerting on the skull (Markey et al. 2006). For example, the configurations of anterior tension and posterior compression in early land vertebrates represent the suction mode, whereas features of compression between the frontals and parietals suggest biting mode (Markey and Marshal 2007). Analysis of the cranial suture suggests that the suction mode was employed by *Polypterus* and *Eusthenopteron* (Markey and Marshal 2007); suction and/or biting was used by *Tiktaalik* and *Acanthostega* (Markey and Marshal 2007; Lemberg et al. 2021); and biting was used by *Phonerpeton* (Long and Gordon 2004; Markey and Marshal 2007). Modifications of the cranial suture among stem species, especially in *Acanthostega*, suggest that biting mode were first emerged in aquatic environment (Markey and Marshal 2007; Clack 2012). Even though the skull roof of mudskippers mainly shares the morphology of typical fish enable flexible framework (Murdy 1989; Michel et al. 2014), they still possess the capability of feeding on land. Some species of genera *Periophthalmus* and *Periophthalmodo*n show the capability of feeding away from water's edge. Given that the early land vertebrates developed biting mode in aquatic environment before expanded their lives on land, the mudskippers is in another hand, which possesses suction structure but shows terrestrial feeding. The capability of terrestrial feeding is endowed by having the pectoral fins and the capability of the oral jaw rotation. The

head of the most terrestrial mudskippers appears to be enlarged (Hui et al. 2019) with the pre-orbital length of the skull being relative short compared to other gobies (Clayton 1993), which could involve in terrestrial activities such as hunting, digging, storing air/water. Little is known about how skull roof morphology involving in terrestrial feeding in mudskippers.

Adaptations of terrestrial grazing in the herbivorous and omnivorous mudskippers

In aquatic environment, planktivorous or herbivorous fishes retain food particles suspended in water column or adhesive surfaces. Their food resources are less admixture of mud particles. In the ingestion stage, they usually employ ram feeding or suction feeding to engulf food (Crownder 1985; Gibson and Ezzi 1985). Some species use comb-like teeth on the oral jaws to encrust algae off surfaces (*Sicyopterus japonicus* Sakai and Nakamura 1979; *Plecoglossus altivelis* Uehara and Miyoshi 1993; blennniod fishes Kotrschal 1989, Hundt and Simons 2018; loricariid fishes Geerinckx et al. 2007). In order to retain food particles, they employ the dead-end filtering (Berry and Low 1970; Drenner and Mummert 1984; Gophen and Geller 1984; Hoogenboezem et al. 1991; van den Berg et al. 1992) or cross-flow mechanism (Sanderson et al. 2001; Weller et al. 2016) with or without using mucus (Sanderson et al. 1996; Smith and Sanderson 2007). Therefore, their gill rakers are extended anteriorly, most numerous and developed on the first arch, and filamentous (Iwata 1976; Gibson 1988; Salman et al. 2005). In the herbivorous and omnivorous mudskippers, their food particles are most density on the top layer of the mud surface and mixed with mud particles (Aleem 1950; Koh et al. 2006,2007). In order to obtain food particles with less admixture of mud, they have to ingest a very top layer of the mud surface. *B. boddarti* and *B. pectinirostris* use their horizontal teeth on the dentary to skim mud surface with side-to-side behavior (Tran et al. 2020,2021). Preliminary observations of the feeding behavior of *O. nexipinnis*, *S. histophorus*, and *Pd. elongatus* show the skimming or scraping movements. Note that all of them show horizontal orientation of dentary teeth. Detail analysis of the feeding behavior and comparison of food composition between the stomach content and different deep levels of the mud surface could partly clarify function of

the dentary teeth. Filtering mechanism in the herbivorous and omnivorous mudskippers is little known. Mucus trapping cannot be used in these species due to retention of both food and mud particles. Data from the morphological features of the gill rakers and comparison of the average space between gill rakers on the last two or three rows and food particles ingested by *B. boddarti*, *B. pectinirostris*, *O. nexipinnis*, and *S. histophorus* suggest that the dead-end mechanism could be employed for sieving. This could be the case of *B. boddarti* and *B. pectinirostris* because their feeding cycle happens on land and water is expelled downward through the gill slits at the end of the feeding cycle allowing the last three rows of gill rakers filtering food particles. In the cases of *O. nexipinnis*, and *S. histophorus*, although the average space between gill rakes suggest possibility of using dead-end mechanism, feeding behavior of these two species resembles the feeding behavior of winnowing in cichlid fish (Weller et al. 2017). The feeding cycle of the two species happens in shallow water and cloudy water expelled slowing during fish gurgling. Further investigation of feeding cycle using electromyography method or hydrodynamic simulation (see China et al. 2017; Provini and van Wassenbergh 2018) could reveal the food retention mechanism in the herbivorous and omnivorous mudskippers. To sum up the grazing in the herbivorous and omnivorous mudskippers, water play an important role in the feeding process in this group of fish. Therefore, even though possession of the ability to emerge on land for extended periods in some species (e.g., *B. boddarti* and *B. pectinirostris*) (Clayton 1993), they have to stick to water's edge.

Adaptations of terrestrial feeding in carnivorous mudskippers

One of primary evolutions during land invasion of vertebrates is the transition of feeding mode from suction to prehension. Aquatic vertebrates employ suction feeding using medium of water for capture and intraoral processes, while terrestrial vertebrates usually utilize teeth on the oral jaws for prehension and the tongue for swallowing (Schwenk and Rubega 2005). The intermediate stage of feeding mode is little known. Recent findings showed that capability of placing the gape on prey is the key factor in capture prey on land (Sponder and Lauder 1981;

Van Wassenbergh 2013; Michel et al. 2014, 2015a,b; Van Wassenbergh et al. 2017; Heiss et al. 2018) and the possession of the tongue allows terrestrial vertebrates swallow prey on land and freely exploit food resources away from water's edge (Schwenk and Rubega 2005). The lowest form of the tongue is found in salamanders, a group of amphibians with highly adapted to terrestrial environment (Schwenk and Rubega 2005; Iwasaki et al. 2019). However, an intermediate form of the tongue evolved from fish and how intraoral transport happens in the early land vertebrates are still mysterious. In the carnivorous mudskippers, they employ the pectoral fins and rotation of the oral jaws to orientate the gape on prey (Michel et al. 2014) or use hydrodynamic tongue for capture (Michel et al. 2015b). The intraoral transport in this group of fish is little known. Michel et al. (2015b) found that fish used hydrodynamic tongue for swallowing but data from Sponder and Lauder (1981) suggested the pharyngeal plates took the role of the intraoral transport. However, these two studies used immobilized prey and implemented in laboratory condition (uniform terrain), which do not reflect the feeding in nature. From observation of feeding behavior of some carnivorous mudskippers, we tentatively presume that the hydrodynamic tongue can only perform near water's edge where the mud surface is smooth and moisture allowing suction mechanism, and uses to capture less evasive prey, e.g., polychaetes, mixed with mud particles. This could be the case of *Ps. modestus* hunting by sucking mouthful of water, protruding and sucking back the water with prey and gurgling the mouth (Fig. VI-2a), but further confirmation is needed. However, this mechanism is impractical when hunting for evasive and durable prey in non-uniform terrain of higher terrestrial environment. We observed that *Ps. chrysospilos* and *Pn. schlosseri* usually hunt by jumping forward with the mouth opened and handling prey by the oral jaws. Their prey are durable, evasive, and occasionally larger than their gape (Figs. VI-2b and VI-2c). Therefore, the hydrodynamic tongue cannot be used in these cases. The strong canine teeth on the oral jaws, high jaw-closing value, and developed adductor mandibulae 2 could serve handling these types prey. *Periophthalmodon. septemradiatus* found feeding mainly on ants (Dinh et al. 2020)

distributed in highly terrestrial environment, and rarely venturing into water (Mai et al. 2019). These raise the question: whether or not they feed without using water, and if not, what mechanism they employ to swallow prey on land. Note that mudskippers have the "tongue adnate" (Murdy 1989; also see Fig. VI-3), which may not function as the muscular tongue in amphibians and tetrapods. Therefore, further investigation of swallowing prey on land of mudskippers could gain more understanding of early stage of feeding transition.

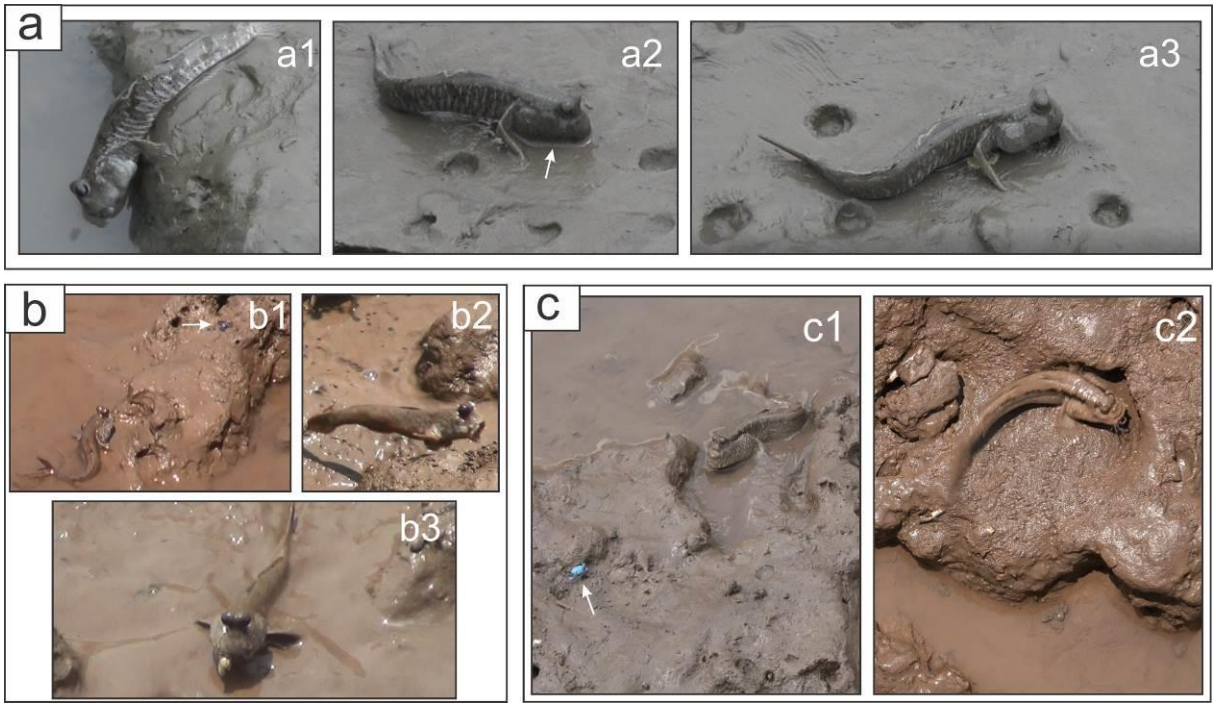

Fig. VI-2 Feeding behavior of *Periophthalmus modestus* (**a**), *Periophthalmus chrysospilos* (**b**), and *Periophthalmodon schlosseri* (**c**). *Ps. modestus* shows the suction mouthful of water (**a1)**, prey suction (**a2**), and mouth gurgling (**a3**) in their feeding cycle, while *Ps. chrysospilos* and *Pn. schlosseri* strike with mouth opened. Arrows indicate water released as suction in *Ps. modestus* (**a2**), small crab in **b1** and **c1**. Photos were taken from video footages recored in Ariake Sea, Saga, Japan (**a**) and in in Mo O mudflat, Soc Trang Province, Vietnam (**b**, **c**)

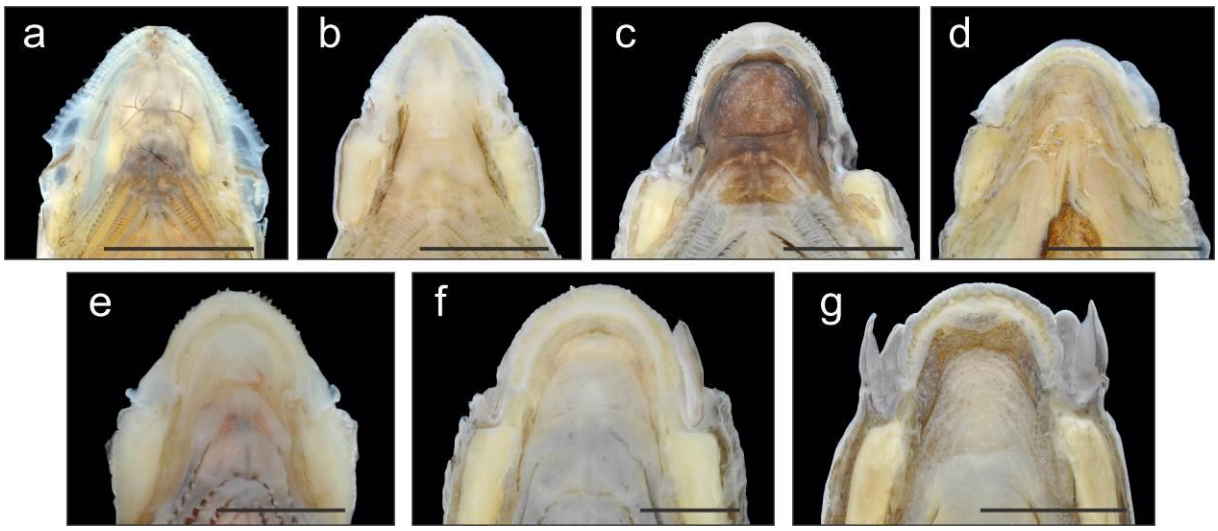

Fig. VI-3 The mouth floor of *Oxuderces nexipinnis* (**a**), *Scartelaos histophorus* (**b**), *Boleophthalmus boddarti* (**c**), *Periophthalmus modestus* (**d**), *Periophthalmus chrysospilos* (**e**), *Periophthalmodon schlosseri* (**f**), and *Periophthalmodon septemradiatus* (**g**) in dorsal views. Scales: 5 mm

REFERENCES

Abdoli L, Kiabi B, Kamrani E, Abdoli A, Rezazadeh Katehsari E, Keshavarz M (2012) Feeding habits of *Scartelaos tenuis* in Bushehr Province, Iran. J Fish Iran J Nat Resource 64:309-318

Abidizadegan M, Saeid EP, Hosein R (2015) Partial morphometrics and meristic evaluation of the two species mudskippers: *Scartelaos tenuis* (Day, 1876) and *Periophthalmus waltoni* (Koumans, 1941) from the Persian Gulf, Bushehr, Iran. Int J Fish Aquat Stud 2:353-358

Aguilar NM, Ishimatsu A, Ogawa K, Khoo KH (2000) Aerial ventilatory responses of the mudskipper, *Periophthalmodon schlosseri*, to altered aerial and aquatic respiratory gas concentrations. Comp Biochem Physiol 127A:285-292

Ahlberg PE, Clack JA (1998) Lower jaws, lower tetrapods – a review based on the Devonian genus Acanthostega. Trans R Soc Edinburgh Earth Sci 89:11.46

Ahlberg PE, Milner AR (1994) The origin and early diversification of tetrapods. Nature 368:507-514

Ahlberge PE (2018) Follow the footprint and mind the gaps: A new look at the origin of tetrapods. Earth Environ Sci Trans R Soc Edinb 109:115-137

Aleem AA (1950) The diatom community inhabiting the mud-flats at Whitstable. New Phytol 49:174-188

Alongi D.M. 2015. The impact of climate change on mangrove forests. Curr Clim Change Rep 1:30–39

Anderson PS, Friedman M, Ruta M (2013) Late to the table: diversification of tetrapod mandibular biomechanics lagged behind the evolution of terrestriallity. Integr Comp Biol 53:197– 208

Ansari AA, Trivedi S, Saggu S, Rehman H (2014) Mudskipper: A biological indicator for environmental monitoring and assessment of coastal waters. Journal of Entomology and Zoology Studies, 2(6):22-33

Ashley-Ross MA, Hsieh ST, Gibb AC, Blob RW (2013) Vertebrate land invasions – Past, present, and future: An introduction to the symposium. Integr Comp Biol 53(2): 192-196

Beon MS, Oh MK, Lee YJ, Kim CH, Park JY (2013) A comparative study on vascularization and the structure of the epidermis of an amphibious mudskipper fish, *Scartelaos gigas* (Gobiidae, Teleostei), on different parts of the body and the appendages. J Appl Ichthyol 29:410-415

Berry PY, Low MP (1970) Comparative studies on some aspects of the morphology and histology of *Ctenopharyngodon idellus*, *Aristichthys nobilis*, and their hybrid (Cyprinidae). Copeia 1970:708-726

Bryan-Brown DN, Connolly RM, Richards DR, Adame F, Friess DA, Brown CJ (2020) Global trends in mangrove forest fragmentation. Sci Rep 10:7117

Bucholtz RH, Meilvang AS, Cedhagen T, Christensen JT, Macintosh DJ (2009) Biological observations on the mudskipper *Pseudapocryptes elongatus* in the Mekong Delta, Vietnam. J World Aquac Soc 40:711-723

Burress ED (2015) Cichlid fishes as models of ecological diversification: patterns, mechanisms, and consequences. Hydrobiologia 748:7-27

Burress ED (2016) Ecological diversification associated with the pharyngeal jaw diversity of Neotropical cichlid fishes. J Anim Ecol 85:302-313

Camp AL, Konow N, Sanford CPJ (2009) Functional morphology and biomechanics of the tongue-bite apparatus in salmonid and osteoglossomorph fishes. J Anat 214:71.-728

Carey N, Goldbogen JA (2017) Kinematics of ram filter feeding and beat-glide swimming in the northern anchovy *Engraulis mordax*. J Exp Biol 220:2717-2725

Carroll RL (2001) The origin and early radiation of terrestrial vertebrates. J Paleont 75(6):1202-1213

Cataldi E, Cataudella S, Monaco G, Rossi A, Tancioni L (1987) A study of the histology and morphology of the digestive tract of the sea-bream, *Sparus aurata*. J Fish Biol 30:135-145

Chapman WM (1941) The osteology and relationships of the isospondylous fish, *Plecoglossus altivelis* Temminck and Schlegel. J Morph 68:425-455

Chaudhuri A, Mukherjee S, Homechaudhuri S (2014) Food partitioning among carnivores within feeding guild structure of fishes inhabiting a mudflat ecosystem of Indian Sundarbans. Aquat Ecol 48:35-51

China V, Levy L, Liberzon A, Elmaliach T, Holzman R (2017) Hydrodynamic regime determines the feeding success of larval fish through the modulation of straking kinematics. Proc R Soc B 284:20170235

Clack JA (2012) Gaining ground: the origin and evolution of tetrapods. Bloomington: Indiana University Press

Clayton D (2017) Feeding behavior: a review. In: Jaafar Z, Murdy EO (eds) Fishes out of water: biology and ecology of mudskippers. CRC Press, Boca Raton, pp 237-275

Clayton DA (1993) Mudskippers. Oceanogr Mar Biol Annu Rev 31:507-577

Clayton DA (2017) Feeding behavior: A review. In: Jaafar Z, Murdy EO (ed) Fishes out of water: Biology and ecology of mudskippers. CRC Press, Taylor & Francis Group, pp 237-275

Cohen KE, Hernandez LP (2018) Making a master filterer: Ontogeny of specialzed filtering plates in silver carp (*Hypophthalmichthys molitrix*). J Morphol 279:925– 935

Collard F, Gilbert B, Eppe G, Roos L, Compere P, Das K, Parmentier E (2017) Morphology of the filtration apparatus of three planktivorous fishes and relation with ingested anthropogenic particles. Mar Pollut Bull 116:182-191

Crownder LB (1985) Optimal foraging and feeding mode shift in fishes. Envi Biol Fish 12(1):57-62

Das BK (1934) The habits and structure of *Pseudapocryptes lanceolatus*, a fish in the first stage of structural adaptation to aerial respiration. Proc Roy Soc Lond 115:422-430

Delariva RL, Agostinho AA (2001) Relationship between morphology and diets of six neotropical loricariids. J Fish Biol 58:832-847

Dingerkus G, Uhler LD (1977) Enzyme clearing of alcian blue stained whole small vertebrates for demonstration of cartilage. Stain Technol 52:229-232

Dinh QM, Qin JG, Dittmann S, Tran DD (2014) Burrow morphology and utilization of the goby (*Parapocryptes serperaster*) in the Mekong Delta, Vietnam. Ichthyol Res 61:332-340

Dinh QM, Qin JG, Dittmann S, Tran DD (2017) Seasonal variation of food and feeding in burrowing goby *Parapocryptes serperaster* (Gobiidae) at different body sizes. Ichthyol Res 64:179-189

Dinh QM, Tran LT, Tran TTM, To DK, Nguyen TTK, Tran DD (2020) Variation in diet composition of the mudskipper, Periophthalmodon septemradiatus, from Hau River, Vietnam. Bull Mar Sci 96(3):487-500

Dinh QM, Tran TT, Phan TT, Bui MT, Nguyen TTK, Tran DD, Vo TT, Mai HV, Tran LX, Ishimatsu A (2020) Borrow structure and utilization in the mudskipper *Periophthalmodon septemradiatus* from the Mekong Delta. J Zoo 314(1)72-83

Drenner RW, Mummert JR (1984) Selective particle ingestion by a filter-feeding fish and its impact on phytoplankton community structure. Limnol Oceanogr 29: 941-948

Dôtu Y (1961) The bionomics and life history of the gobioid fish, *Apocryptodon bleekeri* (Day). Bull Fac Fish Nagasaki Univ 10:133-139

Dôtu Y, Mito S (1955) Life history of a Gobioid fish, *Sicydium japonicum* Tanaka. Sci Bull Fac Agric Kyusyu Univ 15:213-221

Ebeling AW (1957) The dentition of eastern Pacific mullets, with special reference to adaptation and taxonomy. Copeia 1957:173-185

Elgendy SAA, Alsafy MAM, Tanekhy M (2016) Morphological characterization of the oral cavity of the gilthead seabream (*Sparus auratus*) with emphasis on the teeth-age adaptation. Microsc Res Tech 79:227-236

Ferry LA, Paig-Tran EM, Gibb AC (2015) Suction, ram, and biting: deviations and limitations to the capture of aquatic prey. Integr Comp Biol 55(1):97–109

Fink WL (1981) Ontogeny and phylogeny of tooth attachment modes in actinopterygian fishes. J Morphol 167:167-184

Fishelson L, Delarea Y (2014) Comparison of the oral cavity architecture in surfeonfishes (Acanthuridae, Teleostei), with emphasis on the taste buds and jaw "retention plates". Evviron Biol Fish 97:173-185

Friedland KD, Ahrenholz DW, Smith JW, Manning M, Ryan J (2006) Sieving functional morphology of the gill raker feeding apparatus of Atlantic Menhaden. J Exp Zool 305A:974-985

Geerinckx T, Poorter JD, Adriaens D (2007) Morphology and development of teeth and epidermal brushes in loricariid catfishes. J Morphol 368:805-814

Gerking SD (1994) Feeding ecology of fish. Academic Press, San Deago

Ghaffar MA, Yakob F, Nor SM, Arshad A (2006) Foraging behavior and food selection of giant mudskipper (Periophthalmodon schlosseri) at Kuala Gula, Matang Mangrove Reserve, Perak, Malaysia. Coast Mar Sci 30(1):263-267

Gibson RN (1988) Development, morphometry and particle retention capability of the gill rakers in the herring, *Clupea harengus* L. J Fish Biol 32:949-962

Gibson RN, Ezzi IA (1985) Effect of particle concentration on filter- and particulate-feeding in the herring *Clupea harengus*. Mar Biol 88:109-116

Giri C, Ochieng E, Tieszen LL, Zhu Z, Singh A, Loveland T, Masek J, Duke N (2011) Status and distribution of mangrove forests of the world using earth observation satellite data. Glob Ecol Biogeogr 20:154–159

Goldberg L, Lagomasino D, Thomas N, Fatoyinbo T (2020) Global declines in human-driven mangrove loss. Glob Chang Biol 26(10):5844-5855

Gonzales TT, Katoh M, Mazlan G, Ishimatsu A (2011) Gross and fine anatomy of the respiratory vasculature of the mudskipper, *Periophthalmodon schlosseri* (Gobiidae: Oxudercinae). J Morphol 272:629-640

Gophen M, Geller W (1984) Filter mesh size and food particle uptake by Daphnia. Oecologia 64: 408-412

Graham JB, Lee HJ, Wegner NC (2007) Transition from water to land in an extant group of fishes: air breathing and the acquisition sequence of adaptations for amphibious life in Oxudercine gobies. In: Fernandes MN, Rantin FT, Glass ML, Kapoor BG (eds) Fish Respiration and environment. Science Publisher, Enfield, pp 255-288

Grubich J (2003) Morphological convergence of pharyngeal jaw structure in durophagous perciform fish. Biol J Linn Soc 80:147-165

Grubich JR (2005) Disparity between feeding performance and predicted muscle strength in the pharyngeal musculature of black drum, Pogonias cromis (Sciaenidae). Envi Biol Fish 74:261-272

Grubich JR, Rice AN, Westneat MW (2008) Functional morphology of bite mechanics in the great barracuda (*Sphyraena barracuda*). Zool 111:16-29

Günther ACLG (1880) A introduction o the study of fishes. Adam & Charles Black, Edinburgh

Heiss E, Aerts P, Van Wassenbergh S (2018) Aquatic–terrestrial transitions of feeding systems in vertebrates: a mechanical perspective. J Exp Biol 221:jeb154427

Hiatt RW (1947) Food-chains and the food cycle in Hawaiian fish ponds - Part I: The food

and feeding habits of mullet (*Mugil cephalus*), milkfish (*Chanos chanos*), and the ten-pounder (*Elops machnata*). Trans Am Fish Soc 74:250-261

Hoogenboezem W, van den Berg C, Sibbing FA, Lammens EHRR, Terlouw A, Osse JWM (1991) A new model of particle retention and branchial sieve adjustment in filter-feeding bream (*Abramis brama*, Cyprinidae). Can J Fish Aquat Sci 48:7-18

Hora SL (1936) Ecology and bionomics of the gobioid fishes of the Gangetic delta. Compt Rend XII Congr Internat Zool, Lisbonne 1935 12:841-863

Howes GJ (1987) Oral ontogeny of the Ayu, *Plecoplossus altivelis* and comparisons with the jaws of other salmoniform fishes. Zool J Linn Soc 89:133-169

Hui NY, Mohamed M, Othman MNA, Tokiman L (2019) Diversity and behavior of mudskippers of Tanjung Piai, Pontian, Johor. IOP Conf Ser: Earth Envon Sci 269:1-15

Hulsey CD (2006) Function of a key morphological innovation: fusion of the cichlid pharyngeal jaw. Proc R Soc B 273:669-675

Hundt PJ, Iglésias SP, Hoey AS, Simons AM (2014a) A multilocus molecular phylogeny of combtooth blennies (Percomorpha: Blennioidei: Blenniidae): multiple invasions of intertidal habitats. Mol Phylogenetics Evol 70:47-56

Hundt PJ, Nakamura Y, Yamaoka K (2014b) Diet of combtooth blennies (Blenniidae) in Koichi and Okinawa, Japan. Ichthyol Res 61:76-82

Hundt PJ, Simons AM (2018) Extreme dentition does not prevent diet and tooth diversification within combtooth blennies (Ovalentaria: Blenniidae). Evolution 72(4):930-943

Iida M, Watanabe S, Tsukamoto K (2015) Oceanic larval duration and recruitment mechanism of the amphidromous fish *Sicyopterus japonicus* (Gobioidei: Sicydiinae). Reg Stud Mar Sci 1:25-33

Iida M, Watanabe S, Yamada Y, Lord C, Keith P, Tsukamoto K (2010) Survival and behavioral characteristics of amphidromous goby larvae of *Sicyopterus japonicus* (Tanaka, 1909) during their downstream migration. J Exp Mar Biol Ecol 383:17-22

Ishimatsu A, Gonzales TT (2011) Mudskippers: front runners in the modern invasion of land. In: Patzner R, Van Tassell JL, Kovačić M, Kapoor BG (eds) The biology of gobies. Science Publishers, Enfield, pp 609-638

Ishimatsu A, Hishida Y, Takita T, Kanda T, Oikawa S, Takeda T, Huat KK (1998) Mudskippers store air in their burrows. Nature 391:237-238

Ishimatsu A, Ishimatsu M (2021) An annotated translation of "Morphologie und Physiologie der Atmung bei wasser-, schlamm- und landlebenden Gobiiformes" by Elfriede Schöttle (1931). Bull Fac Fish Nagasaki Univ 101:1-149

Ishimatsu A, Yoshida Y, Itoki N, Takeda T, Lee HJ, Graham JB (2007) Mudskippers brood their eggs in air but submerge them for hatching. J Exp Biol 210:3946-3954

Iwasaki S, Erdoğan S, Asami T (2019) Evolutionary specialization of the tongue in vertebrates: structure and function. In: Bels V, Whishaw IQ (eds) Feeding in vertebrates: evolution, morphology, behavior, biomechanics. Springer, Cham, pp333-384

Iwata K (1976) Morphological and physiological studies on the phytoplankton feeders in cyprinid fishes: I. Developmental changes of feeding organs and ingestion rates in Kawachibuna (*Carassius auratus cuvieri*), Silver carp (*Hypophthalmichthys molitrix*) and Nigorobuna (*C. auratus grandoculis*). Jpn J Limnol 37:135-147

Jordan DS (1905) Guide to the study of fishes. Henry Holt and Company

Kashi AM, Tahermanesh K, Chaichian S, Joghataei MT, Moradi F, Tavangar SM, Abed SM (2014) How to prepare biological samples and live tissues for scanning electron microscopy (SEM). GMJ 3:63-80

Katano O, Uchida K, Aonuma Y (2004) Experimental analysis of the territorial establishment of ayu, *Plecoglossus altivelis*. Ecol Res 19:433-444

Khaironizam M, Norma-Rashid Y (2000) A new record of the mudskipper *Parapocryptes serperaster* (Oxudercinae: Gobiidae) from Peninsular Malaysia. Malay J Sci 19:101-104

Koh C, Khim JS, Araki H, Yamanishi H, Koga K (2007) Within-day and seasonal patterns of microphytobenthos biomass determined by co-measurement of sediment and water column chlorophylls in the intertidal mudflat of Nanaura, Saga, Ariake Sea, Japan. Estuar Coast Shelf Sci 72:42-52

Koh C, Khim JS, Araki H, Yamanishi H, Mogi H, Koga K (2006) Tidal resuspension of microphytobenthic chlorophyll a in a Nanaura mudflat, Saga, Ariake Sea, Japan: flood-ebb and spring-neap variations. Mar Ecol Prog Ser 312:85-100

Konow N, Sanford CPJ (2008a) Is a convergently derived muscle-activity pattern driving novel raking behaviors in teleost fishes? J Exp Biol 211:989-999

Konow N, Sanford CPJ (2008b) Biomechanics of a convergently derived prey-processing mechanism in fishes: evidence from comparative tongue bite apparatus morphology and raking kinematics. J Exp Biol 211:3378-3391

Kotrschal K (1989) Trophic ecomorphology in eastern Pacific blennioid fishes: character transformation of oral jaws and associated change of their biological roles. Evn Biol Fish 24(3):199-218

Lazzaro X (1987) A review of planktivorous fishes: Their evolution, feeding behaviours, selectivities and impacts. Hydrobiologia 146:97-167

Lemberg JB, Daeschler EB, Shubin NH (2021) The feeding system of *Tiktaalik roseae*: an intermediate between suction feeding and biting. PNAS 118(7):1-10

Liem KF (1974) Evolutionary strategies and morphological innovations: cichlid pharyngeal jaws. Syst Zool 22:425–441

Liem KF (1990) Aquatic versus terrestrial feeding modes: possible impacts on the trophic ecology of vertebrates. Am Zool 30:209-221

Lombard RE, Wake DB (1986) Tongue evolution in the lungless salamanders, family *Plethodontidae*. IV. Phylogeny of plethodontid salamanders and the evolution of feeding dynamics. Syst Zool 35(4):532-551

Long JA, Gordon MS (2004) The greatest step in vertebrate history: a paleobiological review of the fish-tetrapod transition. Phisiol Biochem Zool 77(5):700-719

Mai HV, Tran XL, Dinh MQ, Tran DD, Murata M, Sagara H, Yamada A, Shirai K, Ishimatsu A (2019) Land invasion by the mudskipper, *Periophthalmodon septemradiatus*, in fresh and saline waters of the Mekong River. Sci Rep 9:14227

Mai VH, Tran LX, Dinh QM, Tran DD, Murata M, Sagara H, Yamada A, Shirai K, Ishimatsu A (2019) Land invasion by the mudskipper, *Periophthalmodon septemradiatus*, in fresh and saline waters of the Mekong River. Sci Rep 9:14227

Mallatt J (1984) Early vertebrate evolution: pharyngeal structure and the origin of gnathostomes. J Zool 204:169-183

Markey MJ, Main RP, Marshall CR (2006) In vivo cranial suture function and suture morphology in the extant fish Polypterus: implications for inferring skull function in living and fossil fish. J Exp Biol 209:2085-2102

Markey MJ, Marshall CR (2007) Terrestrial-style feeding in a very early aquatic tetrapod is supported by evidence from experimental analysis of suture morphology. PNAS 104(17): 7134-7138

Martin KLM, Ishimatsu A (2017) Review of reproductive strategies. In: Jaafar Z, Murdy EO (ed) Fishes out of water: Biology and ecology of mudskippers. CRC Press, Taylor & Francis Group, pp 209-236

Michel KB, Adriaens D, Aerts P, Dierick M, Van Wassenbergh S (2014) Functional anatomy and kinematics of the oral jaw system during terrestrial feeding in *Periophthalmus barbarus*. J Morph 275:1145-1160

Michel KB, Aerts P, Gibb AC, Wassenbergh SV (2015a) Functional morphology and kinematics of terrestrial feeding in the largescale foureyes (*Anableps anableps*). J Exp Biol 218:2951-2960

Michel KB, Heiss E, Aerts P, Wassenbergh SV (2015b) A fish that uses its hydrodynamic

tongue to feed on land. Proc R Soc B. 282:20150057

Mochizuki K, Fukui S (1983) Development and replacement of upper jaw teeth in gobiid fish, *Sicyopterus japonicus*. Jpn J Ichthyol 30:27-36

Morales A, Rosenlund K (1979) Fish bone measurements: An attempt to standardize the measuring of fish bones from archaeological sites. Zoologisk Museum, Kobenhavn, Copenhagen

Munshi JSD, Ghosh TK, Roy PK, Mishra AK (1984) Scanning electron microscopic observation on the structure of gill-rakers of some freshwater teleostean fishes. Proc Indian Natn Sci Acad B50:549-554

Murdy EO (1989) A taxonomic revision and cladistic analysis of the oxudercine gobies (Gobiidae: Oxudercinae). Rec Aust Mus Suppl 11:1-93

Murdy EO, Jaafar Z (2017) Taxonomy and systematics review. In: Jaafar Z, Murdy EO (eds.) Fishes out of water: biology and ecology of mudskippers. CRC Press, Boca Raton, pp 1-36

Nanami A (2016) Parrotfish grazing ability: interspecific differences in relation to jaw-lever mechanics and relative weight of adductor mandibulae on an Okinawan coral reef. PeerJ 4:e2425

Norton SF, Brainerd EL (1993) Convergence in the feeding mechanics of ecomorphologically similar species in the centrarchidae and cichlidae. J Exp Biol 176:11-29

Nursall JR (1981) The activity budget and use of territory by a tropical blenniid fish. Zool J Linnean Soc 72:69-92

Ord TJ, Cooke GM (2016) Repeated evolution of amphibious behavior in fish and its implications for the colonization of novel environment. Evolution 70(8):1747-1759

Parenti LR, Jaafar Z (2017) The natural distribution of mudskippers. In: Jaafar Z, Murdy EO (ed) Fishes out of water: Biology and ecology of mudskippers. CRC Press Taylor & Francis Group, pp37-68

Park JY, Lee YJ, Kim IS, Kim SY (2003) A comparative study of the regional epidermis of an amphibious mudskipper fish, *Boleophthalmus pectinirostris* (Gobiidae, Pisces). Folia Zool 52:431-440

Polgar G (2009) Species-area relationship and potential role as a biomonitor of mangrove communities of Malayan mudskippers. Wetl Ecol Manag 17:157-164

Polgar G, Bartolino V (2010) Size variation of six species of oxudercine gobies along the intertidal zone in a Malayan coastal swamp. Mar Ecol Prog Ser 409:199-212

Polgar G, Crosa G (2009) Multivariate characterisation of the habitats of seven species of Malayan mudskippers (Gobiidae: Oxudercinae). Mar Biol 156:1475-1486

Polgar G, Sacchetti A, Galli P (2010) Differentiation and adaptive radiation of amphibious gobies (Gobiidae: Oxudercinae) in semi-terrestrial habitats. J Fish Biol 77:1645-1664

Polidoro B (2017) Taxa and habitat conservation. In: Jaafar Z, Murdy EO (eds.) Fishes out of water: biology and ecology of mudskippers. CRC Press Taylor & Francis Group, pp 349-368

Provini P, van Wassenbergh S (2018) Hydrodynamic performance of suction feeding in virtually unaffected by variation in the shape of the posterior region of the pharynx in fish. R Soc Open Sci 5:181249

Rao HS, Hora SL (1933) On the ecology, bionomics and systematics of the Blennid fishes of the genus *Andamia* Blyth. Rec Indian Museum 40:377-401

Reilly SM (1996) The metaphorphosis of feeding kinematics in *Salamandra salamandra* and the evolution of terrestrial feeding behavior. J Exp Biol 199:1219-1227

Reilly SM, Lauder GV (1990) The evolution of tetrapod feeding behavior: Kinematic homologies in prey transport. Evolution 44(6):1542-1557

Ridho MR, Patriono E, Sholikah M (2019) Food habits of three species of mudskippers in the Musi River Estuary, South Sumatra, Indonesia. Biodiversitas 20(8):2368-2374

Sahara N, Moriyama K, Iida M, Watanabe S (2013) Unique features of pedicellate attachment

of the upper jaw teeth in the adult gobiid fish *Sicyopterus japonicus* (Teleostei, Gobiidiae): Morphological and structural characteristics and development. J Morphol 274:512-524

Sakai H, Nakamura M (1979) Two new species of freshwater gobies (Gobiidae: Sicydiaphiinae) from Ishigaki Island, Japan. Jpn J Ichthyol 26:43-54

Salman NA, Al-Mahdawi GJ, Heba HMA (2005) Gill rakers morphometry and filtering mechanism in some marine teleost from Red Sea coasts of Yemen. Egypt J Aquat Res 31:286-296

Sanderson SL, Cheer AY, Goodrich JS, Groziano JD, Callan WT (2001) Crossflow filtration in suspension-feeding fishes. Nature 412:439-441

Sanderson SL, Stebar MC, Ackermann KL, Jones SH, Batjakas IE, Kaufman L (1996) Mucus entrapment of particles by suspension-feeding tilapia (Pisces: Cichlidae). J Exp Biol 199:1743-1756

Sanderson SL, Wassersug R (1990) Suspension-feeding vertebrates. Sci Am 262(3):96-102

Schwenk K, Rubega M (2005) Diversity of vertebrate feeding system. In: Starck JM, Wang T (ed) Physiological and ecological adaptation to feeding in Vertebrates. Science Publishers, Enfield, New Hampshire, pp1-41

Schöttle E (1931) Morphologie und Physiologie der Atmung bei wasser-, schlamm- und landlebenden Gobiiformes. Z wiss Zool 140:1-114

Smith JC, Sanderson SL (2007) Mucus function and crossflow filtration in a fish with gill rakers removed versus intact. J Exp Biol 210:706-2713

Sponder DL, Lauder GV (1981) Terrestrial feeding in the mudskipper *Periophthalmus* (Pisces: Teleostei): A cineradiographic analysis. J Zool Lond 193:517-530

Storm TJ, Nolan KE, Roberts EM, Sanderson SL (2020) Oropharyngeal morphology related to filtration mechanisms in suspension-feeding American shad (Clupeidae). J Exp Zool 333:493-510

Suzuki N (1992) Fine structure of the epidermis of the mudskipper, *Periophthalmus modestus* (Gobiidae). Japan J Ichthyol 38:379-397

Tachihara K, Kimura S (1991) Changes in the distribution and food with growth of the landlocked ayu larvae *Plecoglossus altivelis altivelis* of Lake Ikeda in southern Kyushu. Nippon Suisan Gakkaishi 57:797-804

Takeda T, Hayashi M, Toba A, Soyano K, Ishimatsu A (2012) Ecology of the Australian mudskipper, *Periophthalmus minutus*, an amphibious fish inhabiting a mudflat in the highest intertidal zone. Austr J Zool 59:312-320

Takita T, Agusnimar, Ali AB (1999) Distribution and habitat requirements of oxudercine gobies (Gobiidae: Oxudercinae) along the Straits of Malacca. Ichthyol Res 46:131-138

Tattersal A (2018) Open wide. Biogaphic, California Academy of Sciences, http://www.biographic.com/open-wide/ (accessed July 2021)

Taylor WR, Van Dyke GC (1985) Revised procedures for staining and clearing small fishes and other vertebrates for bone and cartilage study. Cybium 9:107-119

Thomson JM (1954) The organs of feeding and the food of some Australian mullet. Aust J Mar Freshw Res 5:469-485

Thomson KS (1967) Mechanisms of intracranial kinetics in fossil rhipidistian fishes (Crossopterygii) and their relatives. Zoo J Linnean Soc 46(310):223-253

Thomson KS (1969) The biology of the lobe-finned fishes. Biol Rev 44:91-154

Thorne KM, Dugger BD, Buffington KJ, Freeman CM, Janousek CN, Powelson KW, Gutenspergen GR, Takekawa JY (2015) Marshes to mudflats – Effects of sea-level rise on tidal marshes along a latitudinal gradient in the Pacific Northwest. US Geological Survey Open-File Report 2015-1204: 54pp

Tran LX, Maekawa Y, Soyano K, Ishimatsu, A (2020) Morphology of the feeding apparatus in the herbivorous mudskipper, *Boleophthalmus pectinirostris* (Linnaeus, 1758). Zoomorphology 139:231-243

Tran X, Maekawa Y, Soyano K, Ishimatsu A (2021) Morphological comparison of the feeding apparatus in herbivorous, omnivorous and carnivorous mudskippers (Gobiidae: Oxudercinae). Zoomorphology doi:10.1007/s00435-021-00530-8

Trapani J (2001) Position of developing replacement teeth in teleosts. Copeia 2001:35-51

Uehara K, Miyoshi S (1993) Structure of comblike teeth of the ayu sweetfish, *Plecoglossus altivelis* (Teleostei: Isospondyli) - I. Denticles and tooth attachment. J Morphol 217:229-238

Van Wassenbergh SV (2013) Kinematics of terrestrial capture of prey by the eel-catfish *Channallabes apus*. Integr Comp Biol 53:258-268

Van Wassenbergh SV, Bonte C, Michel KB (2017) Terrestrial capture of prey by the reedfish, a model species for stem tetrapods. Ecol Evol 2017:3856-3860

Wainwright PC (2006) Functional morphology of the pharyngeal jaw apparatus. In: Shadwick RE, Lauder GV (ed) Fish biomechanics. Elsevier Academic Press, pp77-101

Wainwright PC, Bellwood DR, Westneat MW, Grubich JR, Hoey AS (2004) A functional morphospace for the skull of labrid fishes: patterns of diversity in a complex biomechanical system. Biol J Linn Soc 82:1-25

Wainwright PC, Mcgee MD, Longo SJ, Hernandez LP (2015) Origins, innovations, and diversification of suction feeding in vertebrates. Integr Comp Biol 55:134-145

Weller HI, Mcmahan CD, Westneat MW (2016) Dirt-sifting devilfish: winnowing in the geophagine cichlid *Satanoperca daemon* and evolutionary implications. Zoomorphology 136:45-59

Westneat MW (1995) Feeding, function, and phylogeny: analysis of historical biomechanics in labrid fishes using comparative methods. Syst Biol 44:361-383

Westneat MW (2003) A biomechanical model for analysis of muscle force, power output and lower jaw motion in fishes. J Theor Biol 223:269-281

Westneat MW (2006) Skull biomechanics and suction feeding in fishes. In: Shadwick RE,

Lauder GV (eds) Fish Physiology Vol. 23, Fish Biomechanics. Academic Press, Amsterdam pp29-75

Westneat MW (2006) Skull biomechanics and suction feeding in fishes. In: Shadwick RE, Lauder GV (edd) Fish biomechanics. Elsevier Academic Press, California USA, pp29-76

Yang KY, Lee SY, Williams GA (2003) Selective feeding by the mudskipper (*Boleophthalmus pectinirostris*) on the microalgal assemblage of a tropical mudflat. Mar Biol 143:245-256

Yodnarasri S, Tada K, Montani S (2006) Temporal change of the environmental conditions of the sediment and abundance of the nematode community in the subtidal sediment near a river mouth with tidal flats. Plankton Benthos Res 1(2):109-116

Yokoya S, Tamura OS (1992) Fine structure of the skin of the amphibious fishes, *Boleophthalmus pectinirostris* and *Periophthalmus cantonensis*, with special reference to the location of blood vessels. J Morphol 214:287-297

Zhang J, Taniguchi T, Takita T, Ali AB (2000) On the epidermal structure of *Boleophthalmus* and *Scartelaos* mudskippers with reference to their adaptation to terrestrial life. Ichthyol Res 47:359-366

Zhang J, Taniguchi T, Takita T, Ali AB (2003) A study on the epidermal structure of *Periophthalmodon* and *Periophthalmus* mudskippers with reference to their terrestrial adaptation. Ichthyol Res 50:310-317

van den Berg C, Sibbing, FA, Osse JWM, Hoogenboezem W (1992). Structure, development and function of the branchial sieve of the common bream, *Abramis brama*, white bream, *Blicca bjoerkna* and roach, *Rutilus rutilus*. Environ Biol Fish, 33, 105-124

ACKNOWLEDGEMENTS

Throughout the implementation of the five-year course and this study, I have received a great support and assistance.

I would first like to acknowledge the Ministry of Education, Culture, Sport, Science and Technology (MEXT) for providing scholarship of the five-year program; Keidanren Nature Conservation Fund "Conservation and cleaning up of Mo O mudflat, Mekong river-mouth" and Japan Society for the Promotion of Science for partly funding this study.

I would like to acknowledge my supervisor, Professor Atsushi Ishimatsu, whose expertise was invaluable in formulating the research questions and methodology. I really appreciate your guidance through each stage of the process and supporting my life while I have been in Japan.

I also express my appreciation to my co-supervisor, Professor Kiyoshi Soyano, for providing advice on my study and courses, especially in the last three years of my study.

I would like to thank Professor Katsunori Tachihara (Faculty of Science, University of the Ryukyus) for accepting me in his laboratory during my internship.

I am also thankful to Dr. Yu Maekawa (The University Museum, The University of Tokyo) for her support of the micro-computed tomography scanning and advice on manuscript writing, Dr. Kenjiro Hinode (Institute for East China Sea Research, Nagasaki University) for his guidance for scanning electron microscopy and diatom taxonomy; Dr. Gianluca Polgar (CNR IRSA Water Research Institute, Verbania, Italy) for his great advice on the manuscripts.

I would like to thank Ms. Mizuri Ishimatsu (Institute for East China Sea Research, Nagasaki University), Dr. Mai Van Hieu (College of Aquaculture and Fisheries, Can Tho University), fishermen in the Ariake Sea (Saga, Japan) and Mo O mudflat (Soc Trang, Vietnam) for their help in sample collection; Professor Kei'ichiro Iguchi (Graduate School of Fisheries and Environmental Sciences, Nagasaki University) for providing us with the specimens of *Plecoglossus altivelis*; Dr. Kentaro Hirashima (Wakayama Prefectural Museum of Natural

History) and Dr. Midori Iida (Sado Marine Biological Station, Niigata University) for providing us with the specimens of *Sicyopterus japonicus*; Associate Professor Tran Dac Dinh (College of Aquaculture and Fisheries, Can Tho University) and Associate Professor Nguyen Van Cong (Environment and Natural Resources, Can Tho University) for arranging our trips to Mo O.

I am most grateful to all members of the Institute for East China Sea Research, especially students under supervision of Prof. Atsushi Ishimatsu and Prof. Kiyoshi Soyano, for their assistance in my study and my life in Japan.

I finally acknowledge my wife and my family for their taking care of my children, and standing by me during the past five years.

APPENDICES

Table S1 Comparison of feeding habit and terrestriality among oxudercine gobies

Species	Major food items[#]	Terrestriality
Periophthalmus argentilineatus	*CR*, *NT*, *PC* (16,23)	Moderate to high – *Ps. novemradiatus* occurred on open seashore beaches or up the tidal reaches of rivers (26). *Ps. gracilis* and *Ps. variabilis* were found in the most terrestrial conditions. *Ps. chrysospilos* was in an intermediate position (19). *Ps. minutus* confined themselves in burrows throughout the nine-day, non-inundation period in the dry season (25).
Ps. barbarus	*CR*, *FS*, *PC*, *INS* (5*,9)	
Ps. magnuspinnatus	*CR* (3,4)	
Ps. modestus	*CR*, *PC*, *INS* (4)	
Ps. minutus	*BV*, *CR*, *GP*, *INS (A)* (25)	
Ps. novemradiatus	*CC*, *INS (AQ)*, PP (8)	
Periophthalmodon schlosseri	*CR*, *F*, *INS* (18,29)	High – *Pn. schlosseri*, at Uttarbhag, it is the most terrestrial. It is never found submerged underwater and it is not uncommon to find specimens hopping about on dry beds of pools or on the banks of the channels above tidal limits (14). *Pn. septemradiatus*, during four years of our field survey in the Mekong Delta, we did not see it ventured into water (17)
Pn. septemradiatus	*INS (A)*, D (10)	
Boleophthalmus boddarti	AG, DT, PP (8,14)	Low to moderate – Both *B. boddarti* and *B. pectinirostris* were found only in the second lowest and the lowest strata below mean high water neap in a Malayan swamp (19). *B. boddarti* constructed a burrow in comparatively higher drier locations, most fish leaving the burrow to forage at the water's edge following ebb tides (26).
	DT (our analysis)	
B. dussumieri	DT (22)	
B. pectinirostris	DT (27,28)	

Scartelaos histophorus *S. tenuis*	DT, *PC* (7) DT, *INS(AQ)* (our analysis) *BV*, *CR* (1,2)	Low to moderate – *S. histophorus* spent most of their time in shallow water pools (26).
Zappa	Unknown	Moderate – found in habitats covered by vegetation and plant debris, but never far from the water's edge (20).
Pseudapocryptes elongatus	DT, AG (6,24) *CR*, PP, *ZP* (8)	Low – common at all locations surveyed in this study, preferring shallow stagnant waters on seaward mudflats and tidal reaches of rivers or ponds (26).
Apocryptes bato	AG, M (14) *CR* (21)	Low – lives in burrows within tidal limits. The fish is categorized into semi-aquatic forms (14)
Apocryptodon punctatus	DT, M (13)	None? – The fish was not observed to emerge during low tides but remained in a burrow excavated by the flathead snapping shrimp, crabs, or eel gobies during high tide (13).
Oxuderces nexipinnis	*INS (AQ)*, PP, *ZP* (8) DT (our analysis)	Low – The fish lived in water pools of various sizes and depths on the mudflats. The habitats were located quite low on the intertidal area and were exposed or nearly so for only several days in each lunar cycle (26)**.
Parapocryptes serperaster	DT, AG, D (12,15)	Low – during the field observation, the fish rarely moved out of the burrow (11).

[#]Determined by various methods e.g., biovolume (10), relative volume (16), point method (5) or index of relative importance (4). * Reported as *Ps. koelreuteri*, but the study site, Niger, indicates it is *Ps. barbarus*. ** Reported as *O. dentatus*, but the study site, the Straits of Malacca, indicates it is *O. nexipinnis*. AG, algae; BV, bivalves; CC, cladocerans; CR, crustaceans; D, detritus; DT, diatoms; F, fish; FS, fish scale; GP, gastropods; INS, insects; INS (A), ants; INS (AQ), aquatic insects; M, mud; NT, nematodes, PC, polychaetes, PP, phytoplankton; ZP, zooplankton. Animal food items are in italic.

References

(1) Abdoli L, Kiabi, B, Kamrani E, Abdoli A, Rezazadeh Katehsari E, Keshavarz M (2012) Feeding habits of *Scartelaos tenuis* in Bushehr Province, Iran. J Fish Iran J Nat Resource 64:309-318

(2) Abidizadegan M, Saeid EP, Hosein R (2015) Partial morphometrics and meristic evaluation of the two species mudskippers: *Scartelaos tenuis* (Day, 1876) and *Periophthalmus waltoni* (Koumans, 1941) from the Persian Gulf, Bushehr, Iran. Int J Fish Aquat Stud 2:353-358

(3) Baeck GW, Takita T, Yoon YH (2008) Lifestyle of Korean mudskipper *Periophthalmus magnuspinnatus* with reference to a congeneric species *Periophthalmus modestus*. Ichthyol Res 55:43-52

(4) Baeck GW, Yoon YH, Park JM (2013) Ontogenetic and diel changes in diets of two sympatric mudskippers *Periophthalmus modestus* and *Periophthalmus magnuspinnatus* on the tidal flats of Suncheon Bay, Korea. Fish Sci 79:629-637

(5) Bob-Manuel FG (2011) Food and feeding ecology of the mudskipper *Periophthalmus koelreuteri* (Pallas) Gobiidae at Rumuolumeni Creek, Niger Delta, Nigeria. ABJNA 2:897-901

(6) Bucholtz RH, Meilvang AS, Cedhagen T, Christensen JT (2009) Biological observations on the mudskipper *Pseudapocryptes elongatus* in the Mekong Delta, Vietnam. J World Aquac Soc 40:711-723

(7) Chan KY (1989) The ecology of mudskippers (Pisces: Periophthalmidae) at the Mai Po Marshes Nature Reserve, Hong Kong. Master of philosophy, University of Hong Kong.

(8) Chaudhuri A, Mukherjee S, Homechaudhuri S (2014) Food partitioning among carnivores within feeding guild structure of fishes inhabiting a mudflat ecosystem of Indian Sundarbans. Aquat Ecol 48:35-51

(9) Chukwu KO, Deekae SN (2013) Food of the mudskipper (*Periophthalmus barbarus*) from New Calabar River, Nigeria. IORS-JAVS 5:45-48

(10) Dinh QM, Tran LT, Tran TTM, To DK, Nguyen TTK, Tran DD (2020) Variation in diet composition of the mudskipper, *Periophthalmodon septemradiatus*, from Hau River, Vietnam. Bull Mar Sci 96:487-500

(11) Dinh QM, Qin JG, Dittmann S, Tran DD (2014) Burrow morphology and utilization of the goby (*Parapocryptes serperaster*) in the Mekong Delta, Vietnam. Ichthyol Res 61:332-340

(12) Dinh QM, Qin JG, Dittmann S, Tran DD (2017) Seasonal variation of food and feeding in burrowing goby *Parapocryptes serperaster* (Gobiidae) at different body size. Ichthyol Res 64:179-189

(13) Dôtu Y (1961) The bionomics and life history of the gobioid fish, *Apocryptodon bleekeri* (Day). Bull Fac Fish Nagasaki Univ 10:133-139

(14) Hora SL (1936) Ecology and bionomics of the gobioid fishes of the Gangetic Delta. Compt Rend XII Congr Internat Zool, Lisbonne 1935:840-863

(15) Khaironizam MZ, Norma-Rashid Y (2000) A new record of the mudskipper *Parapocryptes serperaster* (Oxudercinae: Gobiidae) from Peninsular Malaysia. Malay J Sci 19:101-104

(16) Kruitwagen G, Nagelkerken I, Lugendo BR, Pratap HB, Wendelaar Bonga SE (2007) Influence of morphology and amphibious life-style on the feeding ecology of the mudskipper *Periophthalmus argentilineatus*. J Fish Biol 71:39-52

(17) Mai HV, Tran XL, Dinh MQ, Tran DD, Murata M, Sagara H, Yamada A, Shirai K, Ishimatsu A (2019) Land invasion by the mudskipper, *Periophthalmodon septemradiatus*, in fresh and saline waters of the Mekong River. Sci Rep 9:14227

(18) Mazlan AG, Yakob F, Nor SM, Arshad A (2006) Foraging behavior and food selection of giant mudskipper (*Periophthalmodon schlosseri*) at Kuala Gula, Matang Mangrove Reserve, Perak, Malaysia. Coast Mar Sci 30:263-267

(19) Polgar G, Bartolino V (2010) Size variation of six species of oxudercine gobies along the intertidal zone in a Malayan coastal swamp. Mar Ecol Prog Ser 409:199-212

(20) Polgar G, Sacchetti A, Galli P (2010) Differentiation and adaptive radiation of amphibious gobies (Gobiidae: Oxudercinae) in semi-terrestrial habitats. J Fish Biol 77:1645-1664

(21) Rahman MS, Rahman MM, Parvez MS, Rashed-Un-Nabi M (2016) Feeding habit and length-weight relationship of a mudskipper *Apocyrptes bato* (Halminton, 1822) from the coast of Chittagong, Bangladesh. J Bangladesh Acad Sci 40:57-64

(22) Rathod SD, Patil NN (2009) Feeding habits of *Boleophthalmus dussumieri* (Cuv. & Val.) from Ulhas river estuary near Thane City, Maharashtra State. J Aqua Biol 24:153-159

(23) Stebbins RC, Kalk M (1961) Observations on the natural history of the mud-skipper, *Periophthalmus sobrinus*. Copeia 1961:17-27

(24) Swennen C, Ruttanadakul N, Haver M, Piummongkol S, Prasertsongskum S, Intanai I, Chaipakdi W, Yeesin P, Horpet P, Detsathit S (1995) The five sympatric mudskippers (Teleostei: Gobioidea) of Pattani area, Southern Thailand. Nat Hist Bull Siam Soc 42:109-129

(25) Takeda T, Hayashi M, Toba A, Soyano K, Ishimatsu A (2012) Ecology of the Australian mudskipper *Periophthalmus minutus*, an amphibious fish inhabiting a mudflat in the highest intertidal zone. Austr J Zool 59:312-320

(26) Takita T, Agusnimar, Ali AB (1999) Distribution and habitat requirements of oxudercine gobies (Gobiidae: Oxudercinae) along

the Straits of Malacca. Ichthyol Res 46:131-138

(27) Tran LX, Maekawa Y, Soyano K, Ishimatsu A (2020) Morphology of the feeding apparatus in the herbivorous mudskipper, *Boleophthalmus pectinirostris* (Linnaeus, 1758). Zoomorphology 139:231–243

(28) Yang KY, Lee SY, Williams GA (2003) Selective feeding by the mudskipper (*Boleophthalmus pectinirostris*) on the microalgal assemblage of a tropical mudflat. Mar Biol 143:245-256

(29) Zulkifli SZ, Mohamat-Yusuff F, Ismail A, Miyazaki N (2012) Food preference of the giant mudskipper *Periophthalmodon schlosseri* (Teleostei: Gobiidae). Knowl Manag Aquat Ecosyst 405:07

List of published papers

Tran LX, Maekawa Y, Soyano K, Ishimatsu A (2020) Morphology of the feeding apparatus in the herbivorous mudskipper, *Boleophthalmus pectinirostris* (Linnaeus, 1758). Zoomorphology 139: 231-243

Tran LX, Maekawa Y, Soyano K, Ishimatsu A (2021) Morphological comparison of the feeding apparatus in herbivorous, omnivorous and carnivorous mudskippers (Gobiidae: Oxudercinae). Zoomorphology https://doi.org/10.1007/s00435-021-00530-8

Tran LX, Soyano K, Ishimatsu A (2021) Morphology of the feeding apparatus in two oxudercine gobies, *Parapocryptes serperaster* (Richardson 1846) and *Pseudapocryptes elongatus* (Cuvier 1816). Zoomorphology (submitted on July 2021)